DYNAMIC CRUSHING BEHAVIOR OF SANDWICH PANELS WITH BIO-INSPIRED CORES

A Thesis Submitted to
The Graduate School of Engineering and Sciences of
İzmir Institute of Technology
in Partial Fulfillment of the Requirements for the Degree of

MASTER OF SCIENCE

in Mechanical Engineering

by
Erkan GÜZEL

July 2017
İZMİR

We approve the thesis of **Erkan GÜZEL**

Examining Committee Members:

Prof. Dr. Alper TAŞDEMİRCİ
Department of Mechanical Engineering, İzmir Institute of Technology

Prof. Dr. Buket OKUTAN BABA
Department of Mechanical Engineering, İzmir Katip Çelebi University

Assoc. Prof. Dr. H. Seçil ARTEM
Department of Mechanical Engineering, İzmir Institute of Technology

21 July 2017

Prof. Dr. Alper Taşdemirci
Supervisor, Department of
Mechanical Engineering
İzmir Institute of Technology

Prof. Dr. Mustafa GÜDEN
Co-Supervisor, Department of
Mechanical Engineering
İzmir Institute of Technology

Prof. Dr. Metin TANOĞLU
Head of the Department of
Mechanical Engineering

Prof. Dr. Aysun SOFUOĞLU
Dean of the Graduate School of
Engineering and Sciences

ACKNOWLEDGEMENTS

Firstly, I would like to thank to my supervisor Prof. Dr. Alper TAŞDEMİRCİ for his guidance, endless patience and illuminating my career with his great knowledge and experience. Also I am grateful him to let me be a part of a hardworking team in Dynamic Test and Modeling Laboratory. I hope I will keep having his supports and encouragements during my whole engineering life.

I am also thankful to TUBITAK (Scientific and Technical Council of Turkey) for the project with Grant no. 214M339. In this project, my teammates Emine Fulya AKBULUT and Fırat TÜZGEL deserve a tribute for their contributions at least as much as my supervisor.

Furthermore, I would like to thank to all my lecturers Assoc. Professor Hatice Seçil ARTEM, Prof. Dr. Bülent YARDIMOĞLU, Assoc. Professor Selçuk SAATCI, Assoc. Professor Onursal ÖNEN, Prof. Dr. Sedat AKKURT, but notably Prof. Dr. Mustafa GÜDEN who is also my co-supervisor.

Also the other members of Dynamic Test and Modeling Laboratory must be appreciated; Çetin Erkam UYSAL, Semih Berk SEVEN, Mehmet Alper ÇANKAYA, Ali Kıvanç TURAN and Mustafa Kemal SARIKAYA for their big-hearted helps and great supports.

Additionally, I owe my parents a debt of gratitude for their incentive attitudes during this tiring period of my life.

The last but not the least, my girlfriend Gökce GÖKCEN deserves my thankfulness for her all supports and being the source of my motivation.

ABSTRACT

DYNAMIC CRUSHING BEHAVIOR OF SANDWICH PANELS WITH BIO-INSPIRED CORES

In the current study, a new approach was shown to develop an innovative load-carrying and energy absorbing structure which can fulfill the requirements in the fields of automotive, defense and aerospace. Two different topics which have been in great demand in the recent times were combined: sandwich structures and bio-inspiration.

Balanus which is a barnacle living along the seashores and on the ships' surfaces was taken under examination to design a novel sandwich structure core geometry. The designed geometry was manufactured with deep drawing process. The sandwich structures were produced with different face sheets using a pattern to ensure the repeatability of the crushing tests. Firstly, the advantage of the bio-inspired core over the conventional core geometries was shown with a numerical study. Then, the crushing tests were conducted at both quasi-static and dynamic loading rates. Further, the effects of foam filling, confinement, inertia and strain rate sensitivity on the crashworthiness performance of the proposed structure were investigated. In addition to the experimental studies, numerical analyses were also performed using LS-DYNA 971. In the numerical studies, manufacturing process of the core geometry was also modeled to count in the residual stress/strain so that a good proximity was obtained between the experimental and numerical results. Moreover, the penetration and perforation behaviors were inspected. Utility of the proposed geometry where a high resistance is needed against dynamic crushing was demonstrated. Finally, several suggestions were proposed for the future works to elaborate the present study.

ÖZET

DOĞADAN İLHAM ALINAN BİR ÇEKİRDEK MALZEME İHTİVA EDEN SANDVİÇ PANELLERİN DİNAMİK EZİLME DAVRANIŞLARI

Bu çalışmada; otomotiv, savunma ve havacılık-uzay alanlarındaki ihtiyaçları karşılayabilecek yeni bir yük taşıyıcı ve enerji yutucu yapı geliştirmek için farklı bir yaklaşım gösterilmiştir. Son zamanlarda büyük rağbet gören iki farklı konu olan sandviç yapılar ve biyobenzetim birleştirilmiştir.

Özgün bir sandviç yapı çekirdek geometrisi tasarlamak amacıyla deniz kıyılarında ve gemi yüzeylerinde yaşayan bir deniz kabuklusu olan balanus inceleme altına alınmıştır. Tasarlanan geometri derin çekme yöntemiyle üretilmiştir. Sandviç yapılar farklı yüzey malzemeleri ile üretilmiş olup ezilme testlerindeki tekrar edilebilirliği garanti altına alabilmek için kalıp kullanılarak üretilmiştir. İlk olarak, biyobenzetim esaslı çekirdeğin alışılagelmiş çekirdek geometrilerine karşı olan avantajı bir nümerik çalışma ile gösterilmiştir. Daha sonra, kuasi-statik ve dinamik yükleme hızlarında ezilme testleri yapılmıştır. Ayrıca; köpük dolgunun, çevresel sınırlandırmanın, geometri kaynaklı ataletin ve şekil değiştirme hassasiyetinin önerilen geometrinin çarpışma dayanıklılığı performansına etkileri araştırılmıştır. Deneysel çalışmalara ek olarak, LS-DYNA 971 kullanılarak nümerik analizler de yapılmıştır. Nümerik çalışmalarda, artık gerilme ve gerinimleri de hesaba katmak için çekirdek geometrinin üretim süreci de modellenmiştir, böylece deneysel ve nümerik sonuçlar arasında yüksek bir yakınlık elde edilmiştir. Bunlara ek olarak, penetrasyon ve perforasyon davranışları üzerine de çalışılmış olup önerilen geometrinin dinamik ezilmelere karşı yüksek direnç gereken yerlerdeki işe yararlılığı ispatlanmıştır. Son olarak, bu çalışmayı detaylandırmak için yapılabilecek gelecek çalışmalar ile ilgili çeşitli öneriler sunulmuştur.

TABLE OF CONTENTS

LIST OF FIGURES

Figure **Page**

LIST OF TABLES

Table **Page**

CHAPTER 1

INTRODUCTION

Energy absorbing and load-carrying structures serve as protective layers and aim to decrease the effect of applied external loads both statically and dynamically on the inner construction. These structural components are mostly needed in automotive, defense and aerospace industries. Automotive applications primarily require high capability of energy absorption in case of collision to ensure occupants' safety. Defense industry focuses on improving explosion-proof equipments and ballistic resistance in the military vehicles. Aerospace industry demands elevated thermal effectiveness and acoustic comfort in addition to the structural integrity. In these industry fields, the weight of designed structures is another significant factor. Possible lowest weight is desired while the strength of the structure is maximized. If less amount of material is used, manufacturing cost is lowered. Reducing the total weight of these structures has also positive effects on biological environment even it is indirectly. At the present time, most of the mass produced vehicles by aforementioned industry fields work with fossil fuels. Weight reduction in the vehicles decreases required power for propulsion and accordingly fuel consumption is lessened. In the last decades, many investigations have been carried out and it has been shown that sandwich structures can meet these industries' demands. A sandwich structure has markedly higher energy absorbing capability than the solid plate made of the same material with the same mass.

A sandwich panel basically consists of a light core material that is placed between comparatively stiffer and stronger two plates. Mostly these two plates have the same thickness and are made of the same material. Thick and light core exhibits an outstanding resistance to bending and buckling with the cooperation of thin and strong face materials. The most predominant reason of being in demand for the sandwich structures is their high ratio of flexural stiffness to structural weight.

1.1 Sandwich Structures

Besides the naturally occurring ones, the first man-made sandwich structure was manufactured using wood egg-crate cores in the middle 1800s for top compression panel. Then, important development appeared in 1919 and sandwich panels were used on an aircraft. Balsa wood for core layer and mahogany for facing were preferred on the seaplane pontoons. After that, in World War II, balsa wood core and plywood face sheets were used on a military aircraft. In 1945, the first sandwich structure entirely made of aluminum was manufactured with honeycomb core (Bitzer, 1997). From then till now, material variety and popularity of these structures have risen.

In recent years, the interest of scientists working on energy absorbing and load-bearing structures has densely tended to sandwich panels because they can be easily tailored into the most optimal form using numerous combinations of different materials and geometries in the presence of different loading conditions. In existing researches, different materials have been examined in sandwich constructions. In addition to material type, secondary attention has been focused on the effect of various patterns and geometries of the materials in the core layer.

Frequently encountered materials as sandwich structure components have been metals and fibre-reinforced polymer composites. They have been favored for both core and face layers. Honeycomb (both hexagonal and square), foam/solid type, corrugated and truss, Y and I frames have been mainly preferred core geometries, Figure 1.1.

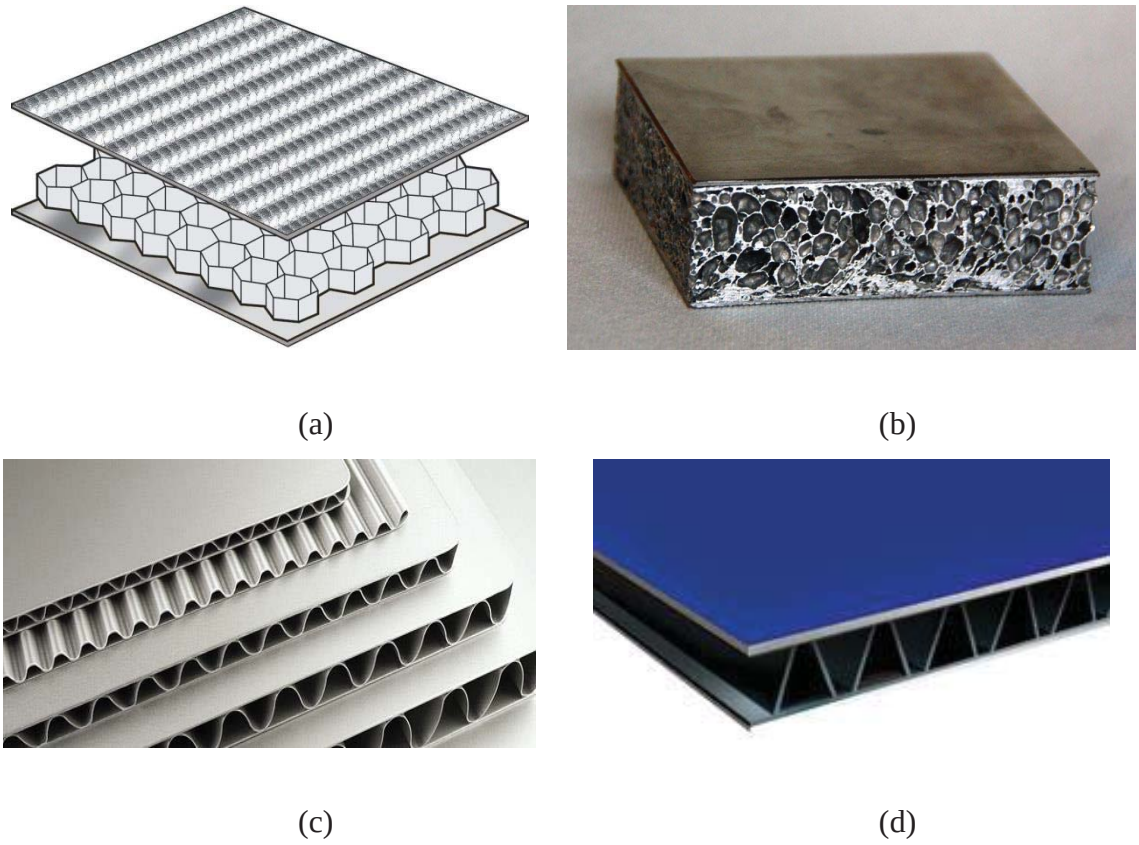

Figure 1.1. Frequently used core geometries in sandwich structures (a) honeycomb, (b) foam, (c) corrugated, (d) truss. (Source: www.nauticexpo.com), (Source: no.pinterest.com), (Source: www.al-honeycomb-panels.com), (Source: www.atas.com)

Aluminum honeycomb sandwich panels have been investigated by several authors. Strength characteristics, low impact velocity response and dynamic crush behaviors of this structures with various cell specifications were documented ((Paik, Thayamballi, & Kim, 1999), (Hazizan & Cantwell, 2003), (Hong, Pan, Tyan, & Prasad, 2008)). The same geometry was also experienced with fibre-reinforced composite face sheets in different papers. Face, core, indenter sizes were varied in the test set-up to determine indentation failure behavior of sandwich panel consisting of glass-fibre/epoxy skins and aramid cores (Lee & Tsotsis, 2000). Furthermore, in order to comprehend the impact damage mechanism of Nomex sandwich structure with carbon epoxy skins, several tests were carried out at different impact energy levels and it has been shown that impact response and energy absorption characteristic are vastly dictated by core compression rather than face delamination (Meo, Vignjevic, & Marengo, 2005).

Polymer and metallic foams have also been presented in many papers as core type. Low velocity impact responses of several polymeric foams were studied and it was shown that failure type in sandwich structure is vastly affected by foam density (Hazizan & Cantwell, 2002). An earlier study had focused on the failure modes of sandwich structure with metallic cores. Additionally, diverse advantages of metallic foam core such as easy to have curve-shape and cancelling the need of adhesive layer were touched upon (McCormack, Miller, Kesler, & Gibson, 2001). In another study, polymeric and metallic foams were compared. Even though energy absorption of these two structures exhibited similarity, remarkable difference was observed between the damage modes of aluminum foam and PVC-based foam (Compston, 2006).

Corrugated and Y frame type cores in sandwich beams have been compared in a study and it has been stated that both two geometries having same masses show similar dynamic responses (Rubino, Deshpande, & Fleck, 2008). Earlier, same authors had also given an attention on truss core sandwich beams. Three-point bend tests were applied on truss-core sandwiches manufacturing from two different materials (aluminum-silicon and silicon brass) to measure collapse responses. Further, weight optimization studies were performed and the advantage of truss core over metallic foams was shown (Deshpande & Fleck, 2001).

In addition to the core types mentioned above, Kagome lattice is another geometry which has been employed in the core layer of the sandwich structures. This geometry can be seen in the molecular patterns of some natural minerals. Thus, it can be evaluated as an example of biomimetic core type. Carbon fiber reinforced Kagome lattice grids were sandwiched by two laminates and failure modes of this geometry have been revealed conducting compression and bending tests. Advantages over other cellular materials were noted whereas debonding was pointed out as the main flaw (Fan, Meng, & Yang, 2007). Another study about Kagome truss core structure focused on the deformation and failure types under compression and shear loadings. This structure exhibits better performance than honeycomb aerospace structure when specific strengths under shear and compressive loadings are compared (Ullah, Elambasseril, Brandt, & Feih, 2014).

With the risen interest on bio-inspiration, different naturally occurring materials have been inspected. Palmetto wood is one of them. Foam core was used between the carbon fiber-epoxy facings and it was reinforced by carbon rods to mimic the wood structure. It has been noted that the sandwich with the bio-inspired core shows

significantly higher performance in terms of flexural strength and elastic energy absorption than the sandwich involving conventional foam does (Haldar & Bruck, 2014).

Contribution of biomimetic concept can not be discarded considering the studies about energy absorbing structures which have been reported in the recent years. It definitely deserves to be concentrated on intensely and more materials must be examined to find solutions for engineering problems.

1.2 Biomimetic

Biomimetic is a compound word (bio- meaning life in Greek, and –mimesis, meaning to copy) which basically means imitating the nature. Nature seems to accomplish numerous actions very well without using high-strength materials contrary to humans do. This skill can be accepted as a gift of billions of years of evolution. At this point, besides the effect of material type, importance of the geometry and the concept of "optimize rather than maximize" become evident.

The idea of mimicking nature goes back a long way although the term of biomimetic was used by Otto Schmitt for the first time in 1950s. For instance, it is known that Chinese people had tried to produce silk artificially more than 3000 years ago (Vincent, Bogatyreva, Bogatyrev, Bowyer, & Pahl, 2006). When considering more recent history, in Renaissance, traces of biomimetic studies can be encountered with. Leonardo Da Vinci who is the designer of the flying machine has obviously inspired of winged animals. Further, he has a saying which emphasizes the importance of directing to the nature. *"Those who are inspired by a model other than Nature, a mistress above all masters, are laboring in vain"*. This saying shows us biomimetic is not that new trend to be concentrated on only in modern science.

In addition to the biomimetic studies previously noted, many other applications can be observed also in daily life. For example, dirt-repellent paints were developed by investigating the lotus flower. Lotus flower is known for the ability of keeping the dust away from its skin. Another extensively known biomimetic product is Velcro. Velcro was produced inspiring of tiny hooks on the burr. Moreover, today's olympic swimmers wear swimsuits which has so many overlapping little scales. These scales closely resemble the microstructure that shark skin has: see Figure 1.2.

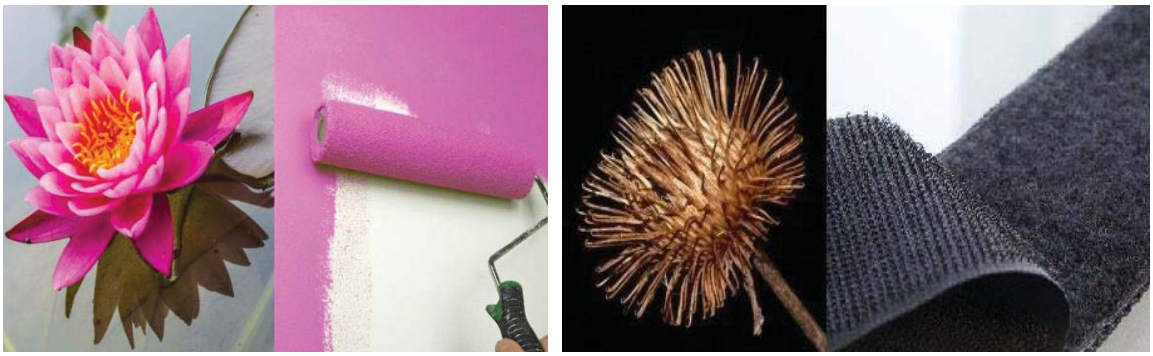

(a) (b)

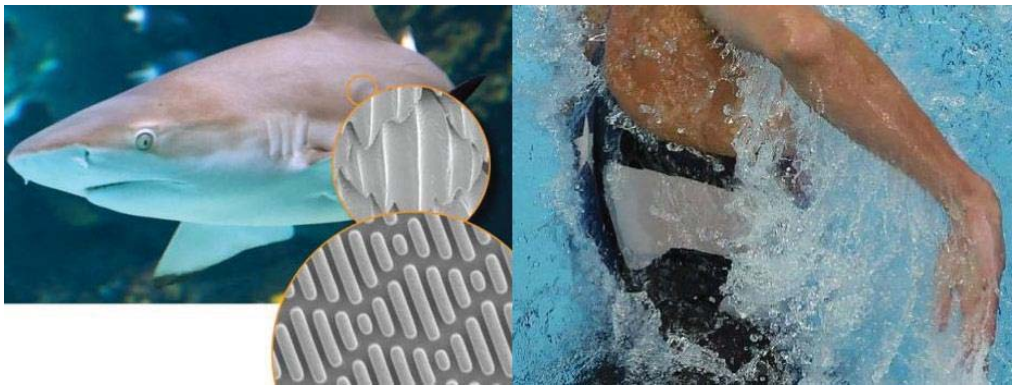

(c)

Figure 1.2. Mostly known biomimetic products (a) dirt-repellent paint, (b) Velcro, (c) swimsuit (Source: www.mnn.com).

Presented examples above consider the characteristics of living creatures such as self-cleaning, being tough to be removed from a surface and lowering the drag friction, respectively. However, in this study, energy absorbing performance is the crucial factor. By taking this factor into consideration, balanus has given the inspiration for a novel geometry in the core layer of a sandwich panel.

1.2.1 **Balanus**

Balanus is a barnacle which is a member of arthropod class in taxonomic classification. It lives along the sea shores sticking on the rocks, wharf piles, buoys and ships' surfaces. It is possible to encounter with several types of balanus along the coasts in Turkey whereas many of them live all around the world's watersides. Balanus starts its life as a larva which is basically a plankton floating freely at the sea. After passing

enough time to reach adulthood, it holds on a convenient surface. Then, it creates an outer shell layer by excreting a material suchlike quicklime to have a safe shelter. In Figure 1.3(a), this structure is seen with the inner half spherical layer which performs as its mouth (Pérez-Losada, Høeg, & Crandall, 2004).

(a)

(b)

(c)

Figure 1.3. (a) a balanus, (b) balanus colony, (c) produced core geometry resembling balanus (Source: http://home.kpn.nl), (Source: http://www.marlin.ac.uk)

Balanus is a hermaphrodite creature which means it is able to fertilize itself and multiply fast. This property enables to live them in colonies and to countervail the external loads such as water pressure and wave impact together with higher resistance due to contribution of confinement effect. In addition to the ability of protecting its shape under water pressure and wave impact, balanus causes deceleration at the ships' speed particularly if a huge colony is being talked about. Inspiring from these properties

of balanus, the geometry that can be seen in Figure 1.3(c) was designed and compared to the conventional core geometries. Balanus geometry is the combination of two concentric thin-walled tubes which are going to be named as inner core and outer shell throughout the study. This geometry was produced with 30 mm of bottom diameter and 25 mm of height in conformity with its common natural dimensions.

1.2.2 **Advantages of Balanus Over Conventional Core Geometries**

A preliminary numerical study was conducted to investigate the performance of balanus geometry in comparison with extensively used core geometries such as cylinder, hexagon and square. These four geometries having the same mass and the same wall thickness were numerically modeled and exposed to dynamic loading. Two different cases were tried. First, the geometries were designed with equal heights and compressed under a plate having constant velocity of 10 m/s until they underwent densification. In the Figure 1.4(a)&(b), force response/crushing displacement and absorbed energy/crushing displacement graphs of the geometries are given. Second, the same procedure was applied by holding the diameters of the geometries constant. Figure 1.5(a)&(b) shows the comparison of the geometries for the second scenario.

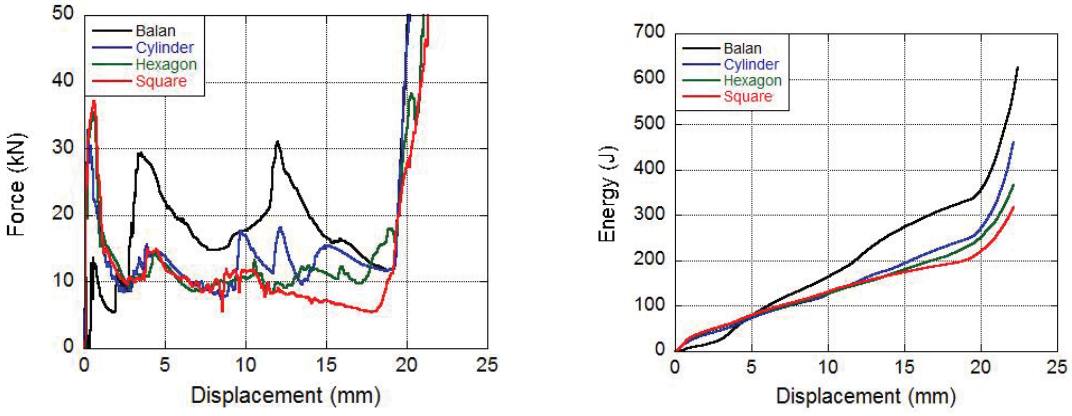

(a) (b)

Figure 1.4. Comparison of balanus geometry with conventional core geometries having same mass, height and wall thickness (a) force response/crushing displacement curves, (b) energy absorption/crushing displacement curves.

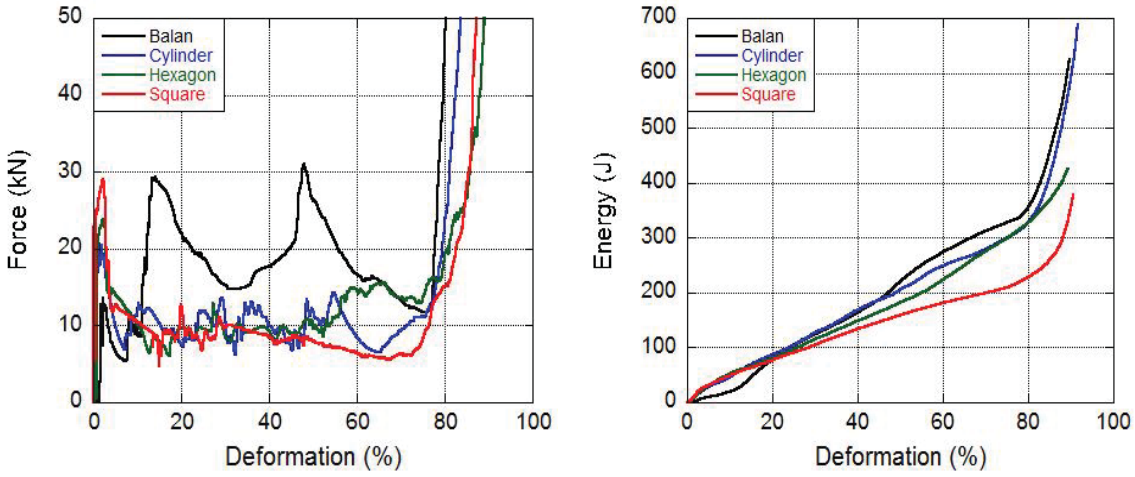

(a) (b)

Figure 1.5. Comparison of balanus geometry with conventional core geometries having same mass, diameter and wall thickness (a) force response/crushing displacement curves, (b) energy absorption/crushing displacement curves.

At both cases, proposed balanus geometry exhibited remarkably higher energy absorption capability. In numerical terms, balanus absorbs 31% more energy at the first case than the cylinder which is the best among conventional geometries. At the second case, even cylinder exhibits better performance compared to its first case, balanus is still better than it with 8% greater absorbed energy. Consequently, it has been proven that balanus geometry is worth to be investigated broadly.

1.3 Aim and Scope of the Study

The current study focuses on the design and optimization of sandwich panels with bio-inspired cores. Even though bio-inspiration has been a widely attention-grabbing topic in the recent years, there are not many researches related to energy absorbing and load-carrying structures, particularly in our country. The present study is a candidate to bridge this gap in the literature.

The sandwich panel with bio-inspired cores proposes many advantages such as easy manufacturability, easy local repair and high strength with low weight. Each detail was specified in the study from the first step of the manufacturing to the dynamic crushing behavior of the specimen. In order to investigate the proposed geometry profoundly, numerical studies were conducted using LS-DYNA 971.

In the first chapter, a brief introductory information was provided with regard to the typical sandwich structures and the concept of biomimetic. Also, balanus which is the source of inspiration of the proposed core geometry was introduced and the results of a simple numerical study were presented to show the advantages of the balanus geometry over the conventional core geometries.

The following chapter was elaborated with the relevant studies previously done and the investigation methods of similar structures. Thin-walled structures and their dynamic crushing behaviors were primarily concentrated on.

In chapter 3, manufacturing methods of each component were presented. Also, test devices were introduced and test methodologies were clarified.

In chapter 4, the details of numerical studies were given. Used material models in the simulations and the material properties were tabulated.

In chapter 5, both experimental and numerical results were illustrated. Various comparisons were made. Static and dynamic crushing behaviors of the proposed sandwich structures were interpreted. Also, the penetration and perforation characteristics were discoursed.

In chapter 6, numerous conclusions were reached and some suggestions were made for the future works.

CHAPTER 2

LITERATURE REVIEW

The main purpose of using sandwich structures as energy absorbers in case of high-speed crashes and ballistic threat is converting the kinetic energy of the impactor into the irreversible plastic deformation energy. In particular, progressively large amount of compression of core material is desired to maximize the energy absorption capacity of sandwich structures. Use of sandwich panels as energy absorbers in military, automotive and aerospace industries makes it a necessity to be extra light in terms of long-term sustainability. Additionally, ease of manufacture and ease of local repair are the properties that enrich a sandwich structure besides its vitally important feature which is promising a reduction in the transmitted force magnitude to the protected structure.It is generally seen when the literature is scanned that thin-walled tubes are widely employed to meet mentioned requirements. Versatility and the efficiency of thin-walled structures move them ahead of other types of core geometries.

2.1 Thin-walled Tubes

Thin-walled tubes are prone to progressively collapse which means they are able to be deformed axially throughout the entire length. When they are subjected to axial loading, they offer higher energy absorption capacity due to the plastic folding formation. In addition to these features, low manufacturing cost makes them prevalent in many application areas ranging from storage vessels, oil rigs to aircrafts and ships.

Cylindrical tubes, square tubes, polygonal tubes and conical tubes in different patterns with various materials have been investigated in the previous studies as the examples of thin-walled structures. Also the performance of the combined thin-walled geometries has been reported. In the following section, the studies in the literature related to aforementioned structure types are going to be given except conical and combined ones. A special attention will be paid to conical and combined geometries because proposed balanus geometry has resembling shape with them. Moreover, bi-

tubular thin-walled structures deserve an extra consideration due to the balanus shape consisting of an inner core and an outer shell.

2.1.1 **Thin-walled Tubes with Circular, Square and Polygonal Cross-sections**

N.K. Gupta performed quasi-static and impact tests to investigate the axial collapse behavior of the cylindrical tubes. Two different materials (aluminum and mild steel) with different dimensions were examined in different conditions (as received and annealed). Also, the effect of drilled circle-form holes at the mid-height of the tubes on the collapse mode was exhibited. He has stated that deformation mode is independent of the test type for identical cylindrical specimens whereas average loads in drop tower tests are approximately 20% greater than the equivalent values in quasi-static tests. Further, the rise in initial peak load reaches about 45%. On the other hand, it is clearly seen that annealing process has significant effect on the collapse modes. Excessively cold worked aluminum tubes are deformed in diamond mode when subsequently annealed ones are collapsed in concertina mode. However, just the contrary case is valid in the crushing of mild steel tubes. Also, the slope at the beginning of the plastic deformation in stress strain curve is affected differently by the annealing process for aluminum and mild steel. Another factor which was studied in this paper is discontinuity along the tube lengths. Opening opposite circular holes at the mid-height of the tubes creates a positive outcome on collapse mode. It helps to avoid global buckling in the use of longer tubes as can be seen in Figure 2.1 (N. K. Gupta, 1998).

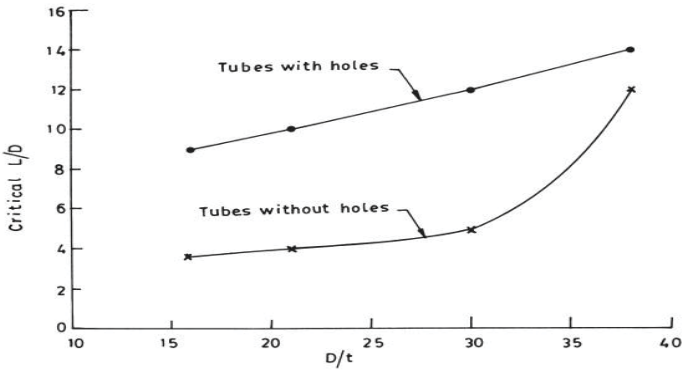

Figure 2.1. Graph of critical buckling length to diameter ratio for overall buckling against the ratio of diameter to thickness (Gupta, 1998).

Deformation rate and the inertial effects on structural response of cylindrical tubes have been studied by Wang and Lu. Aluminum and steel tubes with different thicknesses were tested with different impact velocities varying from 114 m/s to 385 m/s using gas gun test set-up.

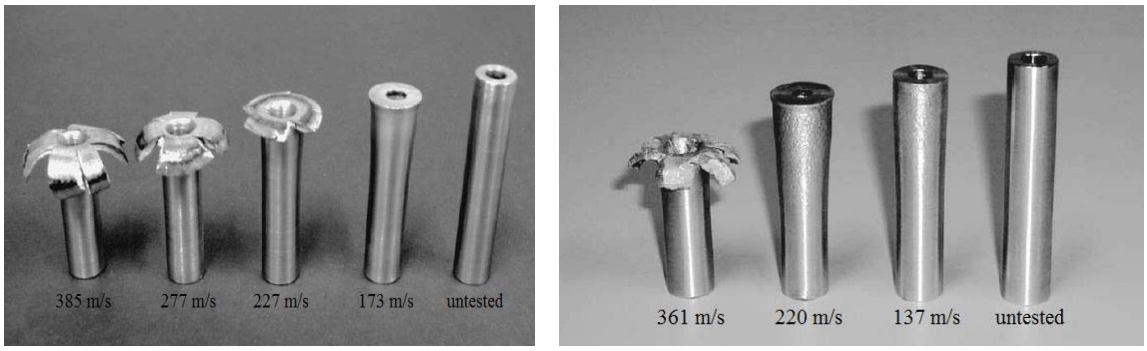

(a) (b)

Figure 2.2. Picture of deformed samples at different strike velocities (a) steel (b) aluminum (Wang & Lu, 2002)

It has been revealed that different deformation modes may occur in dynamic crash other than the modes in static loading. In Figure 2.2, the final states of steel and aluminum tubes with the thickness of 3.13 mm (the thickest specimens) are visualized and mushrooming is displayed. The tubes are folded sequentially at low speed impacts while mushrooming with folds are seen at medium speeds. At high speeds, in addition to mushrooming, wrinkling appears. Also, if the material type is considered it is clearly seen that selecting a more ductile material or annealing the material makes possible to increase crush speeds without cracking (Wang & Lu, 2002).

The foam filling effect on the collapse modes and energy absorption capacity of cylindrical tubes has been searched in several papers. Aluminum tubes were produced with both aluminum and polystyrene foam fillers and exposed to quasi-static compression by Kavi *et al*. It has been stated that all foam-filled tubes are deformed in concertina mode independently of the foam type while the empty ones are collapsed in diamond mode. They also claimed that increasing the wall thickness is more effective than using filler in terms of specific energy which is the ratio of absorbed energy to the mass of tube (Kavi, Toksoy, & Guden, 2006).

Another study with foam-filled cylindrical tubes has been made using hybrid tubes (aluminum & E-glass woven fabric polyester composite) by Guden *et al*. Aluminum closed-cell foam was chosen as filler. As it was declared in previous paper, inefficiency of foam filler from the point of specific absorbed energy was reported. Nevertheless, foam filling showed an alleviant effect on the initial peak force response. On the other hand, hybrid tubes exhibited improved energy absorption performance than the sum of individual performances of their components by means of interaction effect (Guden, Yüksel, Taşdemirci, & Tanoğlu, 2007).

Similar studies have been conducted for both square and polygonal tubes. Zarei and Kröger examined the foam filling contribution on square tubes with different foam densities varying 60-460 kg/m^3 under impact crush loading both experimentally and numerically. Despite the direct proportion between absorbed energy and foam density, specific absorbed energy of foam-filled tubes reaches its maximum value with the foam having 230 kg/m^3 of density. In addition, it has been asserted that foam-filled tube which is even 19% lighter than the optimum empty tube absorbs the same amount of energy with empty one. (Zarei & Kröger, 2008).

Zhang and Huh have made a numerical study to elucidate how the lengthwise grooves on the sidewalls of a square tube influence the crashworthiness parameters. Different groove sizes and arrangements were formed with stamping method as can be seen in Figure 2.3. Also the tubes without groove were axially compressed. Reported results have shown that specific absorbed energy values considerably increase in the compression of grooved square tubes. Further, a reduction was observed in peak force values.

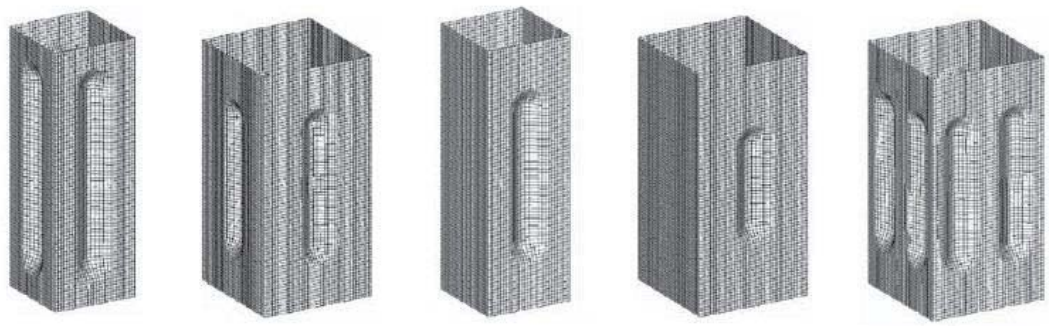

Figure 2.3. Tested specimens with different groove sizes and groove arrangements (Zhang and Huh, 2009)

It has been also pointed out that groove size and number should not be chosen at random. In the compression of the tube having equal size of groove and fold lengths, underperformed energy absorption capacity was obtained (Zhang & Huh, 2009).

Crushing behaviors of polygonal tubes have also been investigated in various studies. Yamashita *et al* concentrated on how crushing strength and deformation mode are affected by the edge number of the polygonal tubes. Numerically analyzed geometries having 4 (square), 5, 6, 12 and 96 (acceptable as nearly circle) edges were subjected to axial compression by a plate which has 10 m/s constant velocity.

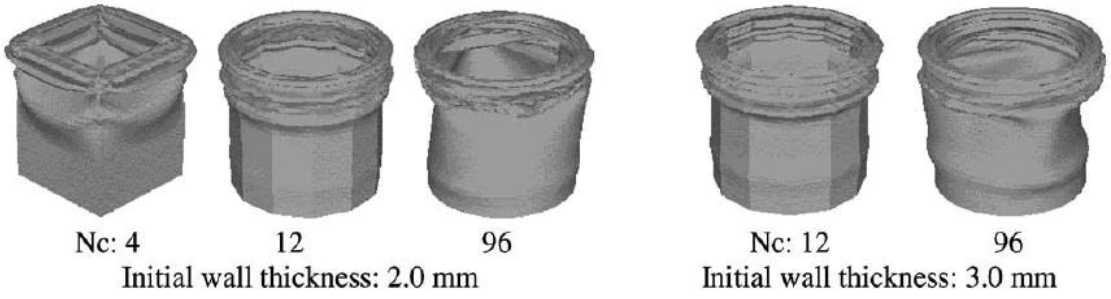

(a)

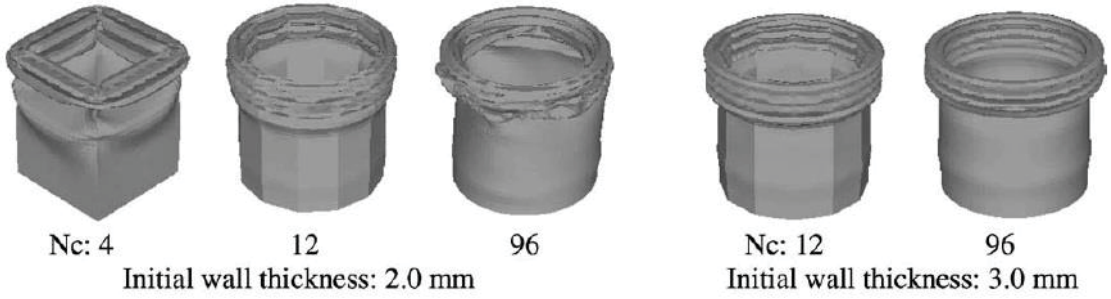

(b)

Figure 2.4. Deformation modes of tubes having different number of corners and different wall thicknesses (a) 100 MPa of strain hardening rate, (b) 300 MPa of strain hardening rate (Yamashita, Gotoh & Sawairi, 2003)

Each polygon has common peripheral length, height, density; hence the masses of the tubes with identical wall thickness are equal to each other. Figure 2.4 shows that increase in the tube thickness, in the number of corners and in the strain hardening rate changes the irregular deformation pattern to orderly collapse mode.

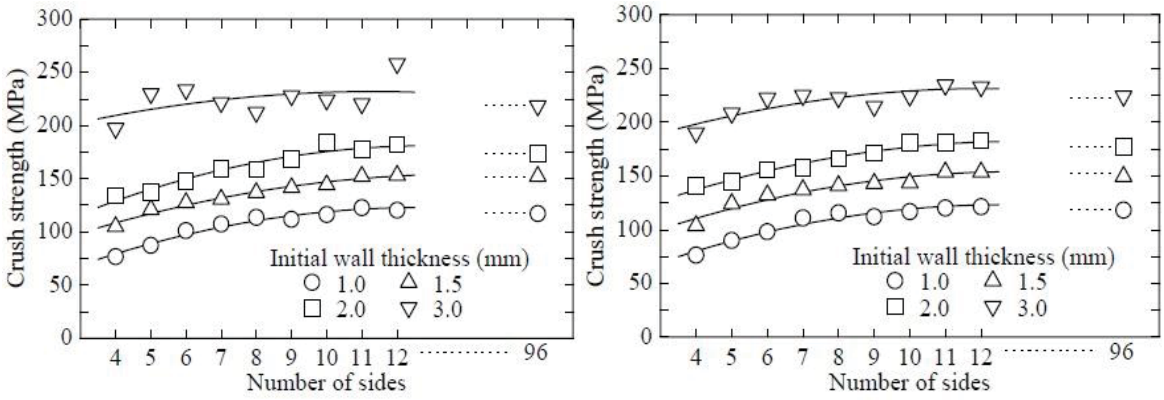

(a) (b)

Figure 2.5. Crushing strength for polygons having different number of sides (a) strain hardening rate: 100 MPa, (b) strain hardening rate: 300 MPa (Yamashita, Gotoh & Sawairi, 2003)

In Figure 2.5, the crushing strength values are illustrated for different polygons. It was calculated by taking the average of oscillatory stress after the initial peak stress. Crushing strength rises as the number of sides increases, however, the tubes with more than 11 sides reach saturation level and do not show big difference. It is also clear that the number of the polygonal sides has an impact upon crushing strength, in particular, considering the tubes having relatively thinner walls (Yamashita, Gotoh, & Sawairi, 2003).

Wangyu Liu *et al.* have compared the axial crushing performance of the tubes with star-shaped lateral cut view and the conventional polygonal tubes both with different number of corners, Figure 2.6. The tubes were crashed with 3.6 m/s of initial velocity and the effect of the number of corners on folding mode and specific absorbed energy were observed. It has been documented that specific absorbed energy value of the tubes having star-shaped cross section reaches maximum when it has 10 corners while the initial peak force increases directly proportional. Not only specific absorbed energy but also average of total absorbed energy and crushing force efficiency (mean crushing force / initial peak force value) reduce beyond 10 corners. In addition, even though a significant rise is observed in the specific absorbed energy values of star-shaped tubes in comparison with polygonal tubes with the same number of corners, crushing force efficiencies are highly close each other. Also, they have claimed that the tubes are collapsed either in small folds mode, in large folds mode or unstable mode

depending on the slenderness which is the ratio of tube length to tube diameter. Deformation with small folds is more desirable than the other two types of deformation mode because the tubes collapsed with small folds exhibit better specific energy absorption (W. Liu, Lin, Wang, & Deng, 2016).

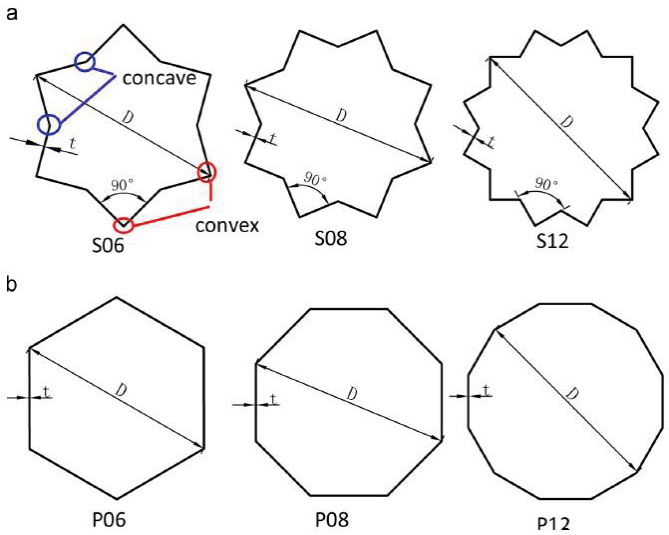

Figure 2.6. Drawing of cross section of (a) star-shaped tubes, (b) polygon tubes (W. Liu et al., 2016)

2.1.2 **Conical Tubes, Combined Geometries and Bi-Tubular Thin-walled Structures**

Alkateb and Mahdi investigated the effects of vertex angle of elliptical cones on the crushing behavior. They chose a composite material for tube manufacturing. Woven roving glass fibre was passed through a resin bath for impregnation process, then, the tubes were shaped with the vertex angles varying 0^o-24^o. To discuss the performance of each tube, some parameters were concentrated on such as initial failure indicator factor (first peak load / maximum load), crush force efficiency (average load / maximum load), stroke efficiency (compression up to distance densification starts / tube height) and specific energy absorption capability (absorbed energy / tube mass). An equation between first peak and maximum peak load which means initial failure indicator factor is 1 causes catastrophic failure in tube crushing. Further, ply failure or matrix failure might be observed first depending upon this factor is more or less than 1, respectively. On the other hand, for the rest of the parameters it can be said that the higher values are

gained the more desired results are gotten. In Figure 2.7, it is clearly indicated that increasing vertex angle decreases initial peak force and boosts the average load up. It makes possible to refrain from catastrophic failure.

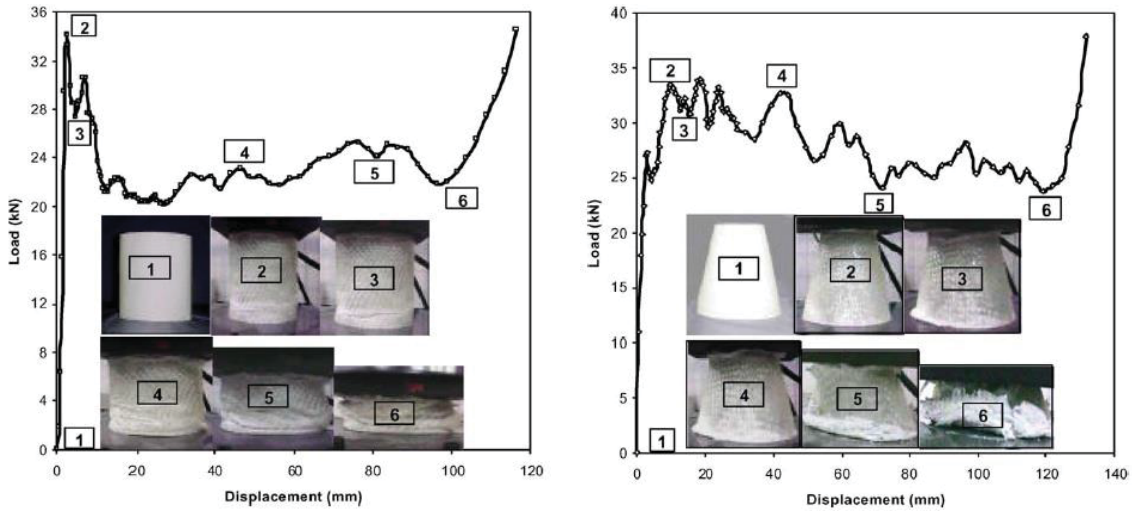

(a) (b)

Figure 2.7. Load-Displacement curves of elliptical cones with vertex angle (a) 0^o and (b) 24^o (Alkateb & Mahdi, 2004)

They have also specified that the tubes having vertex angles of 18^o and 24^o exhibit regular progressive crushing mode which provides better energy absorption capacity whereas the tubes having lower vertex angles are deformed with the combination of initial progressive crushing, local buckling and some local cracks which cause sudden drops in load-displacement curve and affect the energy absorption ability adversely (Alkateb & Mahdi, 2004).

Conical shells made of aluminum with different semi-apical angles and different diameter-to-thickness ratios were tested under impact loading by N.K. Gupta and Venkatesh. Besides the tests that were applied with 34.75 kg of released mass and initial crush velocities ranging from 2.55 to 7.92 m/s using the drop hammer experimental set-up, quasi-static tests were also conducted with the constant velocity of 10 mm/min to compare the collapse modes of shells. It has been noted that load-displacement curves and collapse modes are supremely affected by the semi-apical angle. While in the tubes with low semi-apical angles axisymmetric ring and diamond folding mechanism were observed, in the tubes with greater semi-apical angles axisymmetric rolling plastic hinges and non-axisymmetric stationary plastic hinges were detected. It is difficult to

declare a certain expression related to the effect of semi-apical angle on mean collapse load due to having no direct proportion between them. The highest mean collapse loads are seen in the tubes with semi-apical angles of 30^o and 45^o. Rest of them shows a wavelike performance. Diameter-to-thickness ratio also plays an important role on the energy absorption capability of the conical tubes where diameter refers the average diameter of top and bottom ones. Moreover, higher energy absorption was noticed in the impact tests compared to corresponding static tests (Gupta & Venkatesh, 2007).

Crushing behavior of foam-filled conical tubes was inspected under axial impact using finite element method by Ahmad and Thambiratnam. Impact mass, impact velocity, wall thickness and semi-apical angle were changed in addition to the foam density in numerical models. It has been demonstrated that concertina mode collapse occurs in the presence of foam inside of the conical tube under identical conditions as can be seen in Figure 2.8. Foam-filled tubes absorb higher energy at the same amount of compression compared to the empty counterparts due to having more lobe formation.

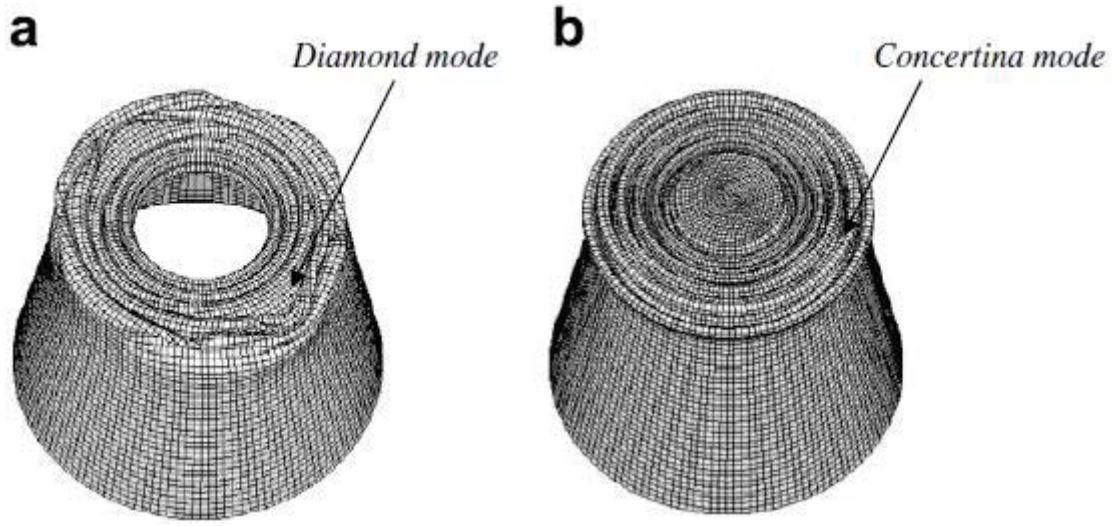

Figure 2.8. Deformation modes of the identical conical tubes (a) empty, (b) foam-filled under the same conditions (Ahmad & Thambiratnam, 2009)

In Figure 2.9, it is clear that increase in semi-apical angle, thickness and foam density affect the amount of absorbed energy positively. However, in empty conical tubes, especially relatively thinner ones, increasing semi-apical angle is not efficient. It is also possible to said that the effect of foam density in thick tubes on the absorbed energy is less than in nearly thinner tubes (Ahmad & Thambiratnam, 2009).

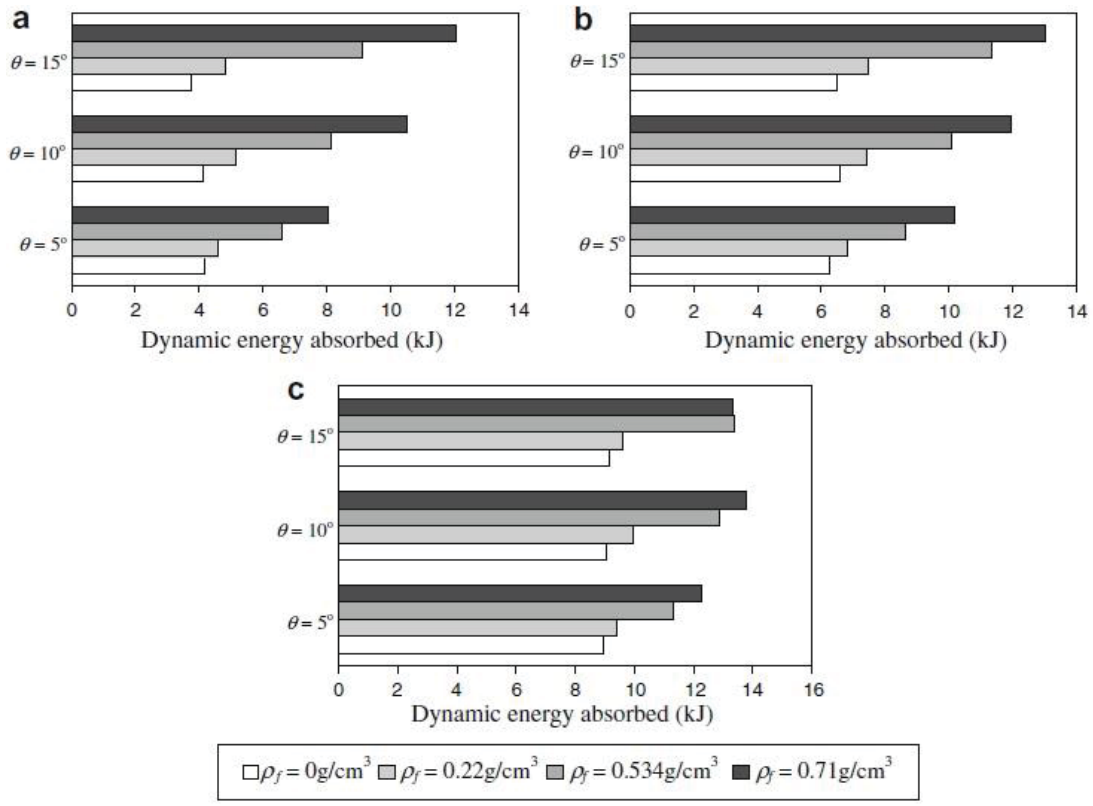

Figure 2.9. Influence of foam density and semi-apical angle on the dynamic energy absorption capability of the tubes with the wall thickness of (a) 1.5 mm, (b) 2.0 mm, (c) 2.5 mm (Ahmad & Thambiratnam, 2009)

Ghamarian *et al.* designed end-capped conical thin-walled tubes and investigated the foam filling effect on crashworthiness of these structures, both experimentally and numerically: see Figure 2.10. A good agreement between experimental and numerical results was noted. Also a comparison was made between cylindrical and conical tubes in terms of specific energy absorption. Polyurethane foam was selected as the filler type. Foams with different densities of 0 kg/m^3, 65 kg/m^3, 90 kg/m^3, 145 kg/m^3 were tested and it was reported that the tube with highest density of foam filler exhibits the topmost specific energy absorption.

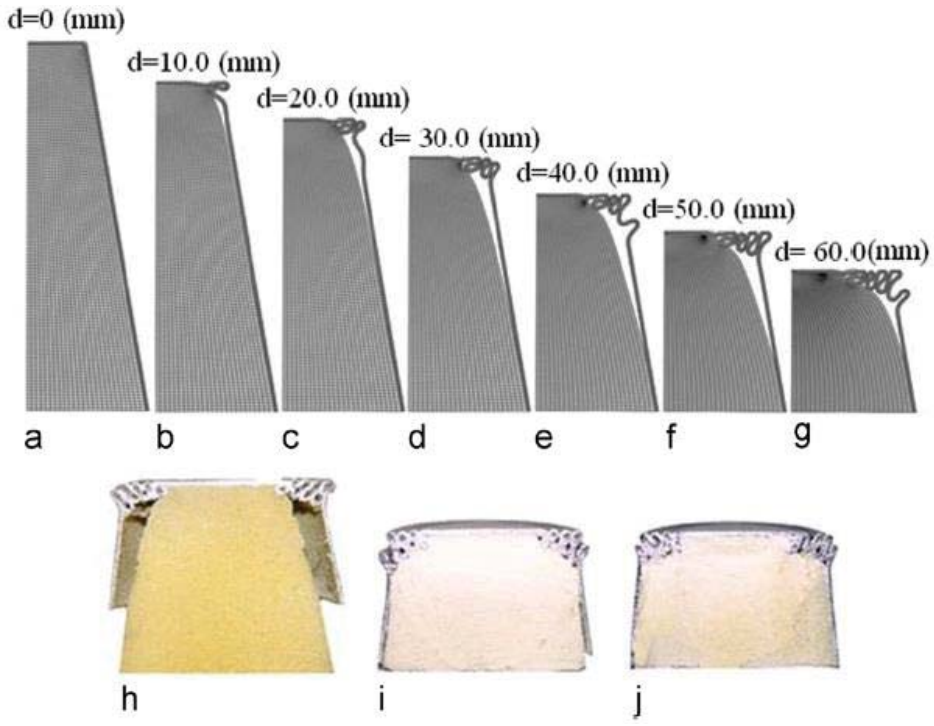

Figure 2.10. (a) to (g) Numerical representation of progressive collapse of the end-capped conical tube with foam density of 145 kg/m3, final state of experiments conducted with the tubes having foam densities of (h) 145 kg/m3, (i) 90 kg/m3, (j) 65 kg/m3 (Ghamarian, Zarei, & Abadi, 2011)

Interaction effect has also a significant role in the crushing of foam-filled conical tubes. Conical tubes with polyurethane foams show better energy absorption capability than the combination of foam and tube separately show. Lastly, they have asserted that empty conical tube with the semi-apical angle of 10^{o} absorbs 18.4% more energy than the cylindrical one absorbs even though they show very much alike performances when they are filled with polyurethane foam (Ghamarian, Zarei, & Abadi, 2011).

Crash behavior of conical tubes under oblique loading has been investigated by Azarakhsh and Ghamarian. Aluminum and polyurethane were preferred as the tube material and the filler type, respectively. Both empty and foam-filled tubes were crushed with the fully clamped boundary conditions under both axial and oblique loadings: see Figure 2.11. It has been demonstrated that increasing the angle of applied load results in a reduction in energy absorption and in mean crush load because collapse mode turns into diamond from axisymmetric fold. Using polyurethane foam filler enhances the resistance of conical tubes against oblique loading. Also increasing the semi-apical angle of foam-filled conical tubes has an absolute positive effect on the

energy absorption capacity. Moreover, empty conical tubes and foam-filled circular tubes are declared as inadvisable structure types under oblique loads (Azarakhsh & Ghamarian, 2017).

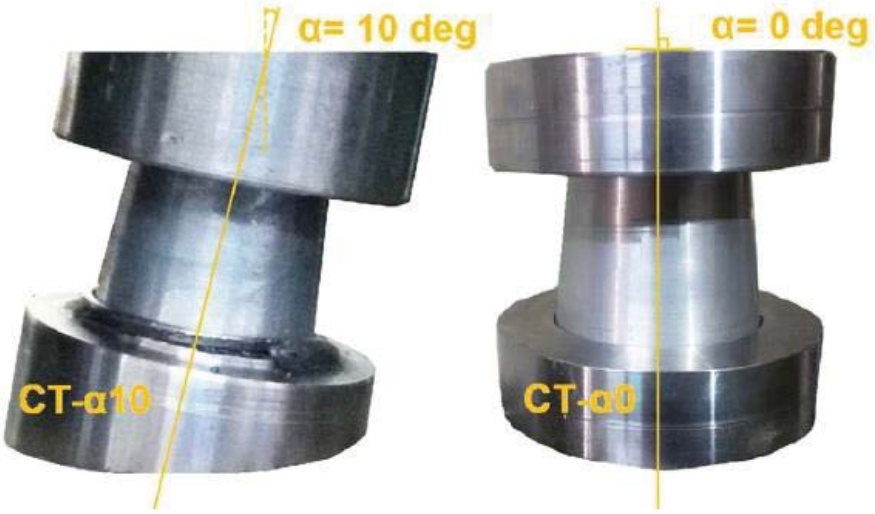

(a) (b)

Figure 2.11. Both-ended-clamped cones under (a) oblique and (b) axial loading (Azarakhsh and Ghamarian, 2017)

Gupta *et al*. have studied the collapse behavior of combined shells consisting of truncated conical base and hemispherical cap illustrated in Figure 2.12. The geometry was subjected to axial impact both experimentally and numerically. A well match was obtained between experimental and numerical results.

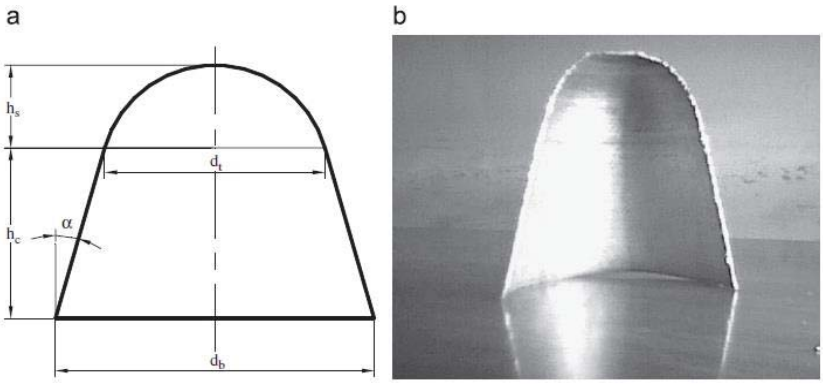

Figure 2.12. (a) Geometrical details and (b) cut-view of untested specimen (Gupta, Mohamed Sheriff, & Velmurugan, 2008)

In the study, mentioned geometry was examined with different semi-apical angles, thicknesses and bottom diameters under both quasi-static and dynamic loadings. The authors have revealed that even a small change of semi-apical angle despite remaining constant of the rest of the parameters affects the crushing behavior of the geometry. In Figure 2.13, zone A and zone B refer the compressions of hemispherical and conical portions, respectively. While the hemispherical portion shows a flat-topped behavior after a linear increase in its load-compression curve, conical one exhibits a sudden drop at the beginning. Also, different portions get an edge over each other in terms of peak loads when the angle is changed. This is attributed to inertia factor which is going to be detailed in the following section.

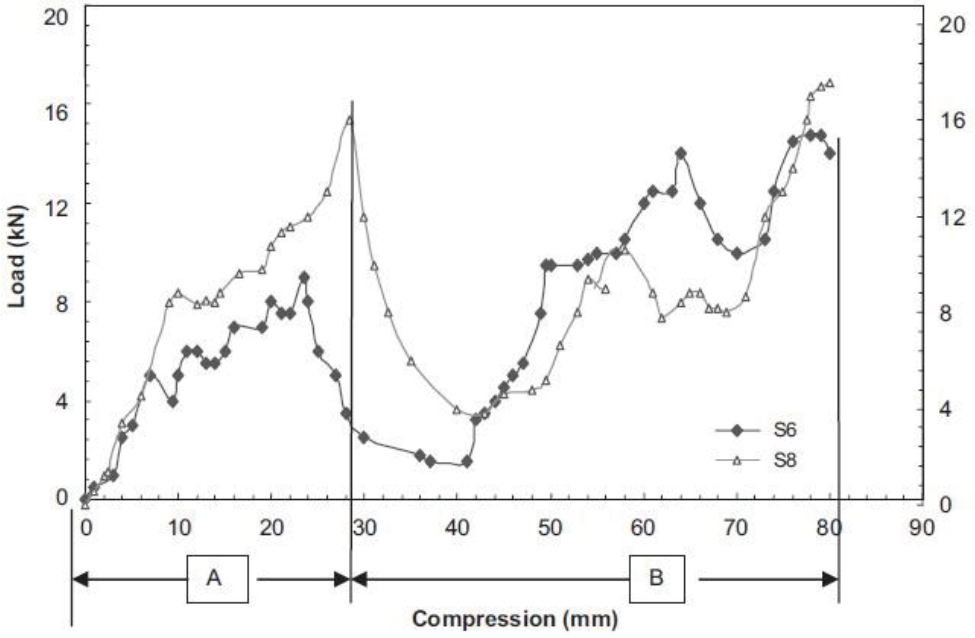

Figure 2.13. Load-Compression curves of two different specimens under static loading (S6: 1.6 mm of thickness, 21^{o} of semi-apical angle, 165 mm of bottom diameter. S8: S6: 1.6 mm of thickness, 25^{o} of semi-apical angle, 165 mm of bottom diameter.) (Gupta, Mohamed Sheriff, & Velmurugan, 2008)

Moreover, another comparison which is given in Figure 2.14 revealed that conical portion of the geometry is much more velocity sensitive than the hemispherical portion. Its energy absorbing performance increases significantly in case of dynamic collision while the hemispherical portion presents an indistinguishable behavior. The

reason of this difference is also going to be investigated further in the following section attributing to strain rate effect (N. K. Gupta, Mohamed Sheriff, & Velmurugan, 2008).

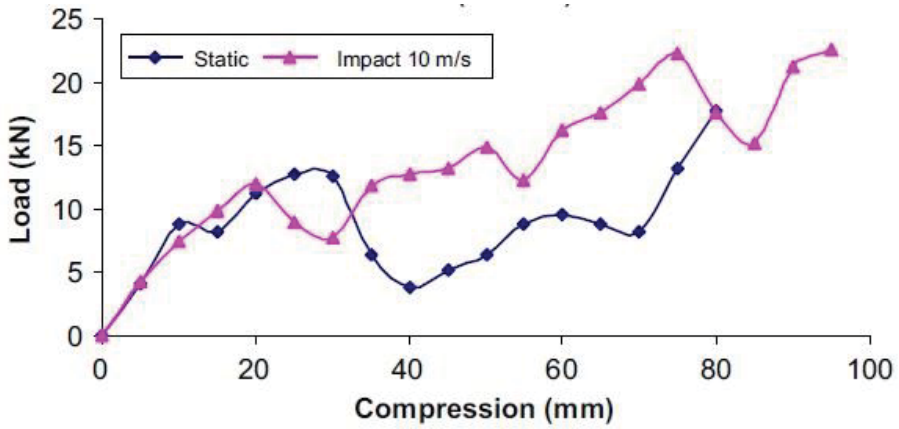

Figure 2.14. Comparison of load-compression curves of the same specimen under static and impact loadings (Gupta, Mohamed Sheriff, & Velmurugan, 2008)

Another type of geometry combining of cone and cylinder has been inspected by Gupta and Gupta. All specimens were fabricated as the combination of upper cylinder portion (one-third of total length) and truncated cone base (two-third of total length). The semi-apical angle and thickness were varied. Not surprisingly energy absorption capacity increased with the increasing shell thickness. They have concluded that the collapse mode of the combined shell geometry is predominantly controlled by the semi-apical angle. The combined geometry having conical base with lower degree of semi-apical angle shows concertina mode deformation whereas mixed mode is observed in the tubes with higher semi-apical angle. It has been also noted that local buckling occurs at the mid-height of the cylindrical portion in thicker tubes while axisymmetric folding is formed at the joint part of the combined geometry in relatively thinner tubes, in the very beginning of the deformation (P. K. Gupta & Gupta, 2013).

Taşdemirci *et al*. have experimentally and numerically studied dynamic crushing behavior and energy absorption capacity of combined geometry shells as core material in sandwich structures. The shell geometry which consists of hemispherical cap and cylinder base was manufactured by deep-drawing process. Hence, the wall thickness is not constant throughout the length of specimen. The compression tests were carried out by using quasi-static and drop-weight test devices. Also direct impact experiments were performed. It has been revealed that, at comparatively lower velocities rate sensitivity and inertia factor both have minor influence on the force-deformation curves of the

samples. Moreover, the confinement effect on buckling loads was considered in the study. The sandwich structures which consist of five shell specimens were compressed under both circumferentially confined and unconfined conditions.

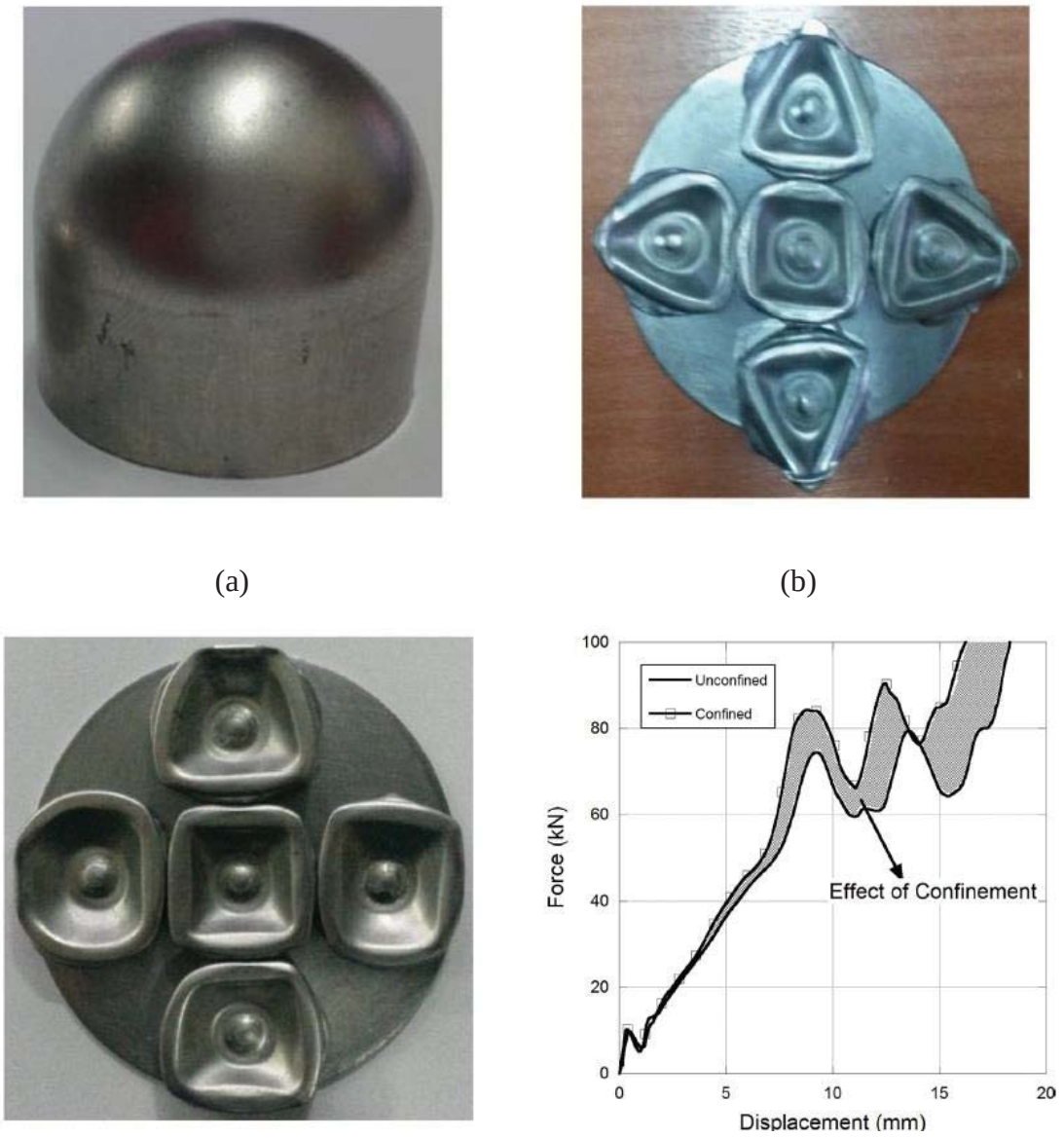

Figure 2.15. (a) a single specimen, the final stages of (b) unconfined and (c) confined sandwich structures under quasi-static compression, (d) comparison of the load-displacement curves of unconfined and confined quasi-static compression tests (Tasdemirci, Kara, Turan, & Sahin, 2015)

In Figure 2.15(d), it can be seen that after a certain compression level confined specimen exhibits higher buckling load due to blocking of lateral displacement of

plastic hinges by the rigid confinement wall. Later than validating numerical models in terms of both energy absorption characteristics and deformation modes, inertial effect and rate sensitivity factor were taken into consideration. Using Johnson-Cook material model, strain rate sensitive and strain rate insensitive numerical simulations were carried out. It has been documented that the effect of inertia is much higher than that of strain rate as can be clearly seen in Figure 2.16(a). The effects of these factors were inspected under different compression velocities with both confined and unconfined conditions: see Figure 2.16(b) (Tasdemirci, Kara, Turan, & Sahin, 2015).

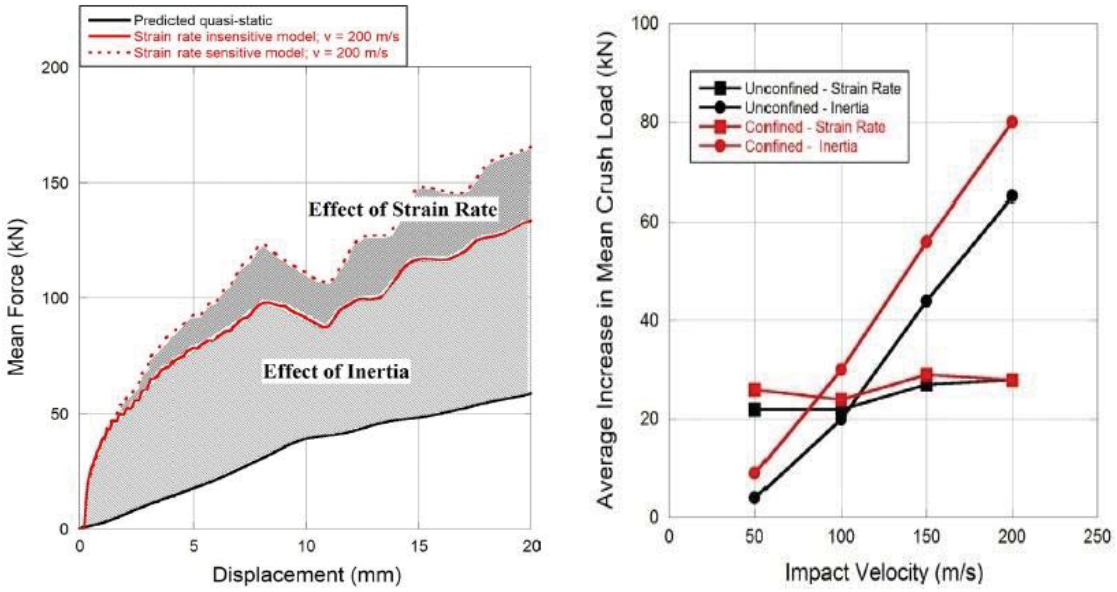

(a) (b)

Figure 2.16. (a) Effect of strain rate and inertia under 200 m/s of compression velocity and (b) average increase in mean crush load for varying impact velocities (Tasdemirci, Kara, Turan, & Sahin, 2015)

Multi-cell and multi-wall tubes have also been studied in several papers as energy absorbers and load-carrying components. Najafi and Rais-Rohani designed multi-cell, multi-corner tubes to be used in vehicles' front rails for providing a reduction in weight together with high energy absorption ability. Axial collapse mechanics of the tubes with different cross-section configurations which are given in Figure 2.17(a) were investigated numerically. Then, they were compared with the results gained by the analytical methods in the literature.

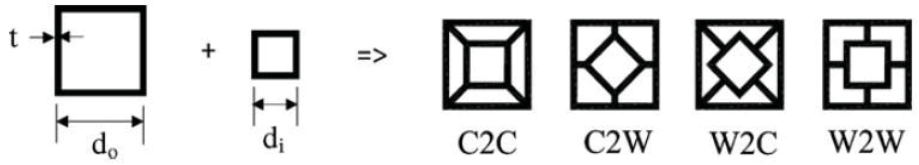

(a)

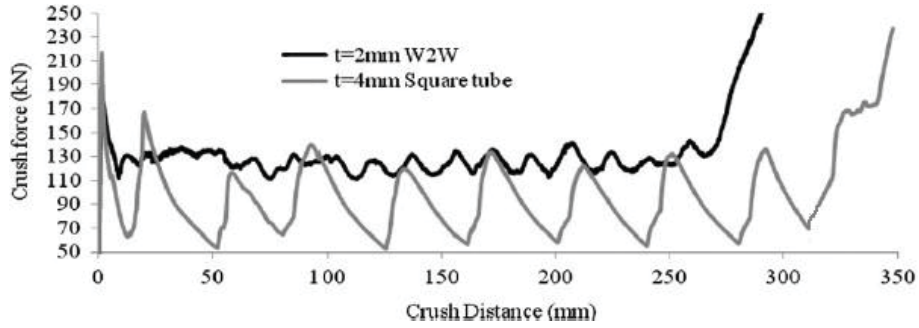

(b)

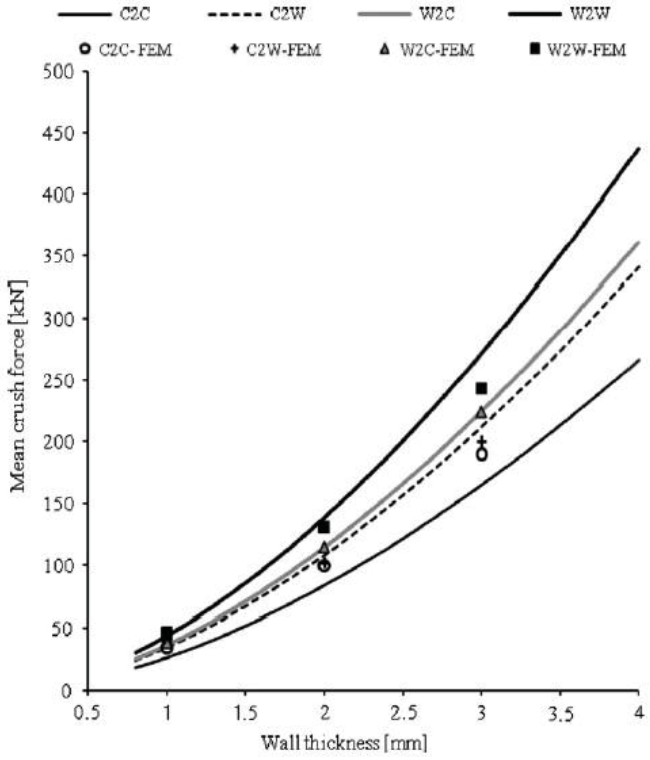

(c)

Figure 2.17. (a) Cross-sections of the tubes, (b) Comparison of W2W multi-cell tube with the wall thickness of 2 mm and single square tube with the wall thickness of 4 mm, (c) Comparison of simulation results and analytical approach results for different wall thickness values (Najafi & Rais-Rohani, 2011).

Figure 2.17(b) shows that multi-cell tube yields a uniformly stable force response while the single tube equivalent in mass exhibits a wavy crush force during the collapse process. On the other hand, the tube with configuration of W2W has the best

crush mean force values for each wall thickness both in numerical and analytical results. It is also clear that the current numerical study matches up with the analytical approach (Najafi & Rais-Rohani, 2011).

A similar numerical study has been conducted by Tang *et al*. for cylindrical multi-cell columns. Number of cells, number of concentric cylinders in the columns and wall thicknesses of the cylinders were varied. As a result of this parametric numerical study, the effects of mentioned parameters on the energy absorption characteristics were reported. Also, a comparison was made between single-square, multi-cell square and multi-cell cylindrical columns.

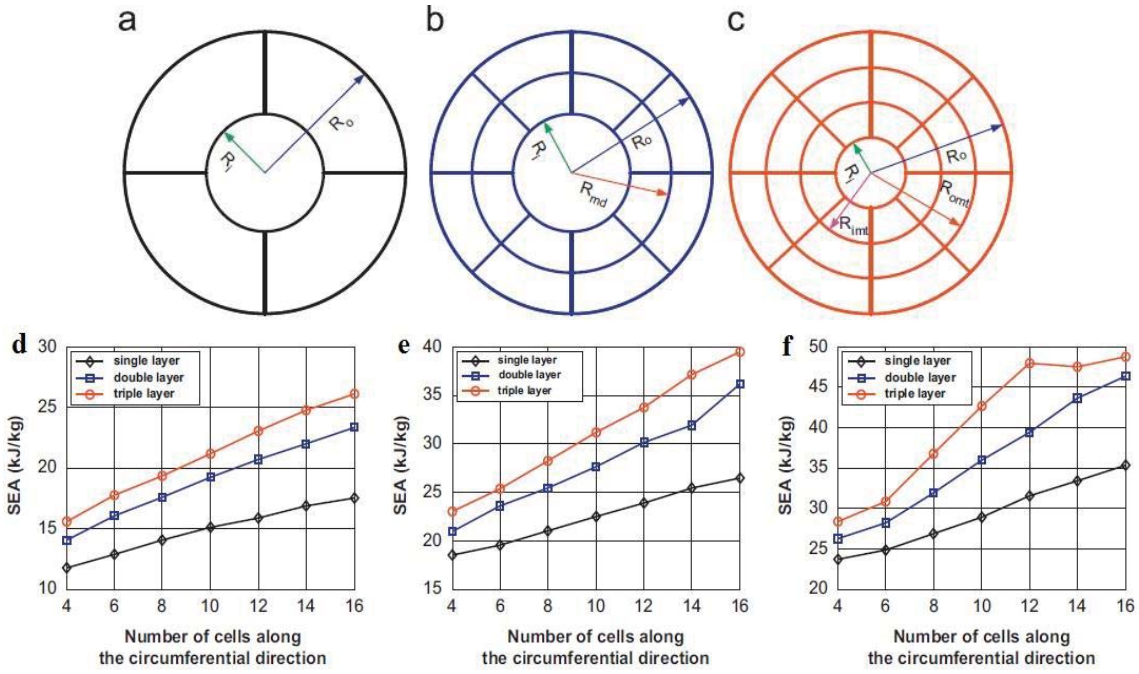

Figure 2.18. Cross-section of cylindrical columns with (a) single layer, (b) double layer, (c) triple layer. Specific absorbed energy variation of single, double and triple layered columns having different number of cells with the wall thickness of (d) 0.5 mm, (e) 1.0 mm, (f) 1.5 mm (Thang, Liu, & Zhang, 2013).

Increasing the number of circumferential cells results in a gradual raise in specific absorbed energy. However, increase in the number of layer is more effective. Additionally, increasing the thickness of the layers and flanges is another way to have a better energy absorption performance. Moreover, it was disclosed that if the same amount of material usage is compelled double layered multi-cell cylindrical columns have the best performance under axial crush even single-square and multi-cell square

columns are considered. No matter how many cells and layers a cylindrical column has, all they are collapsed in a progressive manner as long as they are not unreasonably thick (Tang, Liu, & Zhang, 2013).

Zheng *et al.* conducted a numerical study to inspect the dynamic crushing behavior of single and bi-tubular thin-walled structures. Sixteen different types of foam-filled tubes which are illustrated in Figure 2.19 were modeled and axially crushed.

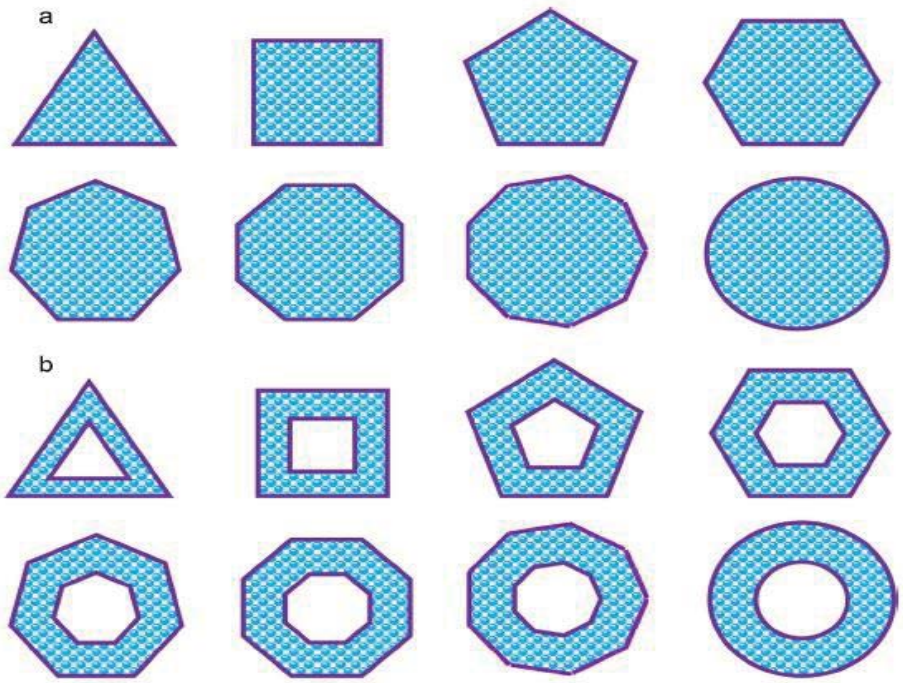

Figure 2.19. Cross-sections of foam-filled (a) single and (b) bi-tubular thin-walled structures (Zheng, Wu, Sun, Li, & Li, 2014)

The results have shown that collapse modes of each foam-filled tube are more regular than the empty counterparts. Additionally, it has been pointed out that increasing the number of sides affects energy absorption and mean crushing force characteristics positively. Bi-tubular foam-filled circular thin-walled geometry has been declared as the best one among all combinations (foam-filled or empty single/multi-wall tubes) considering crashworthiness (Zheng, Wu, Sun, Li, & Li, 2014).

Alavi Nia and Khodabakhsh investigated the crashworthiness of concentric bi-tubular cylindrical tubes by varying the radial distance between inner and outer cylinders both numerically and experimentally. The tubes that are seen in Figure 2.20 were manufactured using aluminum 1050 and loaded axially both quasi-statically and dynamically.

Figure 2.20. Tested bi-tubular concentric thin-walled cylinders with different radial distances (Alavi Nia & Khodabakhsh, 2015)

The tubes were classified into two groups. In the first group, the diameter of the outer cylinder was kept constant and the inner one's was varied. In the second group, a single-tube which is identical with the outer tube in the first group was taken as the reference and then the following bi-tubular samples were fabricated and modeled with different inner and outer diameters so as to have equal mass with the reference single-tube. Considering the second group it can be deduced that using bi-tubular concentric cylinders is much more effective than using its single-tube counterpart. Results have also shown that the bi-tubular specimen with the dimensionless distance of 0.66 in the second group exhibits the best energy absorption capability under both quasi-static and dynamic loadings. For the first group, the optimum value of dimensionless distance was detected as 1. In the study, dimensionless distance was defined as the ratio of the difference between inner and outer tubes' radii to arithmetic average of the radii (Alavi Nia & Khodabakhsh, 2015).

Another crashworthiness analysis about bi-tubular structures has been carried out by Vinayagar and Kumar. Quasi-static compression tests were performed with the specimens which are the combinations of outer cylinder tube and different types of inner polygonal tubes. Together with the diversification of the inner tubes' cross-sections, the dimensions were also changed.

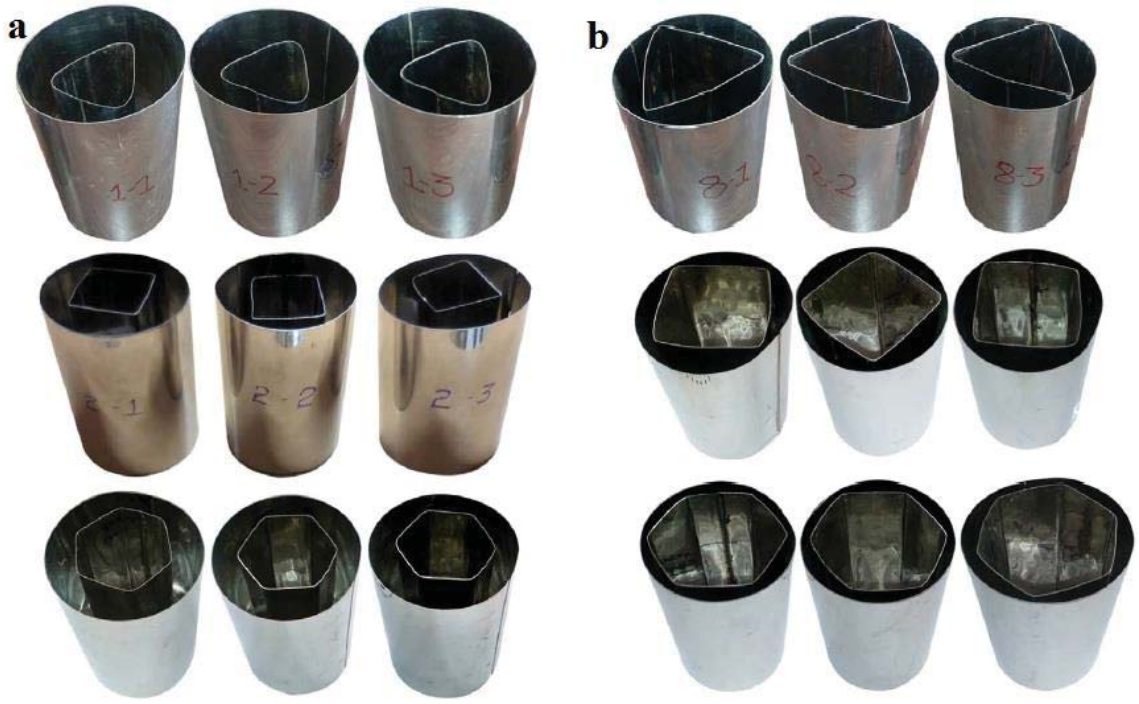

Figure 2.21. Crushed bi-tubular samples involving different types of inner tubes (a) with small size, (b) with large size (Vinayagar & Kumar, 2017).

Documented results have revealed that the bi-tubular structures show noticeably higher energy absorbing performance than the single tubes in parallel with the previous studies. They also stated that the bi-tubular samples which have inner tubes with larger inscribed circles exhibit outstanding energy absorbing capacity in comparison with the tubes having corresponding smaller inner tubes regardless of the geometry. More, the advantage of using hexagonal tube as an inner component rather than triangular or square was demonstrated (Vinayagar & Kumar, 2017).

2.1.3 **A Study on Strain-Rate Sensitivity and Inertial Effect Interaction**

A significant research was conducted on the energy absorbing structures which exhibit different behaviors depending on the geometry despite using same material in the manufacturing. In the research, the effects of the deformation rate on the energy absorbing capacity were also investigated in addition to that of the geometry. The authors, Calladine and English, noted that the geometries showing different load-

carrying characteristics under quasi-static axial compression are also affected differently by the increase of loading rate.

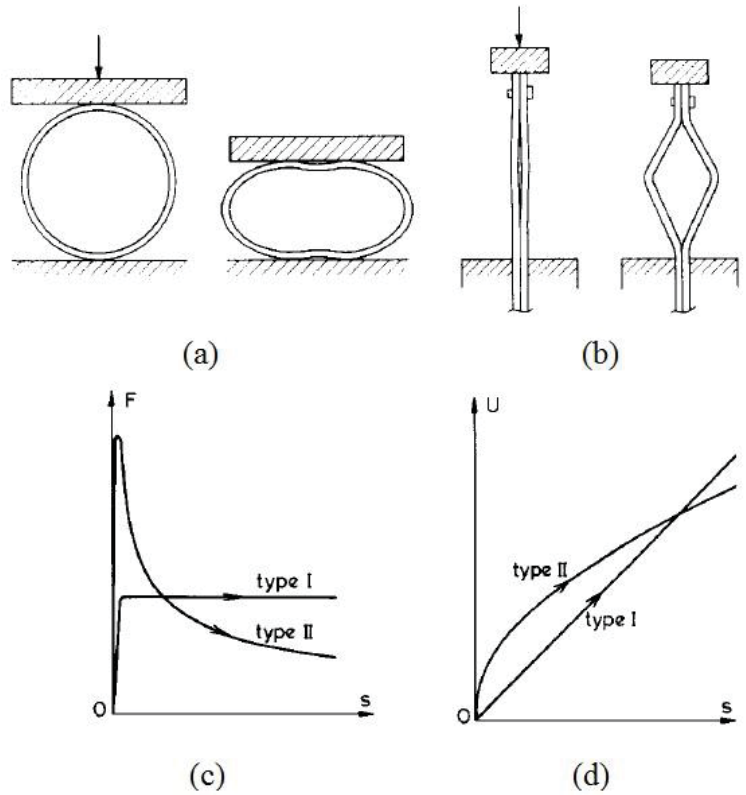

Figure 2.22. Side-views of (a) Type I and (b) Type II experimental samples before and during the loading. (c) Force and (d) Energy responses with respect to amount of deformation (Calladine & English, 1984).

In Figure 2.22, it is obvious that the load-deformation curve of Type I structure shows a relatively slight rise and following flat-topped behavior while the Type II structure exhibits a sudden drop after a sharp increase under same loading conditions. After displaying behaviors of the structures under quasi-static tests, dynamic impact tests were performed. Kinetic energy of impacting plate remained the same in each test by changing the mass and velocity in appropriate proportions. In Figure 2.23, specimen deflections are plotted against different impact velocities. At the same amount of provided kinetic energy with equal impact velocity, type I structure was deformed more than type II structure. These different deformation amounts of the structures are sourced by geometry difference. It can be said that only inertia factor plays a role herein due to the same velocity application. If the structure types are considered separately in order to ignore the effect of geometry, it is still seen difference between deformation amounts.

At that point strain rate sensitivity acts a role because only changing factor is impact velocity. Further, it can be concluded that type II structure is more rate-sensitive than type I structure. Also, inertia factor is more effective in the collapse of type II structure (Calladine & English, 1984).

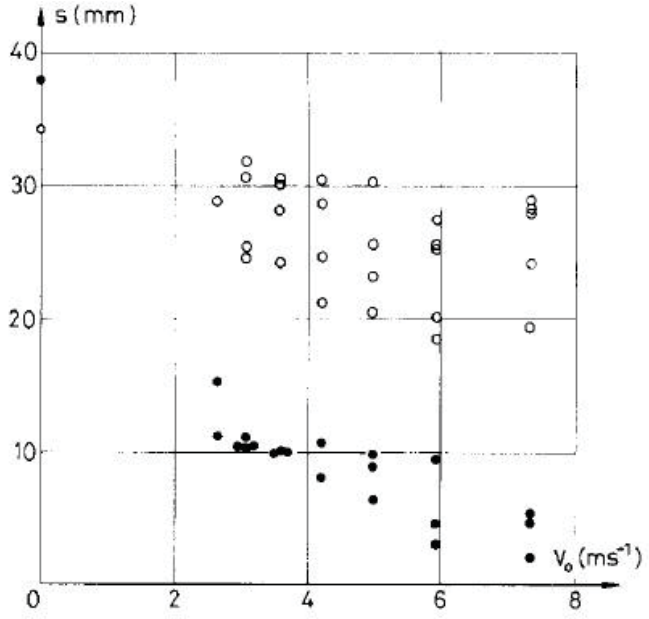

Figure 2.23. Plot of deflection against impact velocity; white points represent Type I structure, black points represent Type II structure (Calladine & English, 1984).

CHAPTER 3

MANUFACTURING AND TESTING

Manufacturing method of a thin-walled structure is critical at least as much as material type and geometry. The present chapter firstly aims to explain manufacturing processes of the bio-inspired core materials and sandwich samples which will be tested during the study. Also, the properties of used materials are introduced. Experimental setups and techniques are also presented in the following sections.

3.1 Manufacturing of Sandwich Structures and Components

3.1.1 Materials

In this section, materials used in manufacturing of sandwich samples are provided superficially. The properties of each material will be detailed within the next sections together with the manufacturing methods of the components.

AISI 304L stainless steel was selected as the core material. It was also used as the face sheets in a group of sandwich samples. In addition to the metal face sheets, E-glass/polyester composite plates were produced and employed in the face layers of the sandwich structures. In several tests, inner cores of balanus-shaped geometries were filled with polyurethane foam. Finally, epoxy adhesive was used in the assembly process of the bio-inspired cores and the face sheets.

3.1.2 Manufacturing of Biomimetic Cores

Core materials were produced with deep drawing process. Deep drawing is a sheet metal forming process which is preferred especially if a final product with combined geometry is aimed. It facilitates a complex geometry without an additional need of welding or adhesion. Firstly, AISI 304L stainless steel sheets were cut into the blanks with the initial thickness of 0.5 mm and the diameter of 60 mm. Then, biomimetic cores took their last shapes in three stages. However, before elaborating the

deep drawing method, mechanical properties of AISI 304L stainless steel have to be introduced and appropriateness of the method and material must be demonstrated.

AISI 304L stainless steel is known for the properties of outstanding formability and high corrosion resistance like other austenitic stainless steels. It can be readily formed without annealing. Also this material does not require an intermediate annealing in case of need of more than one step before having final shape. This property provides benefits in terms of both time and money savings during the production process. Another plus is that welding process can be applied easily in the manufacturing of a construction of AISI 304L stainless steel. Chemical composition of AISI 304L which was used in current study is given in Table 3.1.

Table 3.1. Chemical composition of AISI 304L stainless steel

C (%wt)	Cr (%wt)	Ni (%wt)	Mn (%wt)
0.03	18.0-20.0	9.0-12.0	2.0

As mentioned above, the manufacturing process of the core geometries was completed in three stages. First two stages were drawing, the third one was trimming. The metal-sheet blank was drawn longer than the desired length two times and then wrinkled flange part was cut off. The reason of applying two separate drawings in the process is to avoid any tears on the surface. Shortly, the round metal-sheet blank was placed over the die. Die has a cavity which has the same geometry with the desired final geometry. A punch traveled through the die cavity while the metal-sheet was held by a blank holder. In this process, blank holder is used to apply a certain force on the blank hence reducing or eliminating the wrinkling. At the final stage, the core geometries were trimmed and wrinkled bottom sides were scrapped. Since the outer shell of balanus geometry is a truncated cone, the same trimming process was applied to upper side of this component. Deep drawing process steps of inner core and outer shell are given in Figure 3.1 and in Figure 3.2, respectively. As a natural consequence of deep drawing process, the final wall thickness of the geometry varied through the longitudinal length, but the greatest thickness value was still smaller than the thickness of the initial blank. It is the sign of excessive plastic deformation and increase in strength due to strain hardening.

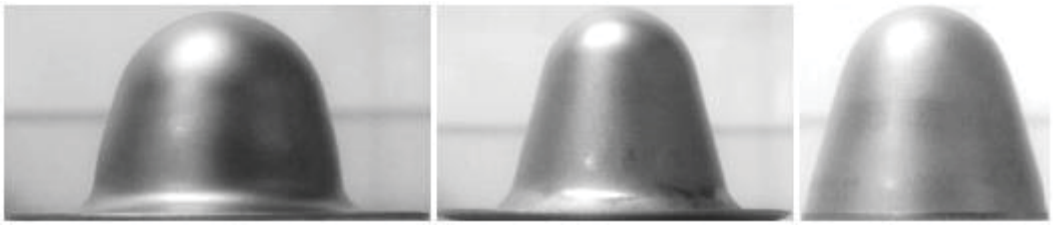

(a) (b) (c)

Figure 3.1. Shapes of inner core at the end of (a) first drawing, (b) second drawing, (c) trimming.

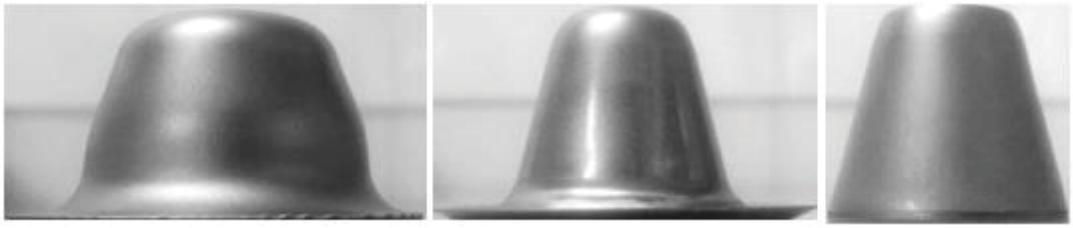

(a) (b) (c)

Figure 3.2. Shapes of outer shell at the end of (a) first drawing, (b) second drawing, (c) trimming.

Final dimensions of the inner core and outer shell are given in Figure 3.3.

The selected manufacturing process is also convenient for the mass production. It enables to manufacture massive amount of core geometries in a short time. Additionally, the potential of the possible commercial application of the proposed core geometries is tremendous due to no requirement of high-tech devices in the manufacturing process.

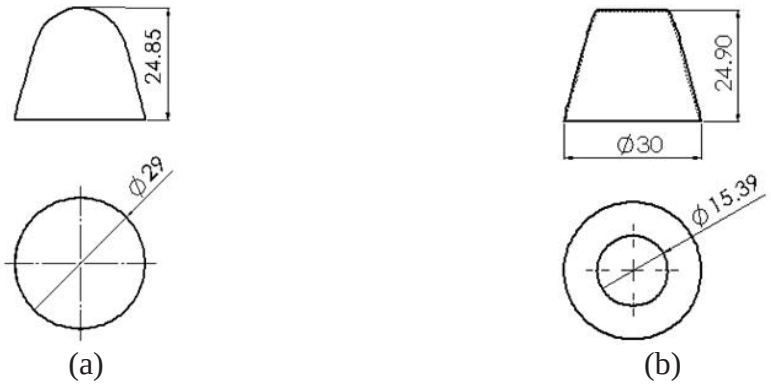

(a) (b)

Figure 3.3. Dimensions of (a) inner core, (b) outer shell.

3.1.3 **Manufacturing of Face Sheets**

Two different materials were employed in the face layers of the sandwich structures; E-glass/Polyester composite material with the ply orientation of $0^o/90^o$ and AISI 304L stainless steel.

E-glass(0.6 kg/m^2)/Polyester(Crystic PAX 703) composite plates were produced with the method of vacuum assisted resin transfer molding (VARTM). VARTM is not an expensive method and can be easily performed in a laboratory environment: Figure 3.4.

In this study, a thick glass in suitable dimensions was used as the working surface. Firstly, thin layer of wax were applied on the glass surface to sever the cured composite plate simply from the glass at the end of the process. Secondly, sufficient amount of fiber to gain minimum desired thickness was laid out. After the placement of tear-off and draining tissues on the fibers respectively, vacuum and resin ramps were fixed. Then, vacuum bag was laid out and air sealing was insured. Finally, infusion process was started by the helping of a vacuum pump.

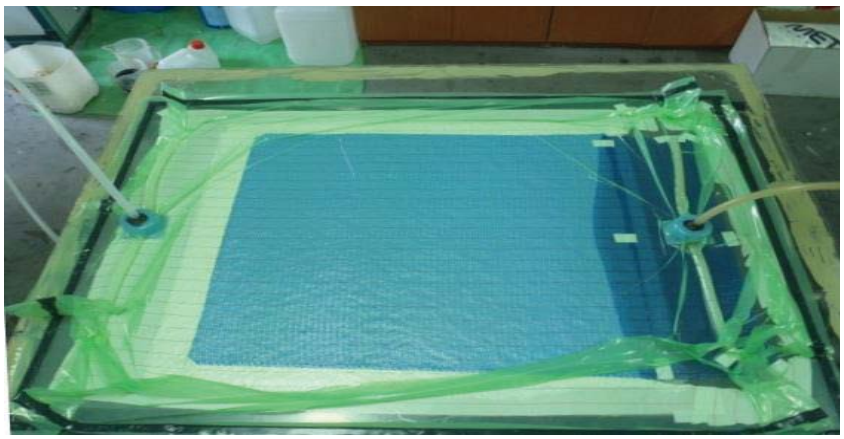

Figure 3.4. Vacuum assisted resin transfer molding setup.

After curing process, to have a better surface and the identical thickness in each plate, surface grinding was applied. Then, the smooth plates having 6 mm thickness was cut into round samples with the diameter of 75 mm using core drilling machine.

AISI 304L stainless steel face sheets were manufactured using sheet metal punch press machine. 3 mm thick metal sheets were pressed and round metal specimens

with the diameter of 75 mm were produced. Both core drilling and punch press machines are given in Figure 3.5 together with final shapes of face sheets.

(a) (b)

(c)

Figure 3.5. (a) Core drill machine, (b) Metal sheet punch press machine, (c) Face sheets

3.1.4 **Manufacturing of Sandwich Specimens**

Above-mentioned bio-inspired cores were sandwiched between identical round face sheets. Each sandwich specimen involves four core materials (one consists of an inner core and an outer shell). Also a group of sandwich specimens were prepared either involving only four inner cores or only four outer shells to investigate the interaction effect during the deformation.

In order to standardize the positions of the core materials and to provide a high repeatability of the tests, a pattern was designed and used in the manufacturing of the

sandwich specimens. Technical drawing of the main part and the final view of the product with additional components are illustrated in Figure 3.6.

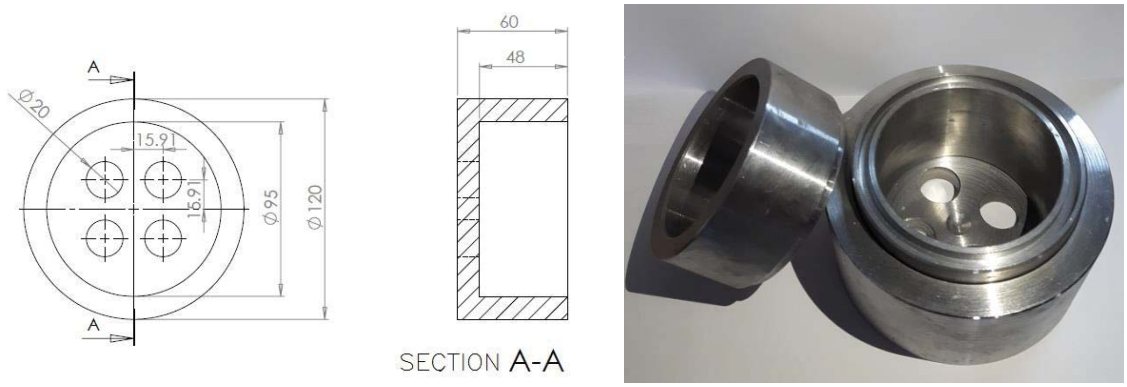

(a) (b)

Figure 3.6. (a) Technical drawing and (b) the final view of pattern.

Firstly, the surfaces of the core materials were cleansed starting from their bottom and top sides. Then, two-component epoxy adhesive was stirred for two minutes on a clean flat platform. After obtaining a homogenous mix, it was applied on the bottom sides of the core materials which were previously placed in the cavities of the pattern. Almost immediately, the first face sheet was attached and a weight was planted until enough time passed for through-dry. Similar steps were applied for the integration of the second face sheet, as well. Manufactured sandwich specimens consisting of only inner cores, only outer shells and bio-inspired geometries (combination of inner cores and outer shells) can be seen in Figure 3.7, with two types of face sheet applications, respectively.

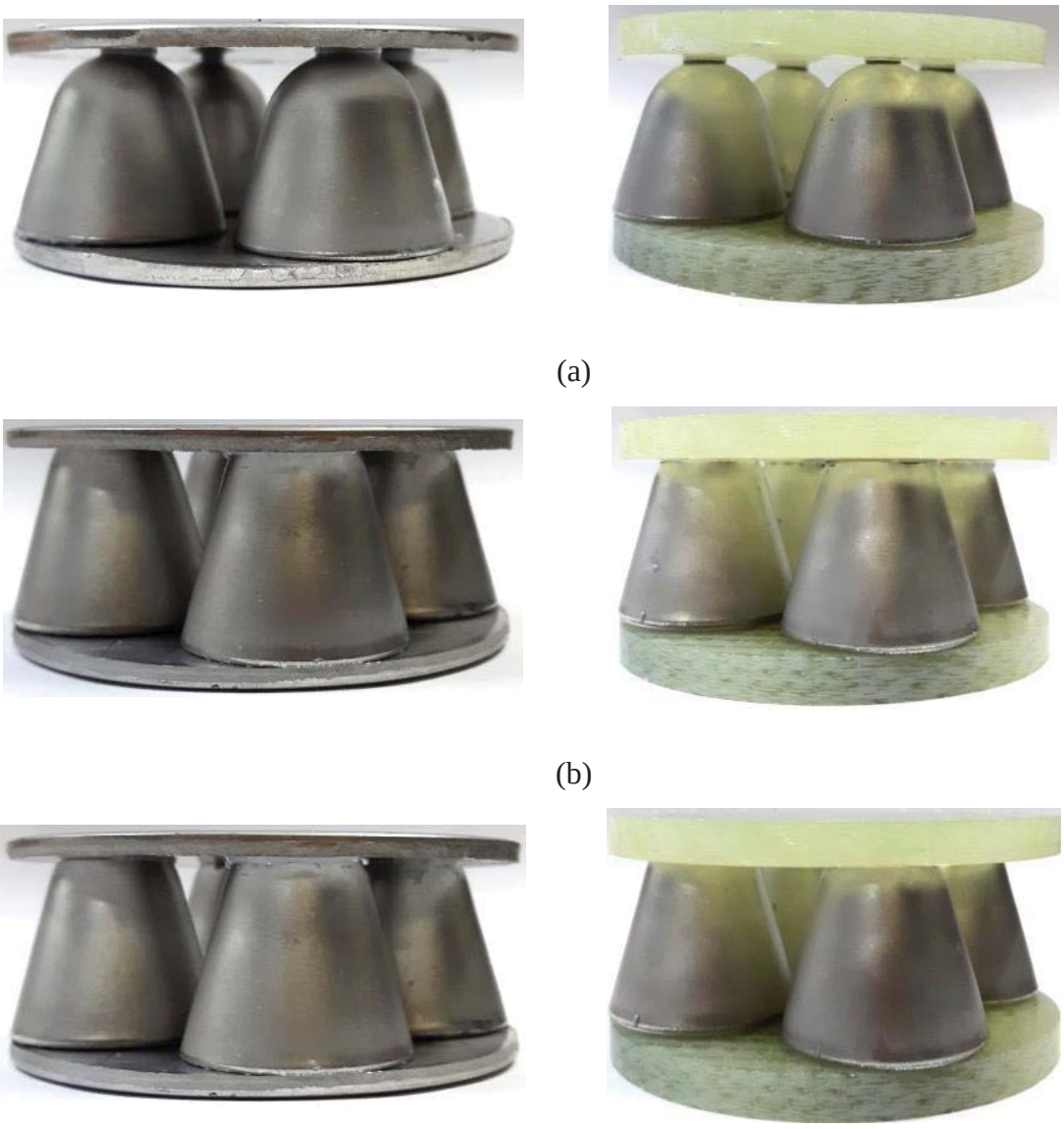

Figure 3.7. Sandwich specimens consisting of (a) only inner cores, (b) only outer shells, (c) bio-inspired geometries both with AISI 304L stainless steel and E-glass/Polyester composite facesheets.

In order to investigate the foam filling effect in the crushing, two-component pourable rigid polyurethane foam was used. The components were mixed in a container 2A:1B by weight and stirred. Before it started expanding, the mixture was poured into the core materials. In case of over-expanding, the residual part was cut off. Finally, the same adhesion process steps were followed also for the sandwich structures with foam-filled bio-inspired cores. The components of the polyurethane foam and the foam filled core geometries are presented in Figure 3.8.

Figure 3.8. Two-component rigid polyurethane foam and foam-filled core geometries.

3.2 Testing Techniques

Three different experiment setups were used in the study. In order to investigate the energy absorption characteristics and the deformation modes of the produced sandwich specimens under quasi-static and dynamic loadings, Shimadzu AG-X universal testing machine and Fractovis drop-weight tower were used, respectively. Also, to examine penetration and perforation behaviors of the proposed core geometries sandwiched by E-glass/Polyester plates, gas gun test setup was used. The working principles and the test details will be specified in the following sections.

3.2.1 **Quasi-static Compression Tests**

Shimadzu AG-X universal testing machine which is seen in Figure 3.9(a) has the maximum capacity of 300 kN. In the quasi-static compression tests, specimens were placed on the fully constrained highly rigid lower plate. Then, they were compressed under upper rigid plate moving with different constant velocities. Applied crushing velocities were selected considering strain rates. In order to calculate crushing velocity, the formula which is given in equation 3.1 was used.

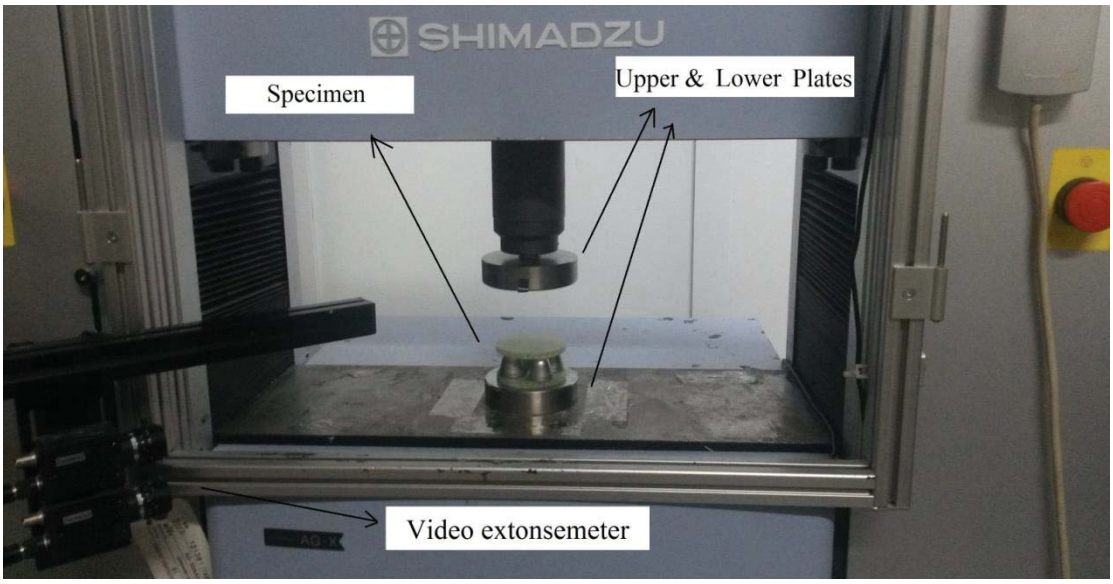

(a)

(b)

Figure 3.9. (a) Shimadzu AG-X universal testing machine, (b) Apparatus used in confined compression tests

$$\dot{\varepsilon} = \frac{V}{l} \tag{3.1}$$

where $\dot{\varepsilon}$ is the strain rate, V is the velocity of upper plate and l is the height of the core material. The tests with the strain rates of 10^{-3} s^{-1}, 10^{-2} s^{-1} and 10^{-1} s^{-1} were conducted and the effect of deformation velocity on the crushing behavior of sandwich structures was investigated. In addition, a video extensometer working integrated with compression test machine was used to eliminate the errors in stroke values caused by the elastic deformations of the test machine. Especially in case of applying high amount of force, error in stroke values, accordingly in strain values, shows dramatic increase.

Also, each test was recorded by the help of a camera to examine the deformation histories of core geometries. Moreover, highly stiff confinement ring and additional crushing apparatus which perfectly fits in confinement ring are given in Figure 3.9(b).

3.2.2 **Drop Weight Impact Tests**

Fractovis Plus drop weight test device was used to investigate the energy absorption capabilities and the dynamic crushing behavior of the sandwich structures under axial impact. Test setup is given in Figure 3.10.

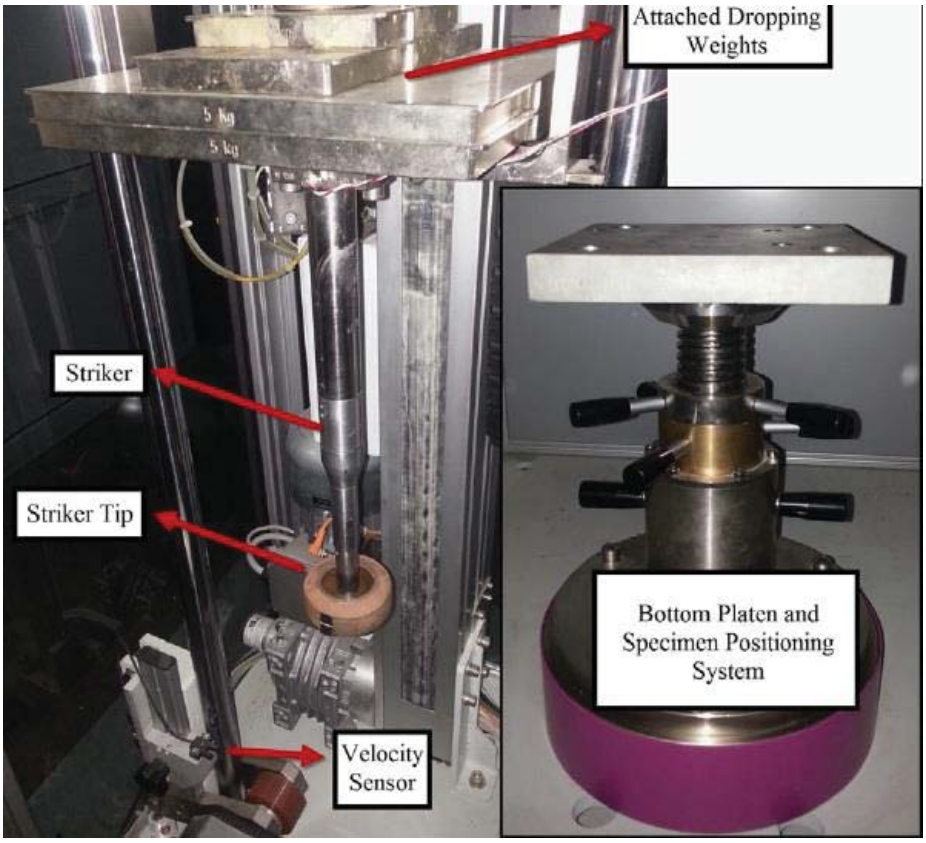

Figure 3.10. Fractovis Plus drop weight test device (Tasdemirci et al., 2015).

The test setup mainly consists of a striker which is able to measure 222 kN maximum force, a rigid bottom plate which is used for placing the specimen down, the extra dropping weights which provide needed kinetic energy, a velocity sensor which detects the certain impact velocity and the compression springs which provide higher impact velocity in which free fall of the weights are insufficient to apply required velocity.

In the impact tests of the current study, a flat striker tip with the diameter of 70 mm was used. Time, displacement, force and energy values during the deformation were gained using DAS 16000 advanced data acquisition system. Also a high speed camera was employed for both being able to follow the folds of thin-walled bio-inspired cores at a certain amount of deformation and verifying the displacement value particularly in the tests with relatively higher impact velocities. In the drop weight impact tests, kinetic energy is adjusted varying impact velocity and impact mass while the compression amount and strain rate are provided as input data in the quasi-static tests.

3.2.3 **Gas Gun Tests**

Penetration and perforation behaviors of the sandwich structures with bio-inspired cores were also studied by carrying out gas gun tests. Experimental setup is given in Figure 3.11 with its main lines. It consists of a gas gun with long gun barrel, a specimen holder and two chronographs. Chronographs are placed both front and back sides of the specimen. The chronograph placed the behind of the specimen measures the terminal velocity of the projectile in case of piercing. Also in these tests, high speed camera was used same as previous tests to record deformation history. Other constituents of the test setup are illustrated in Figure 3.12.

Figure 3.11. Gas gun, gun barrel and target chamber

(a)

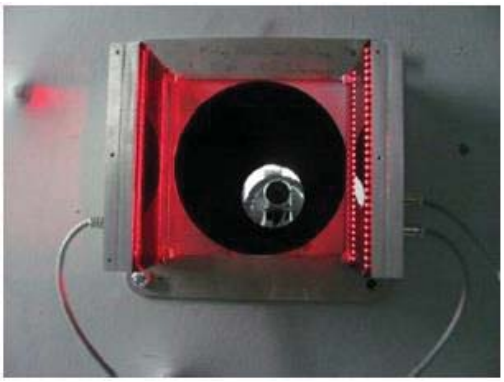

(b)

(c)

Figure 3.12. (a) Specimen holder, (b) inlet chronograph, (c) terminal chronograph.

Firstly, the projectile was placed in a pre-prepared sabot made of polyurethane foam. Polyurethane foam sabot assists the projectile while it travels inside the barrel until it crashes the sabot stripper. After that point, projectile moves alone towards the specimen. Sabot is not used only for centering the target also material choice of the sabot is effective on easy acceleration. Secondly, the gas tank was filled with air using a compressor. After ensuring the data acquisition of the chronographs and the high speed camera are on, the system was triggered.

Two different types of penetrators with different masses were tried in the tests. The first one of the penetrators which can be seen in Figure 3.13(a) has spherical geometry with the diameter of 30 mm and mass of 110 g. The second one is a cube. It has 11.9 mm edge length and 13 g mass.

In the gas gun tests, E-glass/Polyester plates were cut into the square-shaped face materials and the sandwich structures were produced with bigger dimensions differently from previous experiments to provide a larger crush surface. Composite face sheets have 25 cm side length and 5.5 mm thickness. 49 bio-inspired cores were arrayed between the plates and each is in touch with its adjacent cores, Figure 3.13 (b)&(c).

(a)

Figure 3.13. (a) Spherical and cubical projectiles, (b) Configuration of bio-inspired cores, (c) Side view of sandwich specimen.

(cont. on next page)

(b)

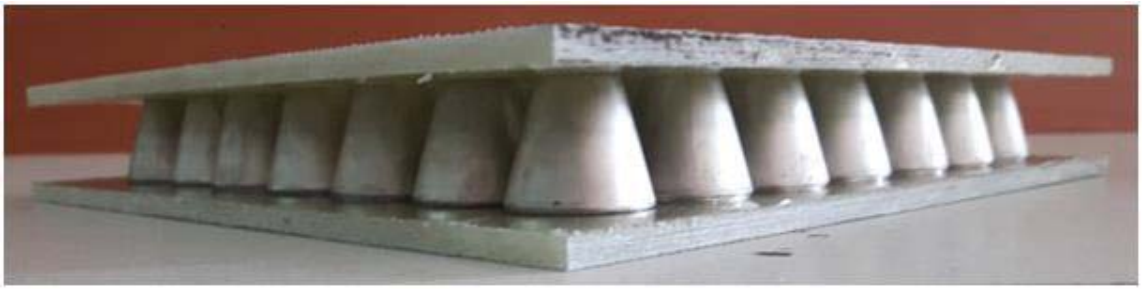

(c)

Figure 3.13 (cont.)

CHAPTER 4

NUMERICAL STUDIES

In the present study, dynamic crushing behavior of sandwich specimens was analyzed conducting numerical studies in addition to previously mentioned testing methods. Numerical analysis facilitates a comprehensive investigation in the solving of engineering problems. Any identified output can be detected in any time interval of the simulated test using numerical analysis techniques. Moreover, a numerical analysis method is mainly used for predicting the responses of the investigated material under the conditions which cannot be fulfilled in a laboratory environment. However, to take the advantage of the numerical methods, all parameters and material constants must be determined well and the numerical results must be verified. A good agreement between experimental and numerical results must be noted under the conditions that can be actualized with laboratory facilities.

LS-DYNA 971 numerical solver was employed in the simulations of the current study. Quasi-static, drop weight and gas gun tests were modeled in accordance with the test conditions. Further, deep drawing process was also simulated to regard the effects of residual stress/strain which occurred throughout the manufacturing due to work hardening.

First of all, material model constants were determined by carrying out several tension tests both quasi-statically and dynamically at various deformation rates. Then, explicit finite element code was prepared using LS-PrePost. Convenient material models, contact definitions and boundary conditions were identified and the code was made ready to run. Material models used in the numerical analyses of deep drawing and experiments are tabulated together with the related manufacturing and experimental set-up constituents in Table 4.1.

Table 4.1. Material models used in numerical simulations

Material Model in LS-DYNA	Corresponding Constituents in Set-up
001-ELASTIC	Striker Tip in Drop-weight Tests, Projectile in Gas Gun Tests
015-JOHNSON_COOK	AISI 304L Stainless Steel Core Material in Drop-weight Tests
020-RIGID	Die, Punch and Blank Holder in Deep Drawing, Upper and Lower Plates in Quasi-static Tests, Bottom Plate in Drop-weight Tests
063-CRUSHABLE_FOAM	Polyurethane Foam Filler
098-SIMPLIFIED_JOHNSON_COOK	Blank Metal Sheet in Deep Drawing, AISI 304L Stainless Steel Core Material and Face Sheets in Quasi-static Tests, Face Sheets in Drop-weight Tests
162-COMPOSITE_MSC_DMG	Face Sheets in Gas Gun Tests

Material properties and material model parameters are given in the following tables. Details of the determination of the properties and material constants of AISI 304L stainless steel and polyurethane foam were specified in a related study performed by Akbulut (Akbulut, 2017). For E-glass/Polyester mechanical properties, another study which was carried out by Tunusoğlu must be shown as reference. (Tunusoğlu, 2011)

Table 4.2. Johnson-Cook material model parameters of AISI 304L stainless steel (Akbulut, 2017)

ρ (kg/m^3)	G (GPa)	E (GPa)	υ	A (GPa)	B (GPa)	n	C
7830	80	193	0.305	0.218	1.905	0.88	0.11429

$D1$	$D4$	T_R (^{o}K)	T_m (^{o}K)	m
0.85677	-0.01105	296	1698	1.0

Table 4.3. Material properties of polyurethane foam (Akbulut, 2017)

ρ (kg/m^3)	E (GPa)	υ
1335	0.024444	0.01

Table 4.4. Material properties of composite face sheets (Tunusoğlu, 2011)

ρ (kg/m^3)	EA (GPa)	EB (GPa)	EC (GPa)	$PRBA$	$PRCA$	$PRCB$	GAB (GPa)
1850	23.11	23.11	7.38	0.08	0.14	0.15	2.15

GBC (GPa)	GCA (GPa)	SAT (GPa)	SAC (GPa)	SBT (GPa)	SBC (GPa)	SCT (GPa)	SFC (GPa)
1.83	1.83	0.437	0.361	0.437	0.361	0.0547	0.547

SFS (GPa)	SAB (GPa)	SBC (GPa)	SCA (GPa)
0.217	0.0328	0.0328	0.0328

In the all tables, ρ, G, E and υ refer the values of density, shear modulus, Young's modulus and poisson ratio, respectively. A, B, n, C, D1 and D4 are Johnson-Cook (J-C) material model constants. T_R and T_M represent room temperature and melting temperature, respectively.

In Table 4.4 since E-glass/Polyester is an anisotropic material, more parameters are detailed and tabulated as the mechanical properties of composite face sheets. *EA*, *EB* and *EC* are the moduli of elasticity in longitudinal, in transverse and through thickness

directions, respectively. *PRBA, PRCA, PRCB* are the poisson ratios in the planes of ab, ac and bc. Shear moduli in ab, ac and bc planes are represented by *GAB, GBC* and *GCA*, respectively. Longitudinal tensile and compressive strengths are denoted by *SAT* and *SAC* whereas transverse tensile and compressive strengths are symbolized with *SBT* and *SBC*. *SCT* refers through thickness tensile strength. *SFC* is the crush strength. Lastly, *SFS* is the fiber mode shear strength and *SAB, SBC, SCA* are the matrix mode shear strengths.

4.1 Modeling of Deep Drawing

Numerical model of deep drawing consists of four parts; die, punch, blank holder and blank. Firstly, die, punch and blank holder were sketched in Solidworks which is a computer aided design software. Secondly, mesh for each part was generated individually in HyperMesh and they were exported to LS-DYNA 971 to be run. The blank was sketched and meshed using Ansys Workbench differently from the other parts. All parts were identified as shell elements using Belytshchko-Tsay element formulation. The initial blank material with the thickness of 0.5 mm was placed between blank holder and die. After the definition of the constraints in needed axial and radial directions, the drawing process was started with constant velocity while the blank holder was applying a certain amount of force to prevent wrinkling. FORMING_SURFACE_TO_SURFACE contact type was selected in the deep drawing simulations. The static and dynamic friction coefficients were assumed as 0.2 and 0.17 between punch and blank, respectively. The same values were chosen as 0.1 and 0.05 for the contacts of die-blank and blank holder-blank. Numerical modeling of deep drawing was performed realistically in three different stages to catch the best results in subsequent test simulations. Output data of the first step was taken as the input data of the second step. After trimming, obtained geometries were used in the crushing simulations. Each deep drawing step of inner core in LS-DYNA is illustrated in Figure 4.1, Figure 4.2 and Figure 4.3. In the final states of the steps, die and punch were viewed in transparent mode to provide a more understandable image. The same procedure was followed also for the manufacture of outer shell.

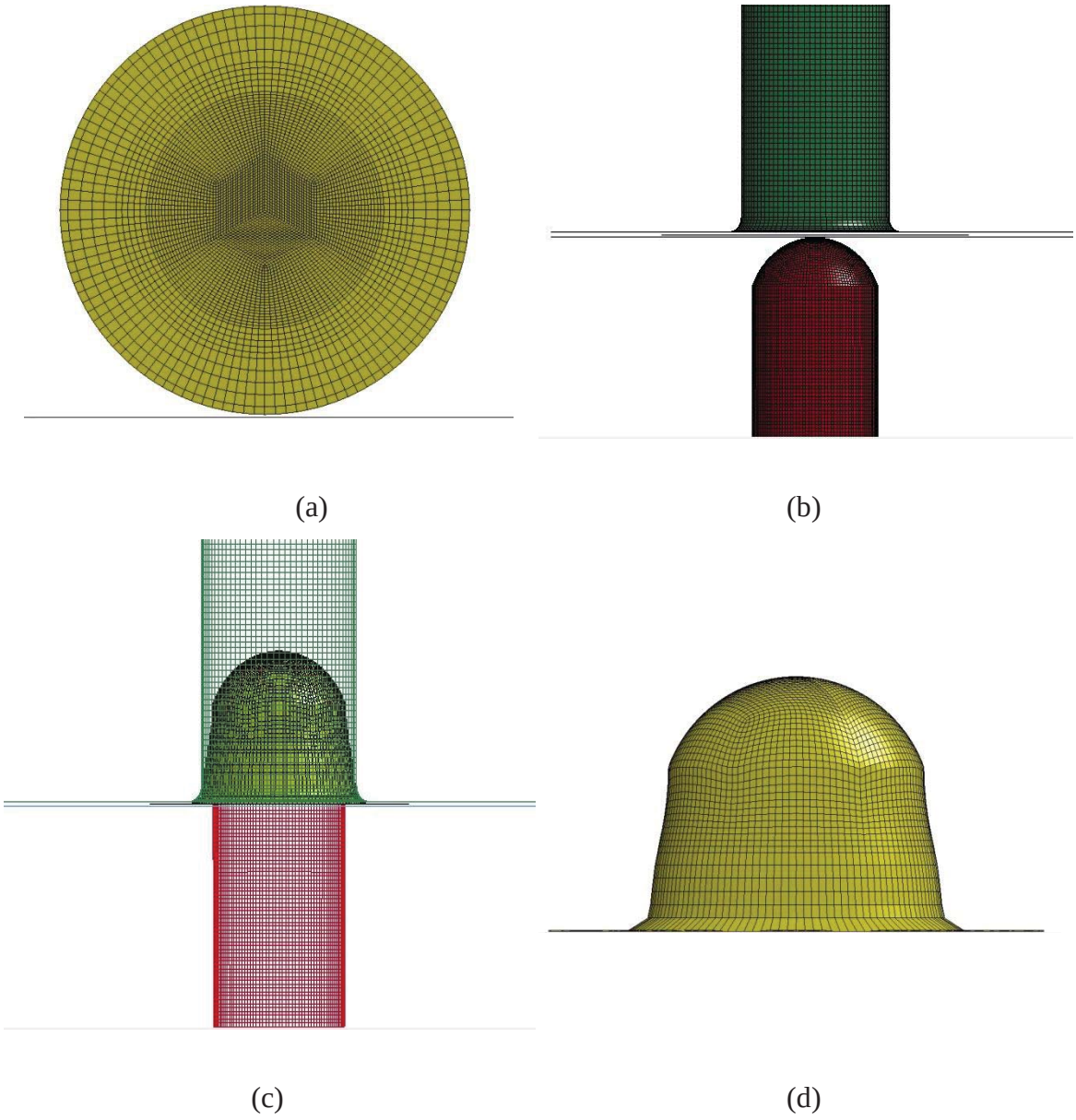

Figure 4.1. Illustration of the first deep drawing step of inner core (a) top view of blank as input material, (b) the first state of the first step, (c) the final state of the first step, (d) output material.

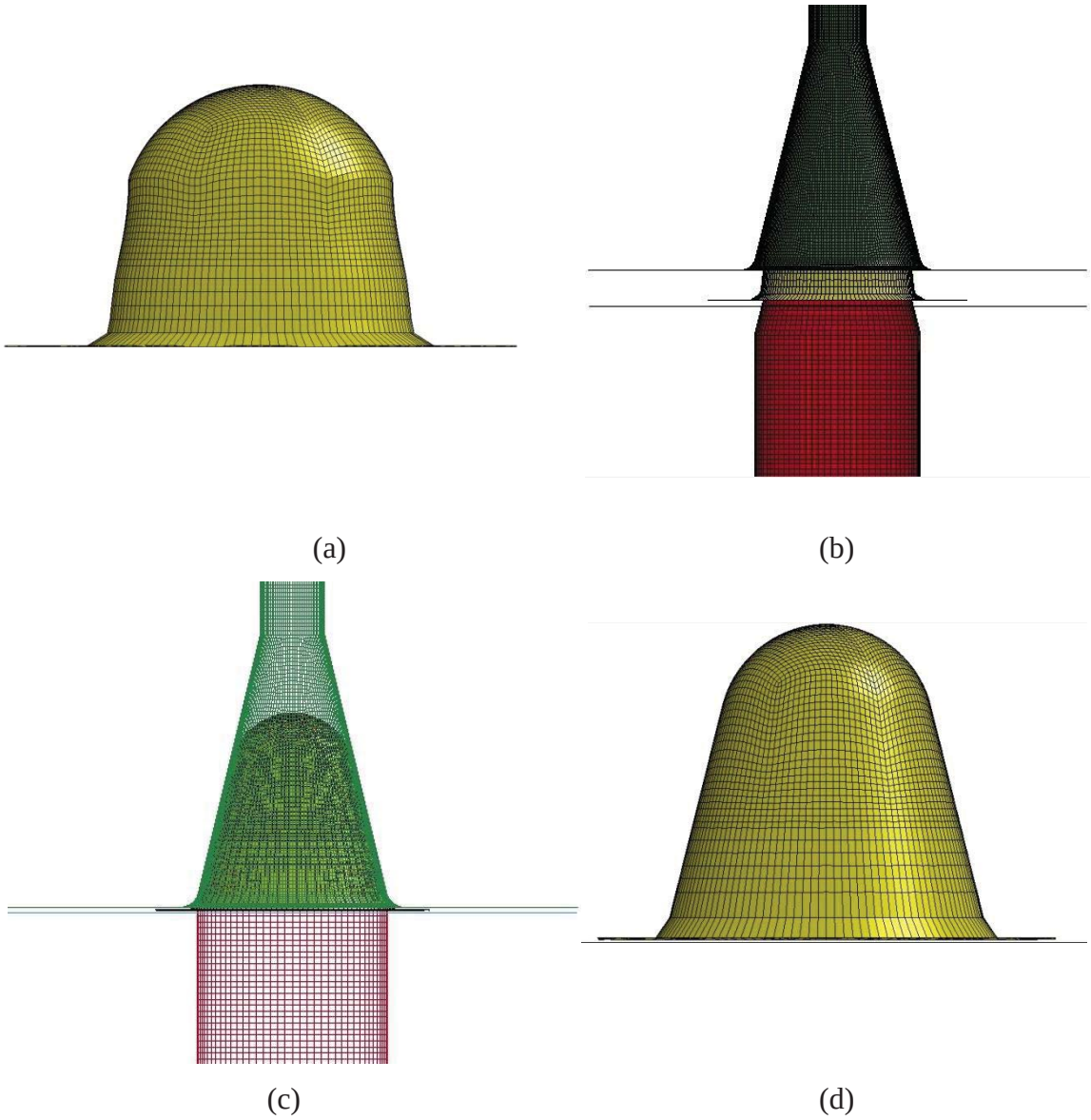

Figure 4.2. Illustration of the second deep drawing step of inner core (a) input material, (b) the first state of the second step, (c) the final state of the second step, (d) output material.

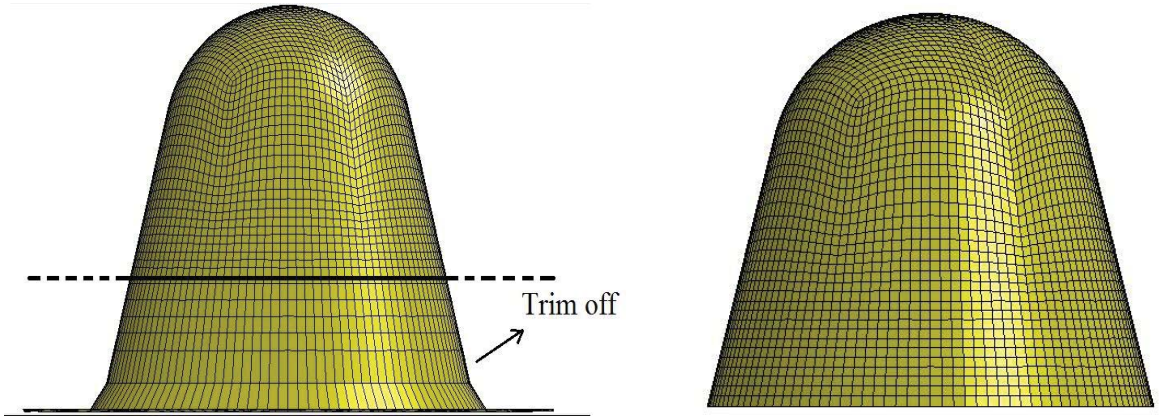

(a) (b)

Figure 4.3. Trimming process (a) Output material in the second drawing, (b) The final shape of inner core.

Modeling of deep drawing was completed with trimming process. Thicknesses in the final states of both numerically prepared inner core and outer shell varied between 0.21 mm and 0.53 mm. Then, these thickness variations were compared with the specimens. After demonstrating a well agreement, the core materials exported to crushing simulations. Thickness variations in both numerically prepared and manufactured specimens are plotted against the distance from the top points of the final geometries in Figure 4.4.

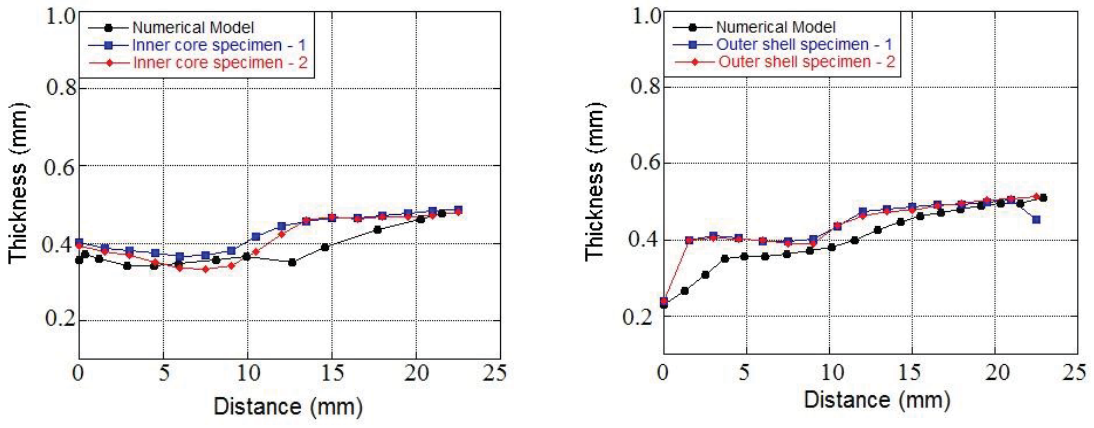

(a) (b)

Figure 4.4. Thickness variation comparison of numerical models and specimens (a) inner core, (b) outer shell.

Before proceeding with crushing simulations, the contribution of modeling manufacturing method was demonstrated. First, the proposed core geometry was sketched using computer aided drawing software. Second, it was obtained using deep-drawing numerical models. Then, both of them were crushed under the same conditions. Even though the first one has a constant shell thickness of 0.5 mm while the thickness of the second one varies densely between the values smaller than 0.5 mm, the second one reached higher load-carrying and energy-absorbing capability due to the positive effects of residual stress/strain. The force-displacement curves of both core geometries are given in the following figure.

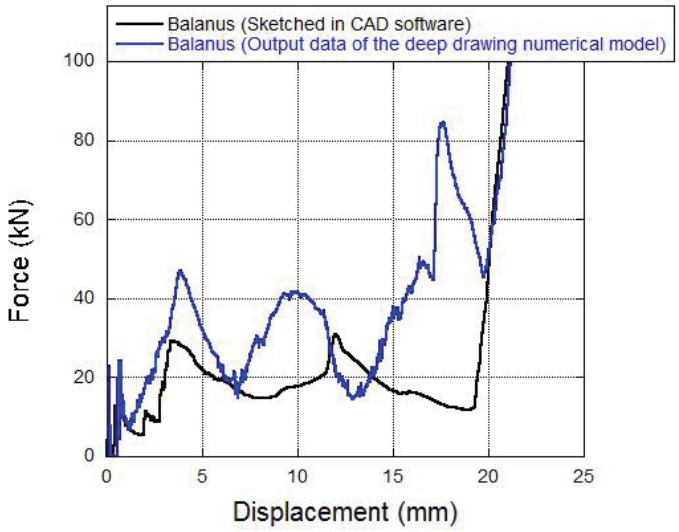

Figure 4.5. Contribution of the deep drawing to the load-carrying capacity.

4.2 Modeling of Experiments

Numerically prepared drawn thin-walled structures were imported into crushing simulations as input data. Thickness variation and residual stress/strain occurred due to plastic deformation during the manufacturing were preserved.

In the quasi-static simulations, lower and upper plates were defined as fully integrated solid elements while Belytshchko-Tsay shell element formulation was used for the core materials. Lower plate was constrained in each direction and each rotation. Upper plate was allowed to move with constant velocity only through the axial direction of sandwich specimens. Two different contact types were defined in the quasi-static

compression numerical models: AUTOMATIC_SINGLE_SURFACE for the folds in the collapse of core materials and AUTOMATIC_SURFACE_TO_SURFACE for the contacts of the plates and core materials. The static and dynamic friction coefficients were assumed as 0.18 and 0.09 in the folding contacts, respectively. In order to catch the finest match between the load-deformation curves of experiments and numerical models, the static and dynamic friction coefficients in the contacts between the plates and core materials were varied in reasonable range. 0.12 and 0.09 were opted for the contact of lower plate-core materials, 0.3 and 0.2 were chosen for that of upper plate-core materials. Prepared numerical sandwich specimen with bio-inspired cores and quasi-static model are given in Figure 4.6.

LS-DYNA is a dynamic explicit numerical solver. Since the strain rate is comparatively low in the quasi-static tests, the method of mass scaling was applied to keep the termination time in a moderate time span. Material density of the specimen was reduced 1000 times and the loading velocity was increased 100 times. In this method, the ratio of kinetic energy to total internal energy is aimed to be kept as low as possible. In all quasi-static numerical models, time step size value in the control card was chosen with caution so as to ensure the ratio of kinetic energy to total internal energy is lower than 10 %.

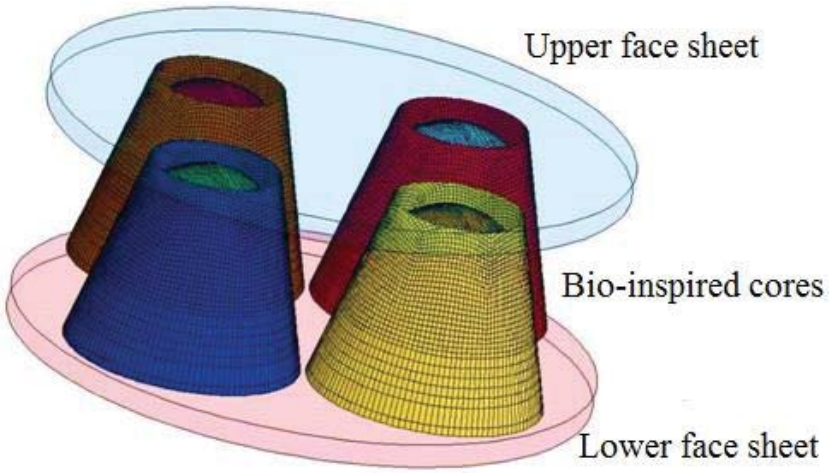

(a)

Figure 4.6. (a) Numerically prepared sandwich specimen and (b) quasi-static model.

(cont. on next page)

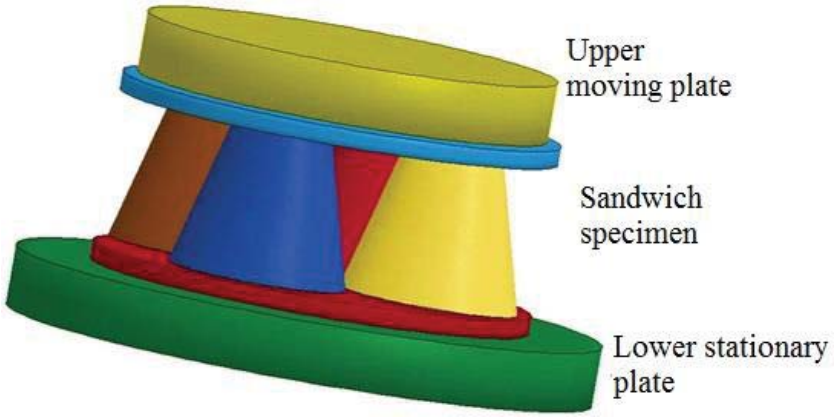

(b)

Figure 4.6 (cont.)

In the drop-weight simulations, initial velocity and additional mass were given to the upper plate unlike the quasi-static models. Also, the method of mass scaling was not needed. To consider the damage parameters, JOHNSON_COOK material card was activated instead of SIMPLIFIED_JOHNSON_COOK as previously mentioned in Table 4.1. In these simulations, as a difference from quasi-static simulations, contact definitions were changed. ERODING_SINGLE_SURFACE was used to delete the elements that were subjected to erosion due to material failure. To gain the force responses against the amount of displacement between the plates and sandwich specimen, FORCE_TRANSDUCER_PENALTY contact definition was preferred. Additionally, a positive touching was made thanks to the high speed camera in the validation of the results. In the drop-weight tests, it was revealed that the bottom plate which is supposed to be fully constrained in each direction was moving down particularly in the tests with relatively higher impact velocities. Thus, a time-displacement curve was defined for the bottom plate in the drop weight simulations. The amount of displacement was detected accurately by image processing.

Finally, a full-scale model of gas gun test setup was prepared. ERODING_SINGLE_SURFACE and ERODING_SURFACE_TO_SURFACE were chosen as the contact definitions similar with drop-weight simulations. The deformation modes of the core materials and the front composite facing were compared with the test results. The gas gun model is illustrated in Figure 4.7.

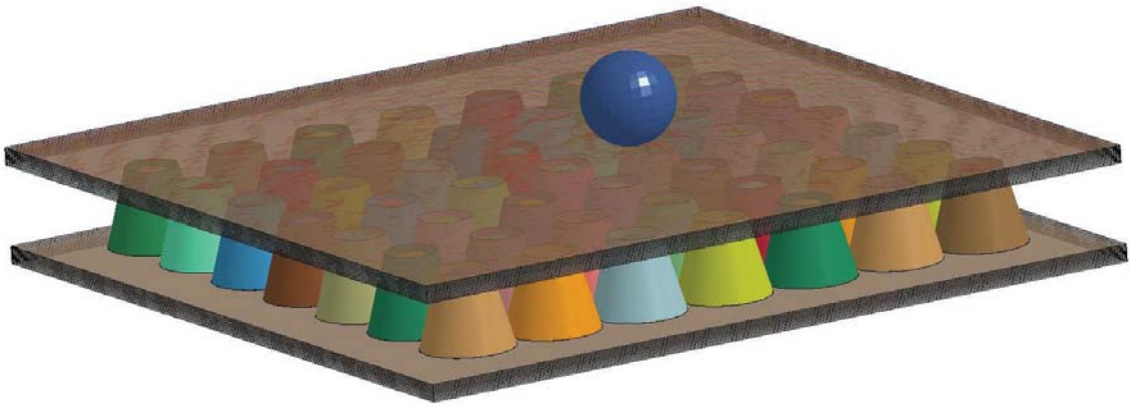

Figure 4.7. Numerical model of gas gun tests.

CHAPTER 5

RESULTS AND DISCUSSIONS

In the present chapter, all obtained results will be reported by the help of graphs, high speed camera views, simulation screenshots and the tables. Also, various deductions are going to be made related to the presented results.

Firstly, three quasi-static compression tests were conducted with the strain rate of 10^{-3} for each type of sandwich specimen (involving only inner cores (IC), only outer shells (OS), bio-inspired cores (BIC)). In the following figures, force-displacement curves are presented. It is confirmed that the tests are repeatable and there is a satisfactory consistency between the experiments.

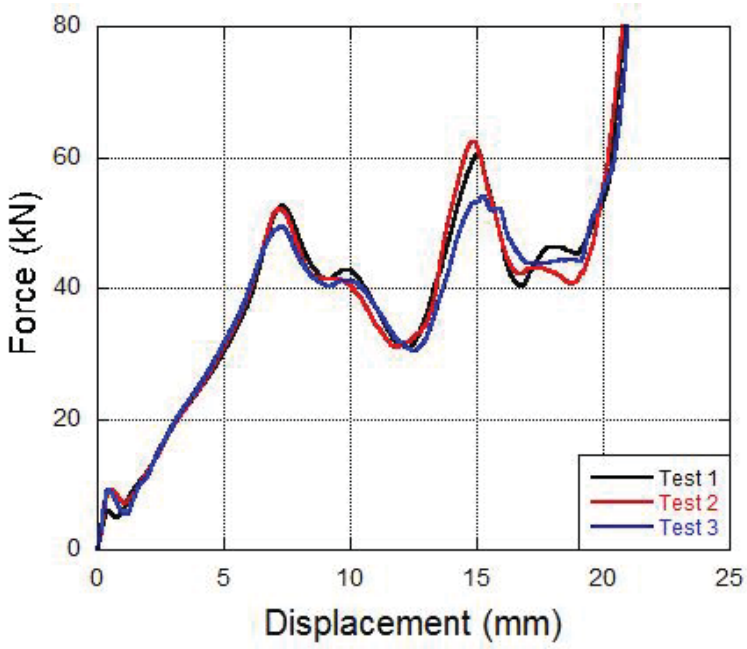

Figure 5.1. Quasi-static compression behavior of IC sandwich specimens

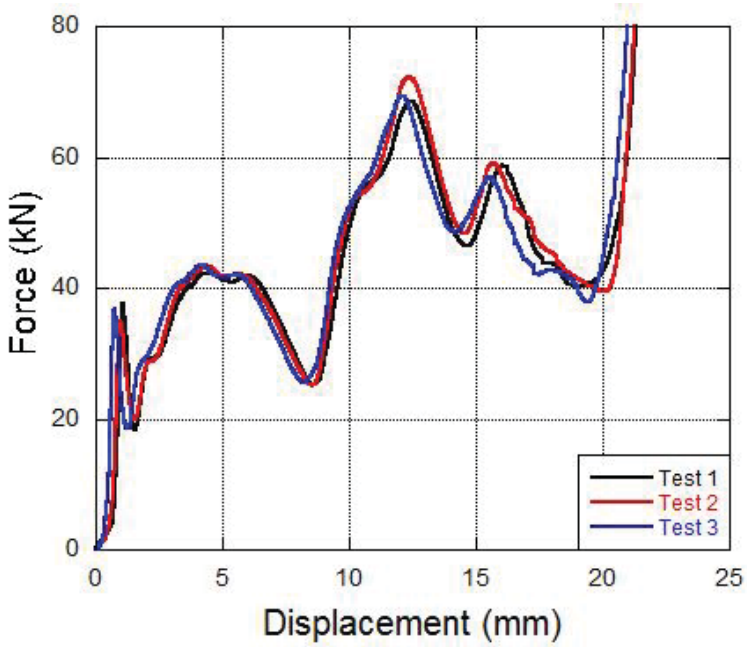

Figure 5.2. Quasi-static compression behavior of OS sandwich specimens

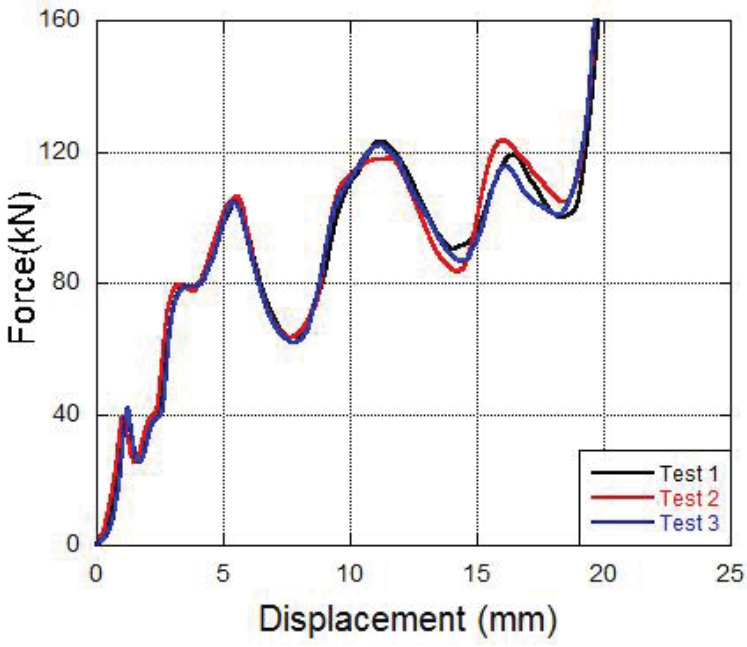

Figure 5.3. Quasi-static compression behavior of BIC sandwich specimens

Then, the force-displacement curves of IC and OS sandwich specimens were added arithmetically. The result was given on the same graph with the force-displacement curve of BIC sandwich specimen. The force-displacement curve of the

arithmetical addition reaches lower peak values than that of sandwich specimen BIC as can be seen in Figure 5.4. It is sourced due to the interaction effect between inner cores and outer shells during the fold formation.

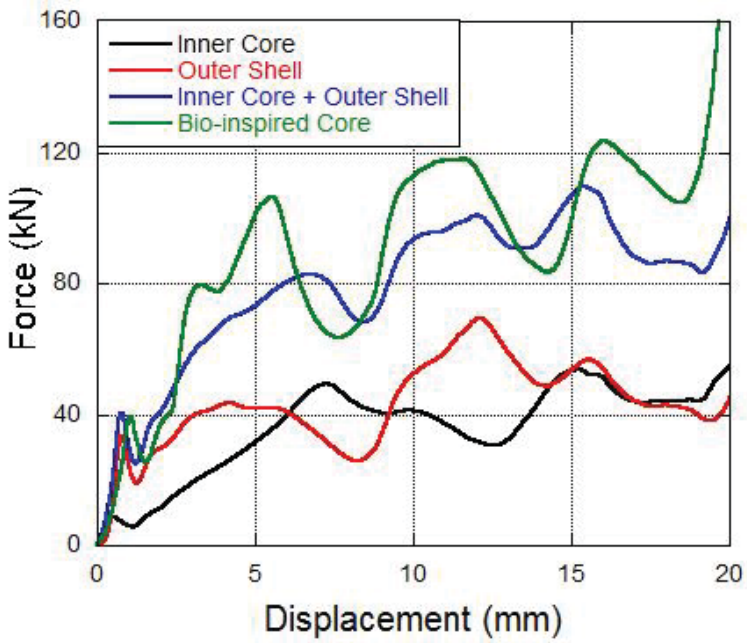

Figure 5.4. Interaction of inner core and outer shell

Further, the interaction between each bio-inspired core in a sandwich specimen was exhibited with a similar method. Inner cores, outer shells and bio-inspired cores were crushed individually at first. Later, the force responses of individual thin-walled structures were multiplied by 4 and compared with corresponding sandwich specimens. It is clearly seen on the graphs given in Figure 5.5, Figure 5.6, Figure 5.7, energy absorption characteristics are enhanced particularly after a small amount of compression when the formation of folds becomes more difficult due to the prevention of lateral displacement of the folds between the adjacent cores.

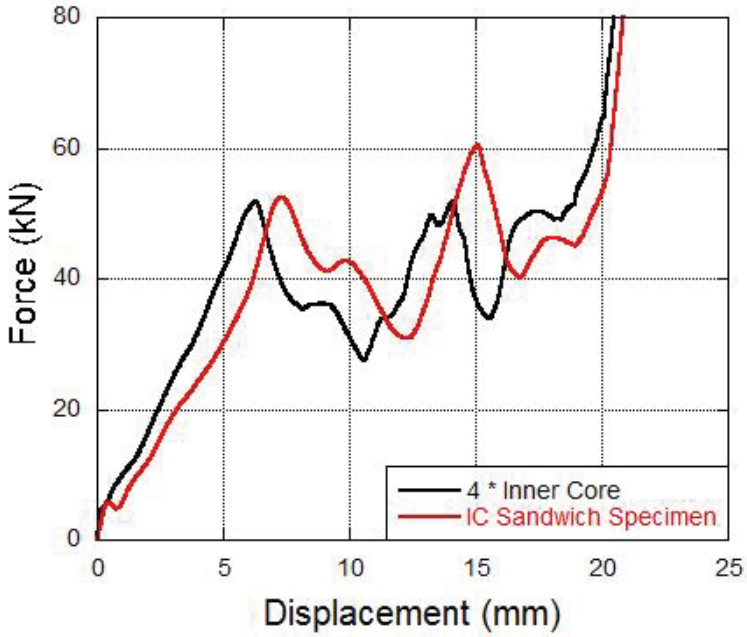

Figure 5.5. Interaction of inner cores in the sandwich specimen.

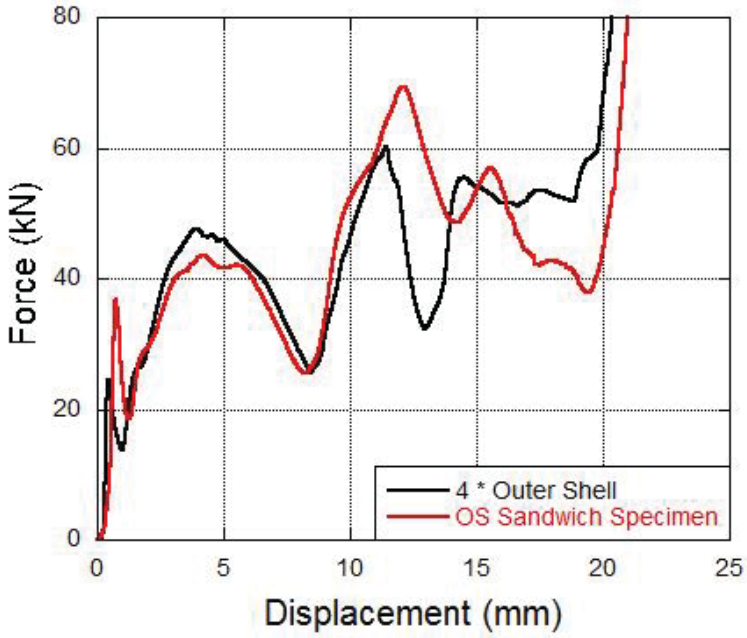

Figure 5.6. Interaction of outer shells in the sandwich specimen.

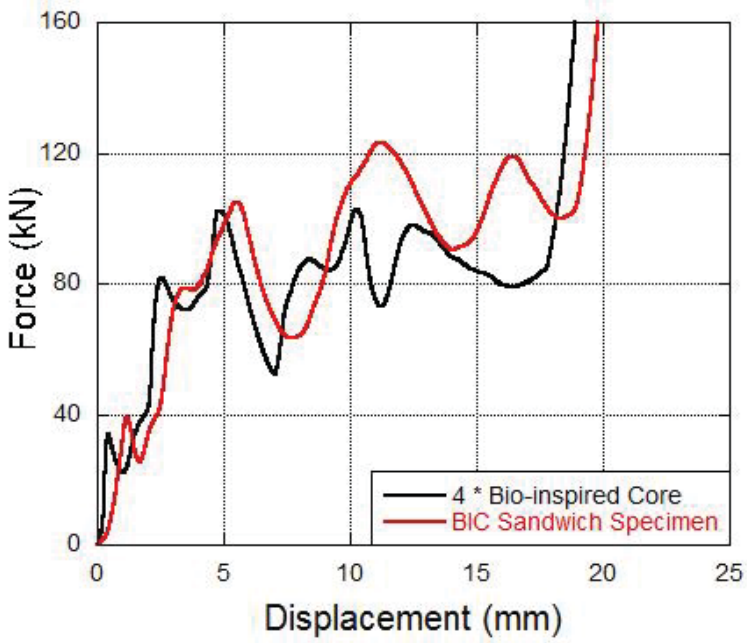

Figure 5.7. Interaction of bio-inspired cores in the sandwich specimen.

In the next figure, the comparison of the sandwich specimens with different face materials is presented. Both two specimens involve bio-inspired cores. Even though the force-displacement curves do not match perfectly, the deformation modes and the energy absorption characteristics are close enough. The third peak was not observed in the quasi-static compression curve of the sandwich specimen with composite face sheet. Each peak formation in the curve corresponds to a fold formation during the deformation. Since the investigated core geometry has thin and sharp bottom edges it easily penetrates the composite face sheet. Therefore, the last fold formation was not seen.

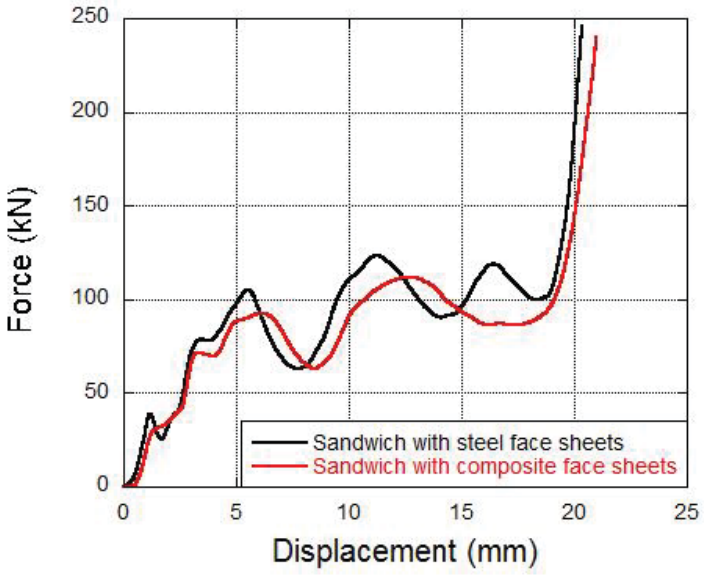

Figure 5.8. Comparison of sandwich specimens with different face sheets.

To investigate the foam filling effect, sandwich specimens were prepared with polyurethane foam filled core materials. Force-displacement curves of the sandwich structures involving foam-filled inner cores, outer shells and bio-inspired cores are given in Figure 5.9, Figure 5.10, Figure 5.11, respectively. Polyurethane foam filler, in particular at higher amount of compression level, increases the load-carrying capacity of the sandwich structures noticeably. In order to express it in numerical terms, the percentage increase of absorbed energy amounts was calculated at 20 mm of compression level where the densification starts in each type of sandwich structures. This value was detected as 15%, 24%, 10% for inner cores, outer shells and bio-inspired cores, respectively.

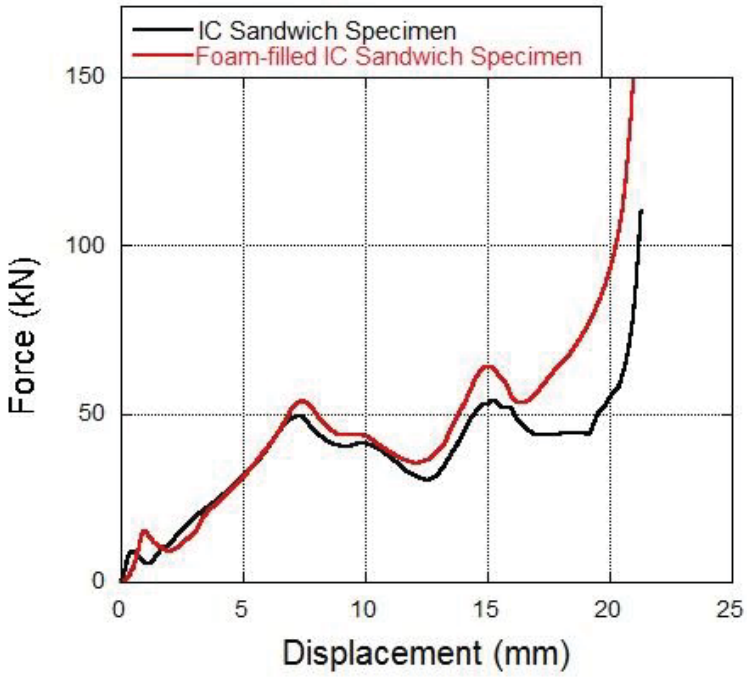

Figure 5.9. Foam filling effect in the quasi-static compression of IC sandwich specimen

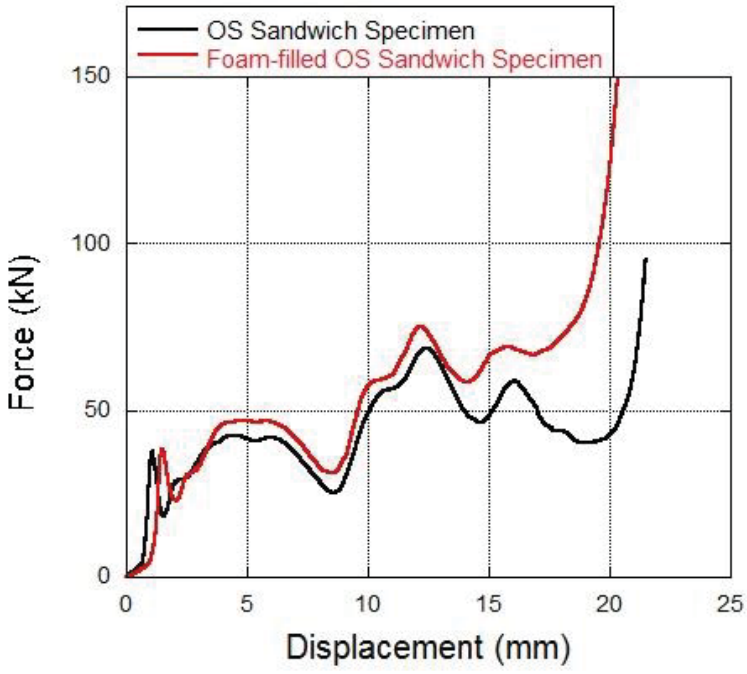

Figure 5.10. Foam filling effect in the quasi-static compression of OS sandwich specimen

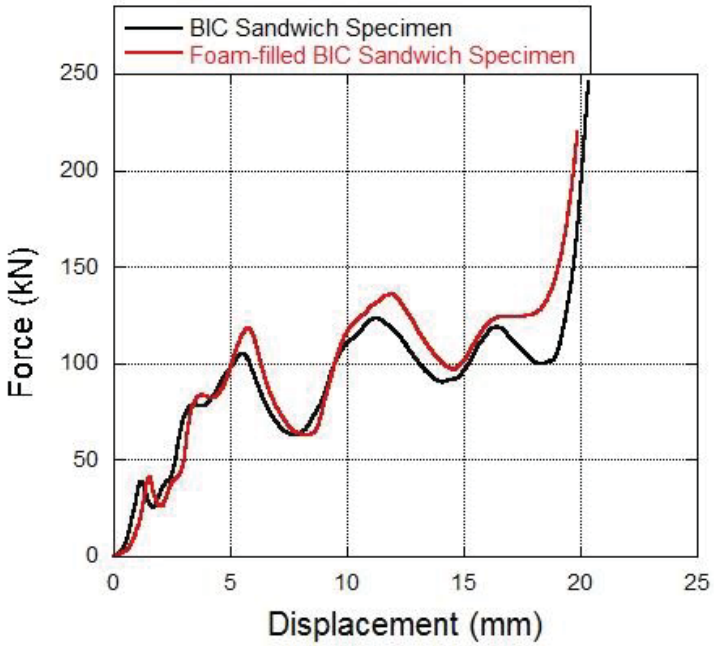

Figure 5.11. Foam filling effect in the quasi-static compression of BIC sandwich specimen

Next, the deformation histories of the sandwich specimens with composite face sheets were recorded under quasi-static loading and the presented views were marked on the corresponding points of the force-displacement curves.

In Figure 5.12, Figure 5.13 and Figure 5.14, above-mentioned deformation histories of the sandwich specimens are given. Mainly, the local minimum and the local maximum points are illustrated on the graphs.

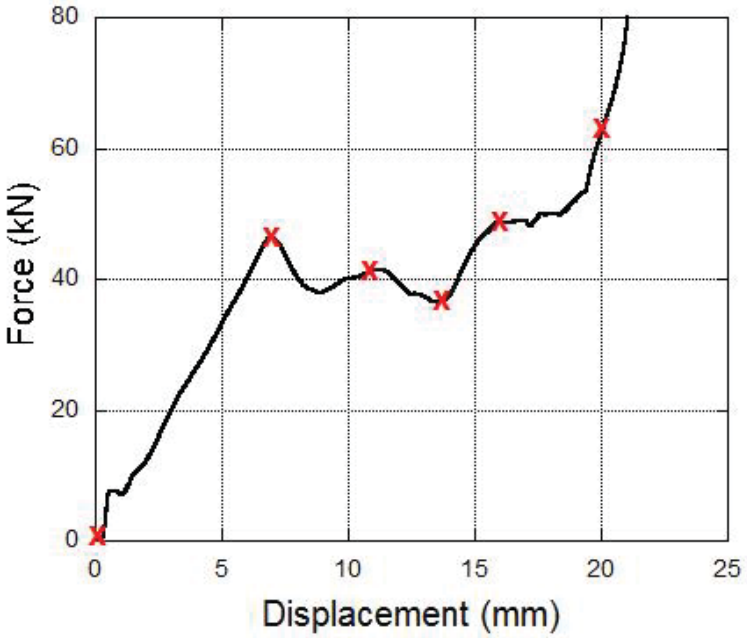

0 mm

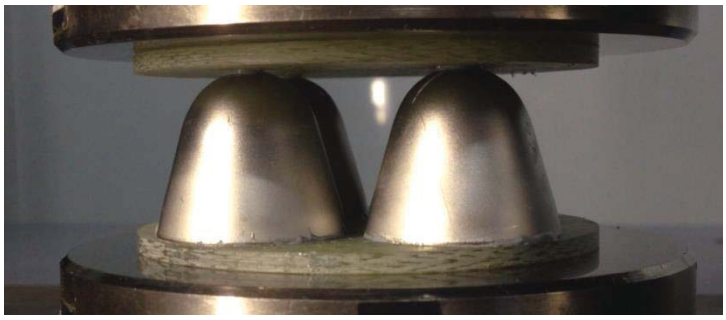

7 mm

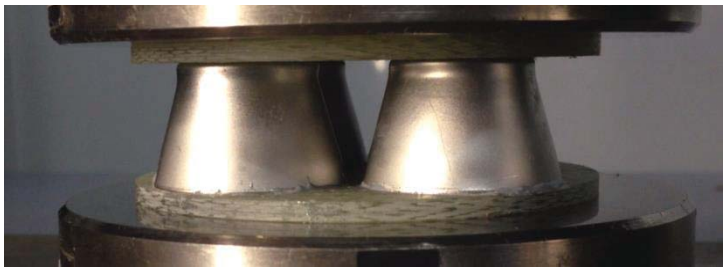

11 mm

Figure 5.12. Deformation history of IC sandwich specimen

(cont. on next page)

14 mm

16 mm

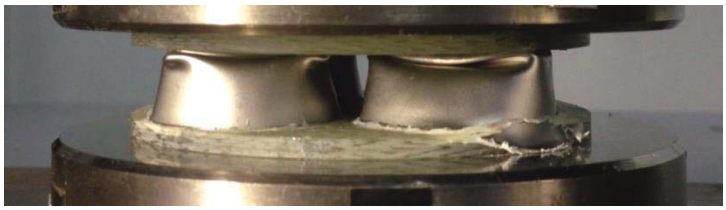

20 mm

Figure 5.12. (cont.)

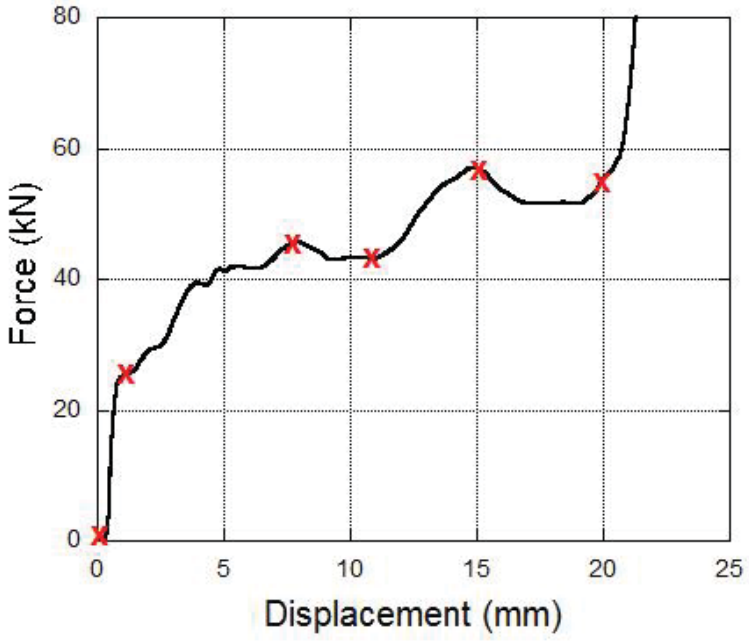

Figure 5.13. Deformation history of OS sandwich specimen

(cont. on next page)

0 mm

1 mm

7,5 mm

11 mm

15 mm

20 mm

Figure 5.13. (cont.)

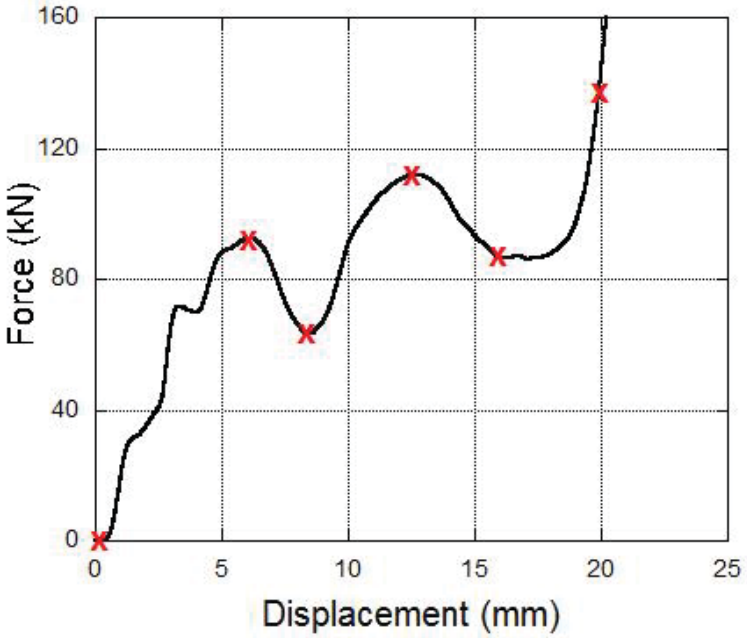

0 mm

6 mm

8 mm

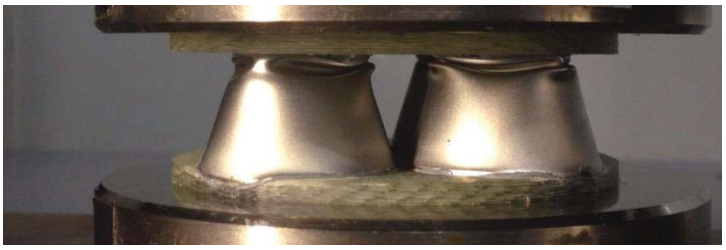

Figure 5.14. Deformation history of BIC sandwich specimen

(cont. on next page)

12,5 mm

16 mm

20 mm

Figure 5.14. (cont.)

After all, the force-displacement curves of the numerical models were compared with the experimental results. The comparisons are provided in the following three figures together with the numerical deformation histories. In Figure 5.15, IC sandwich specimen is presented.

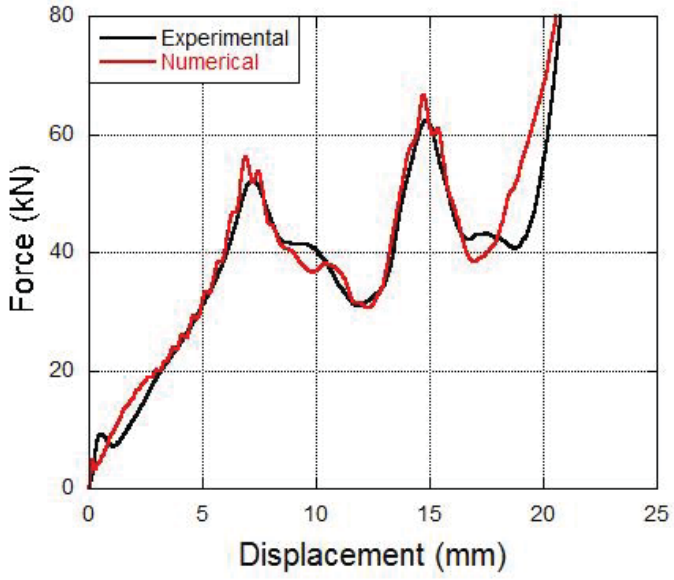

Figure 5.15. Comparison of the force-displacement curves of experimental and numerical quasi-static compression of IC sandwich specimen and the numerical deformation history

(cont. on next page)

0 mm

8 mm

13.1 mm

15.5 mm

18 mm

(cont. on next page)

20 mm

Figure 5.15. (cont.)

OS sandwich specimen has also a quite good agreement between the force-displacement curves of experimental and numerical results as can be seen in Figure 5.16.

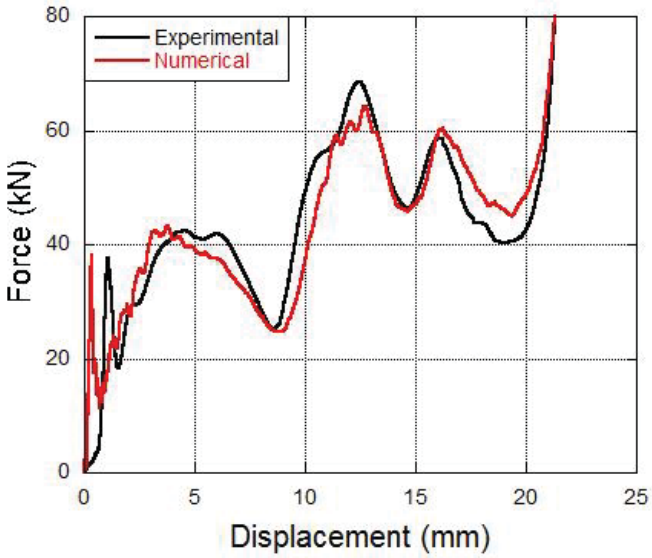

Figure 5.16. Comparison of the force-displacement curves of experimental and numerical quasi-static compression of OS sandwich and the numerical deformation history

(cont. on next page)

0 mm

4.3 mm

9 mm

12 mm

16 mm

(cont. on next page)

20 mm

Figure 5.16. (cont.)

Lastly, the same illustrations are displayed for BIC sandwich specimen in Figure 5.17.

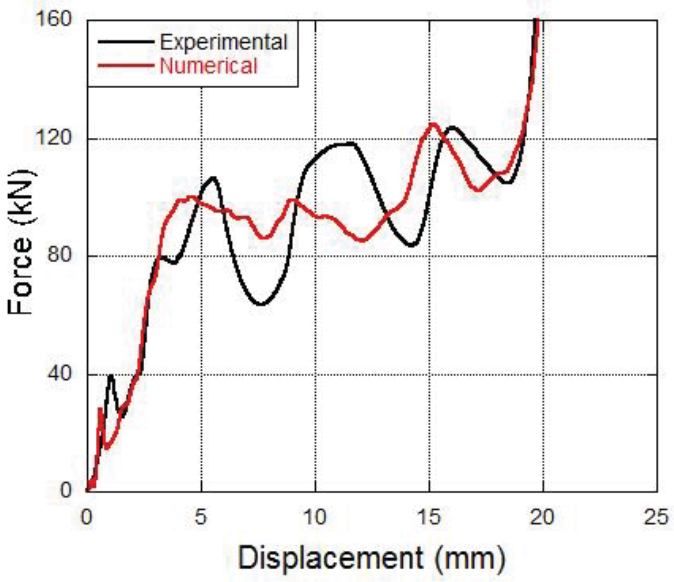

0 mm

Figure 5.17. Comparison of the force-displacement curves of experimental and numerical quasi-static compression of BIC sandwich specimen and the numerical deformation history.

(cont. on next page)

5 mm

9.5 mm

13 mm

15.5 mm

20 mm

Figure 5.17. (cont.)

The final views of each deformed sandwich type are given in Figure 5.18, both numerically and experimentally. In addition to the good agreement in force-displacement curves, a high similarity was obtained in the deformation modes.

(a)

(b)

Figure 5.18. Final top views of experimentally and numerically deformed (a) IC, (b) OS and (c) BIC sandwich specimens under quasi-static loading.

(cont. on next page)

(c)

Figure 5.18. (cont.)

The influence of the circumferential confinement during the quasi-static loading on the load-carrying capacities of the sandwich specimens was also investigated. The results are given in the following figure.

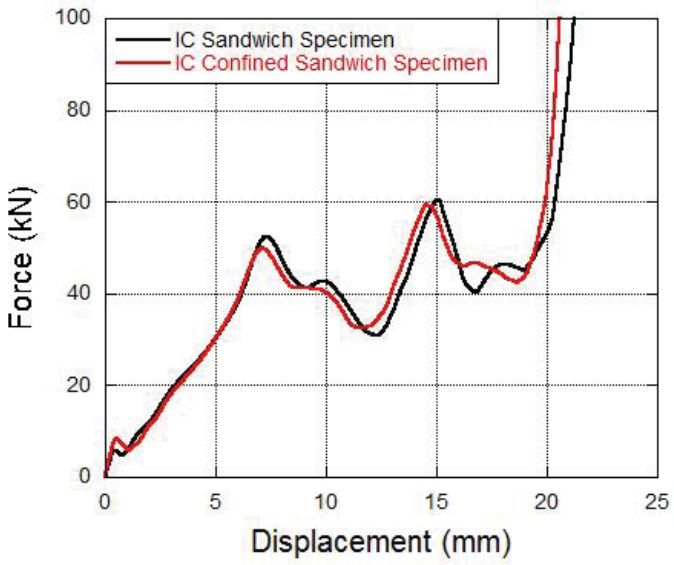

(a)

Figure 5.19. Confinement effect on the load-carrying capacities of the (a) IC, (b) OS, (c) BIC sandwich specimens.

(cont. on next page)

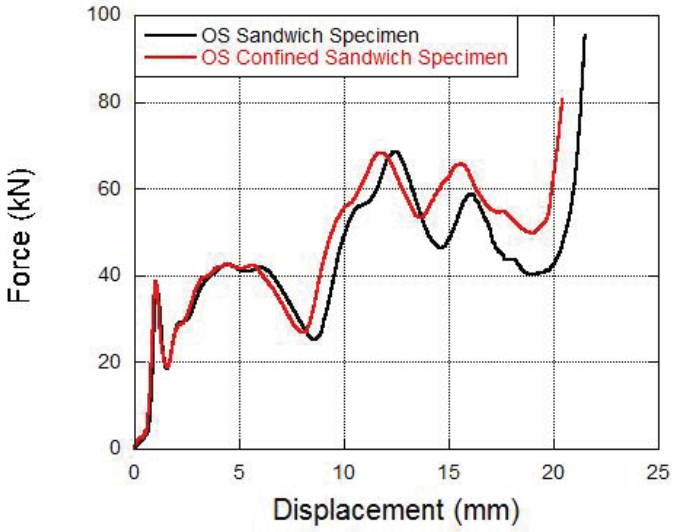

(b)

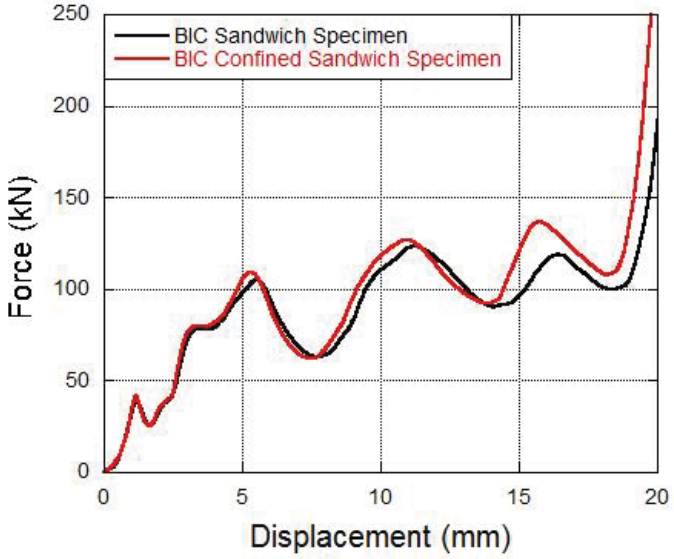

(c)

Figure 5.19. (cont.)

Since the outward buckling of the thin–walled structures was prevented by the rigid confinement wall during the deformation, peak points in the load-displacement curves reached higher values in each sandwich specimen. However, OS and BIC sandwich specimens gave a more pronounced reaction against the confinement effect because of having larger core material diameters.

After the completion of the quasi-static compression tests and the verification of the numerical models, the study was continued with the drop-weight experiments and their numerical studies. The absorbed energies were calculated by taking the integration of the force-displacement curves for each sandwich type. Then, applied mass and

impact velocity were decided in the drop-weight experiments. IC sandwich specimen absorbed energy of 740 joule approximately up to the point where densification started. Corresponding kinetic energy was provided with the striker mass of 15.63 kg and the impact velocity of 10 m/s. The force-displacement curves of experimentally and numerically crushed IC sandwich specimens are presented in Figure 5.20. Also, the experimental and numerical deformation histories are given in the same figure.

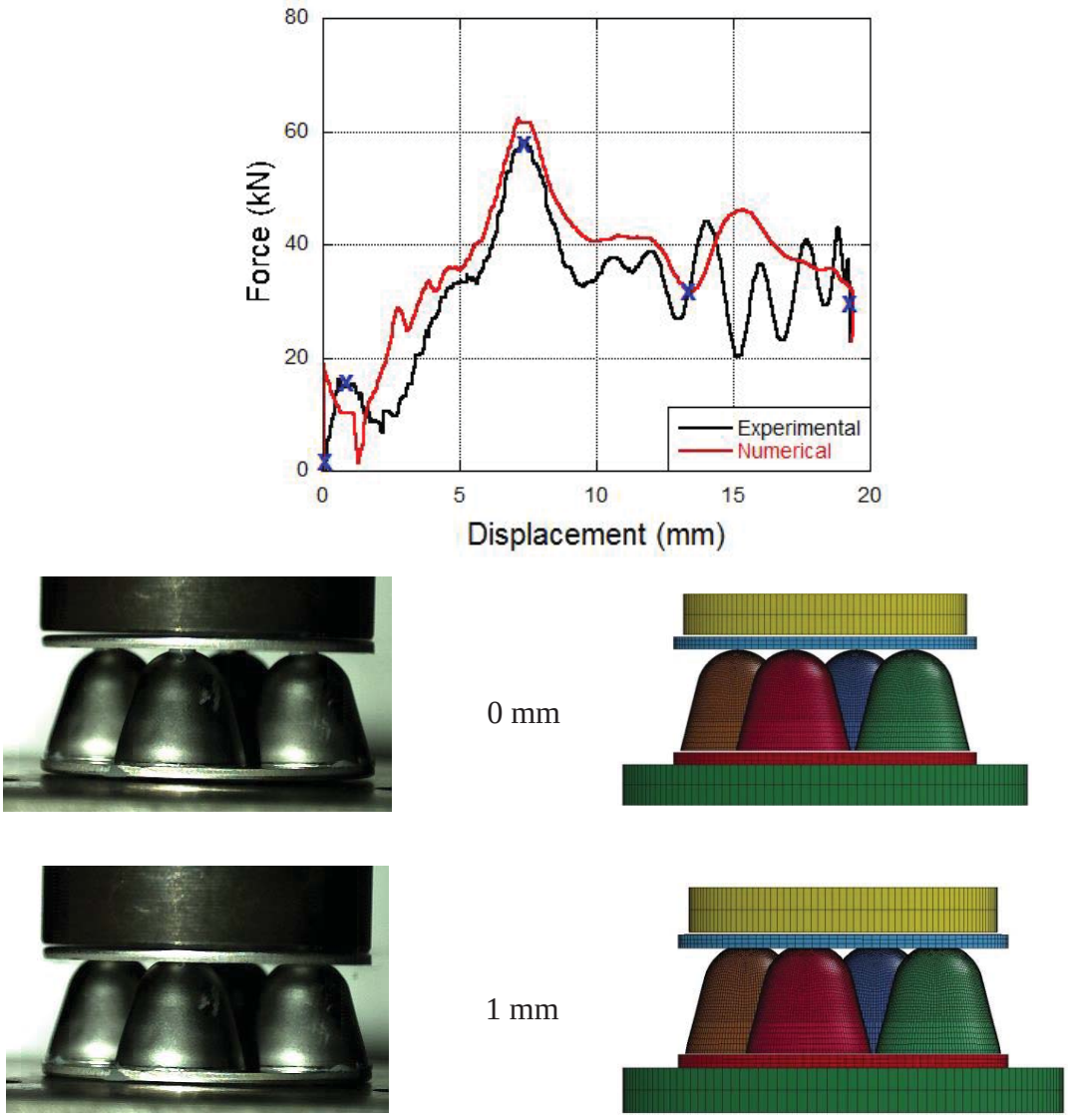

Figure 5.20. The comparison of the force-displacement curves of experimentally and numerically crushed IC sandwich specimens under dynamic loading and the deformation histories.

(cont. on next page)

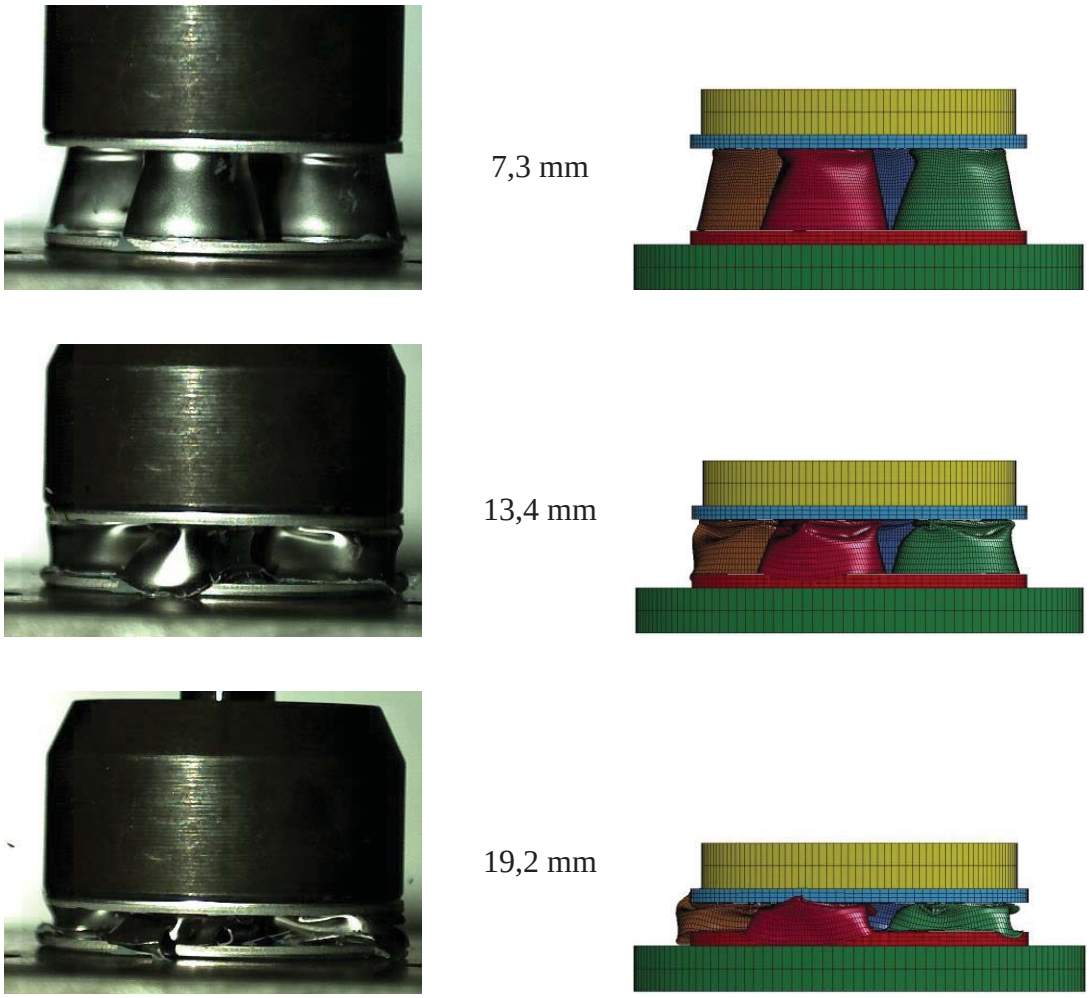

Figure 5.20. (cont.)

In the drop-weight studies, a well agreement was noted same as in quasi-static studies as seen in the figure given above. The deformation histories and the comparison of the force-displacement curves are also provided for OS and BIC sandwich specimens in Figure 5.21 and Figure 5.22, respectively. Both types of sandwich specimens were crushed with the striker mass of 18.63 kg and the impact velocity of 10 m/s.

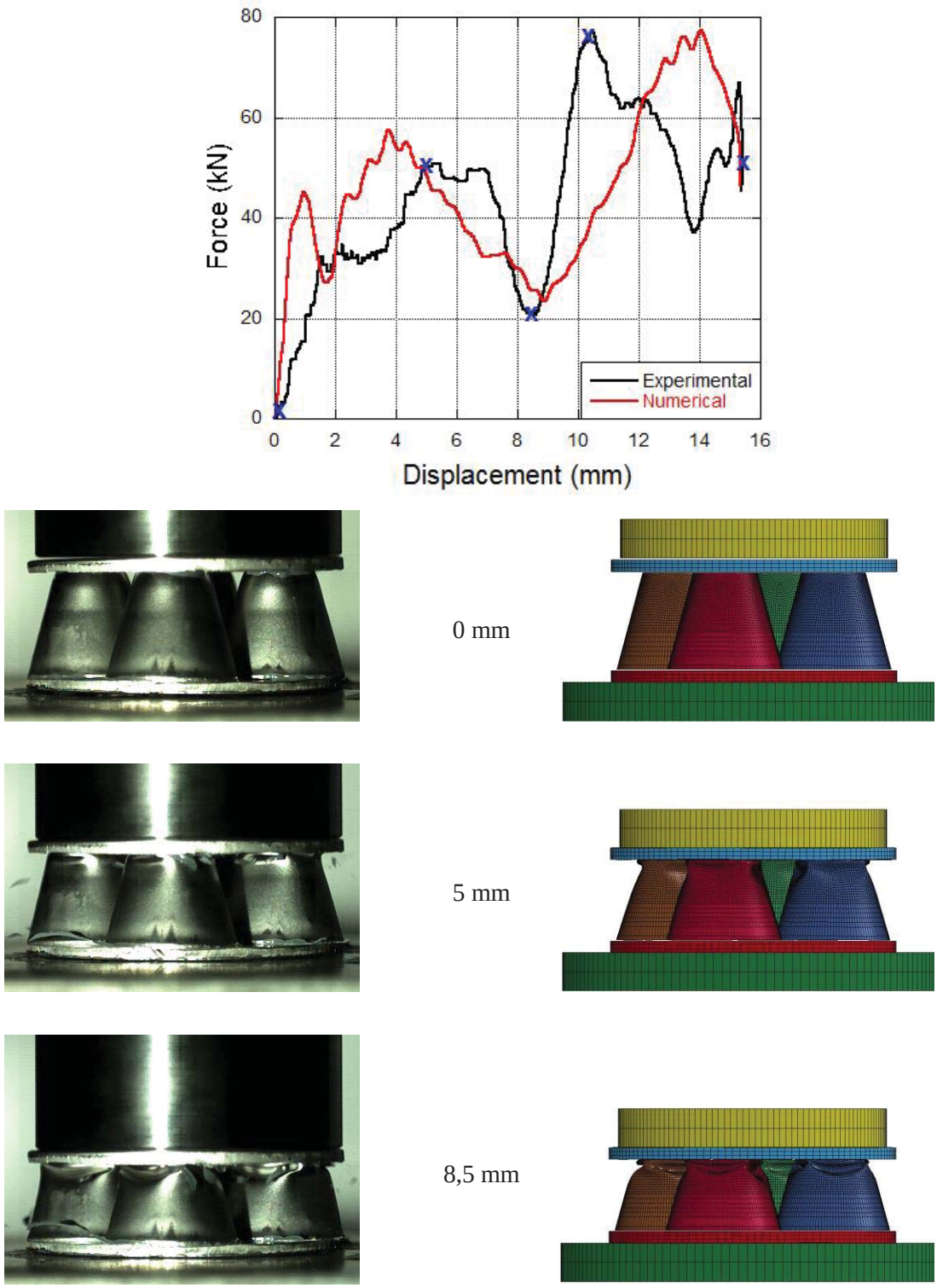

Figure 5.21. The comparison of the force-displacement curves of experimentally and numerically crushed OS sandwich specimens under dynamic loading and the deformation histories.

(cont. on next page)

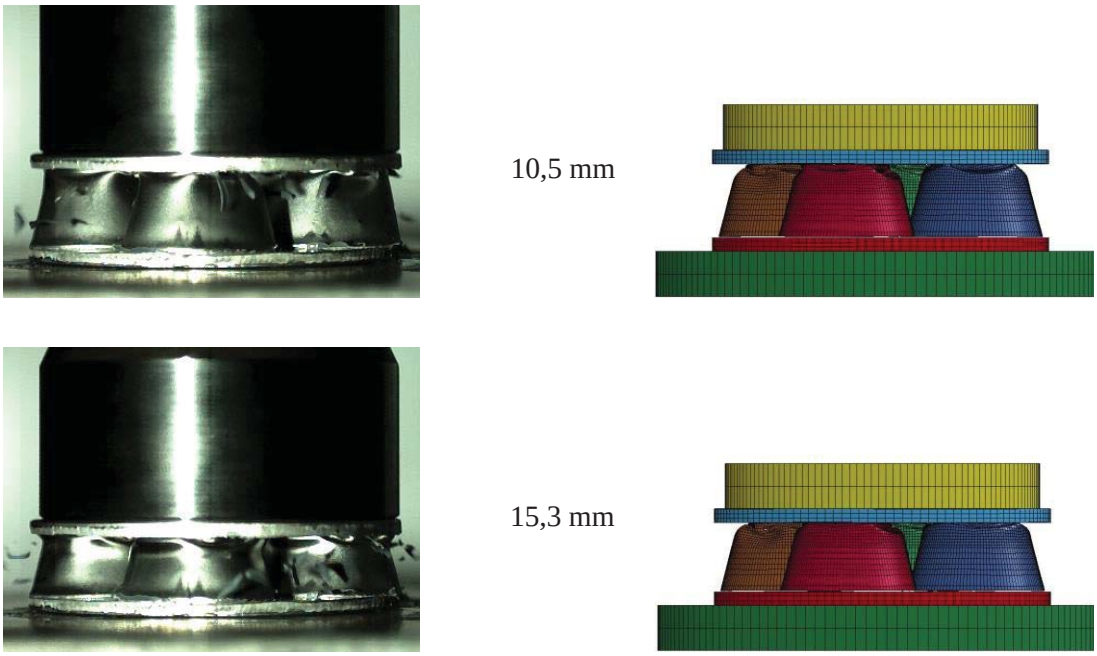

Figure 5.21. (cont.)

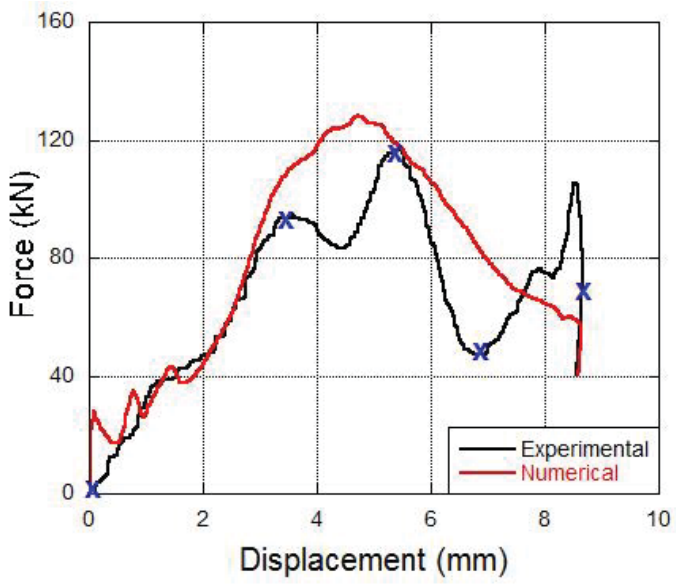

Figure 5.22. The comparison of the force-displacement curves of experimentally and numerically crushed BIC sandwich specimens under dynamic loading and the deformation histories.

(cont. on next page)

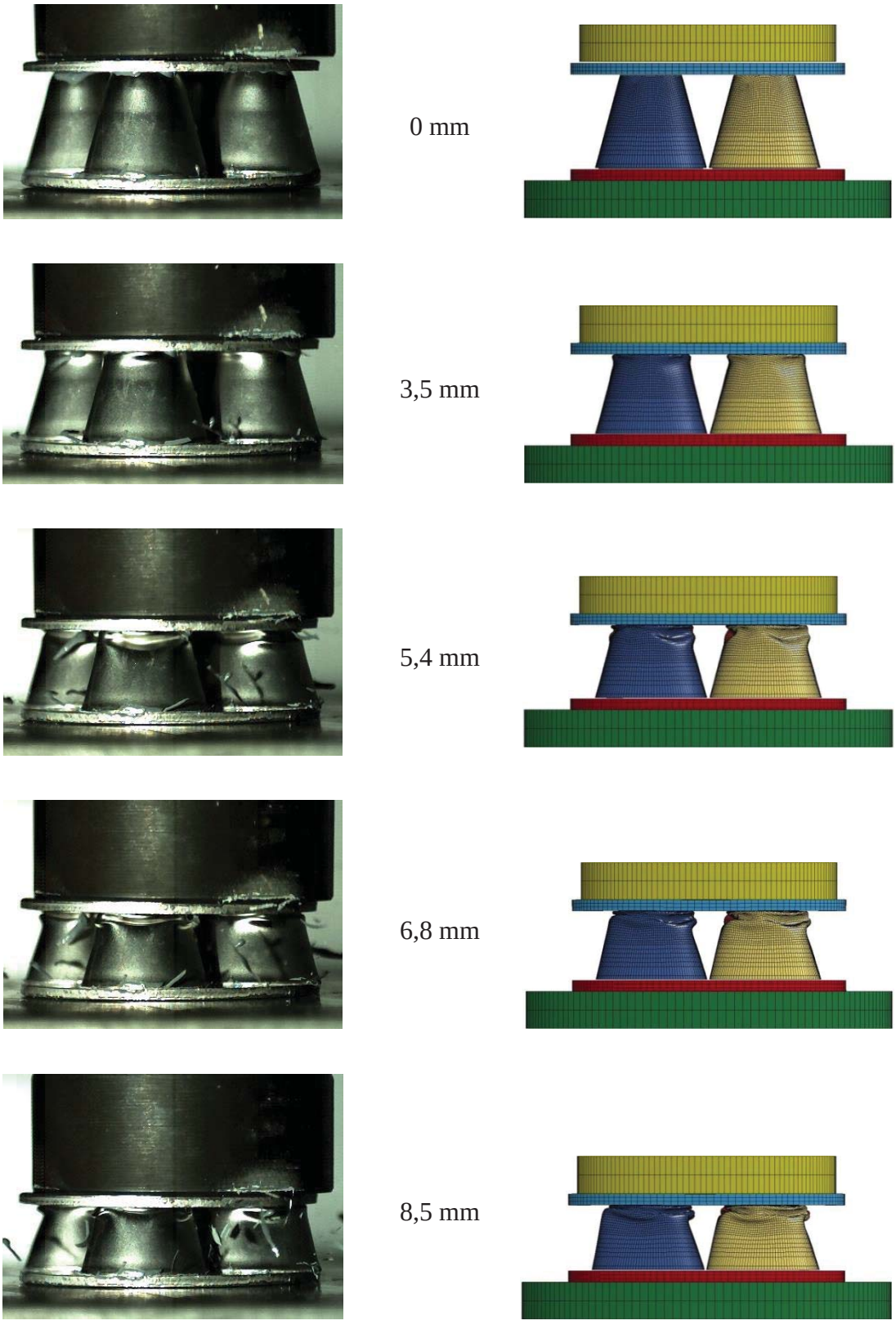

Figure 5.22. (cont.)

At the beginning of the deformation, while the sharp top edge of the outer shell folds inward in small-size, hemispherical portion of the inner core inverts down. It results in a local peak in the force-displacement curve up to the point where the initial actual fold forms. It is followed by the collapse in diamond mode during the deformation and each fold causes local minimum and local maximum points in the force-displacement curve. At the end of the deformation, local outward bending is observed.

The final top views of each type of dynamically crushed sandwich specimens are presented in the following figure. A high similarity in the deformation modes of experimentally and numerically crushed specimens is seen.

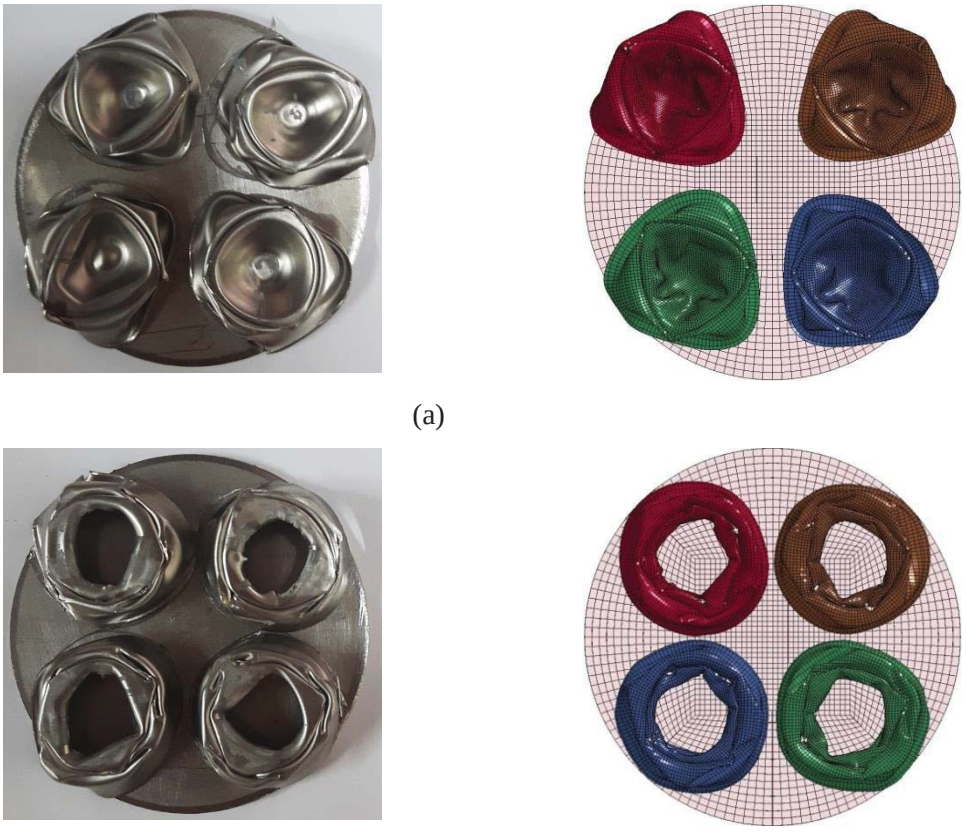

Figure 5.23. Final top views of experimentally and numerically crushed (a) IC, (b) OS and (c) BIC sandwich specimens under dynamic loading

(cont. on next page)

(c)

Figure 5.23. (cont.)

The foam filling effect was also inspected under dynamic loading. Inner cores and bio-inspired cores were filled with polyurethane foam and they were crushed under the same conditions with their empty equivalents. A decrease was observed in their compression amounts while the same amount of energy was absorbed. The force-displacement curves are provided in the following figure.

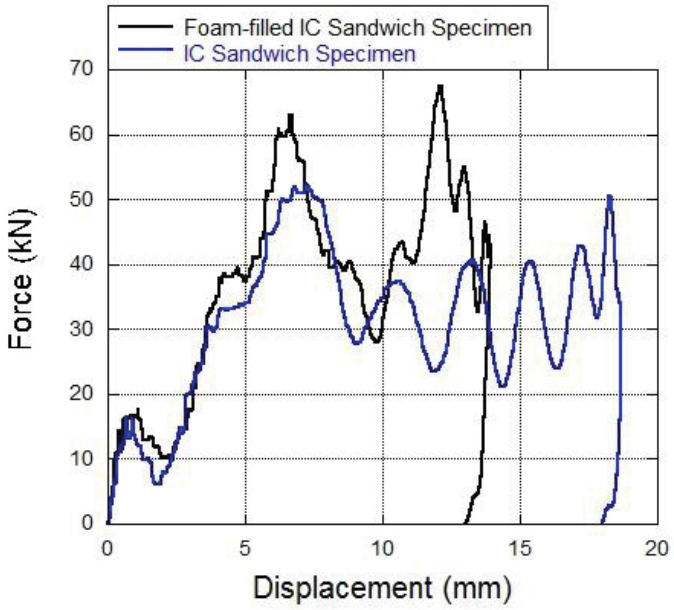

(a)

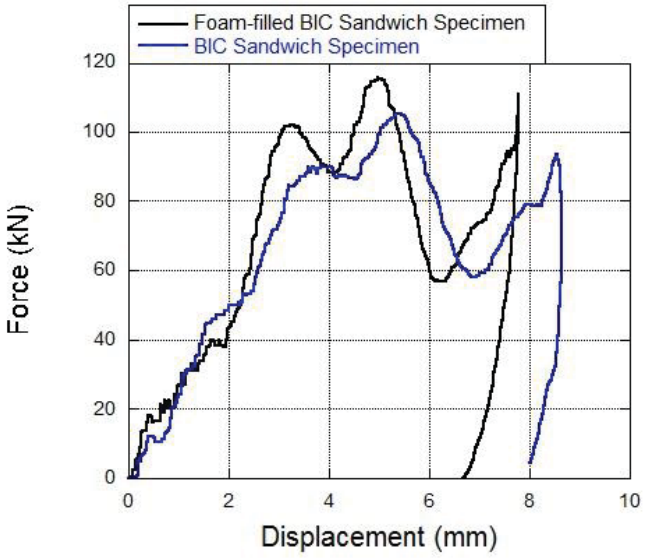

(b)

Figure 5.24. The comparison of (a) foam-filled and empty IC sandwich specimens, (b) foam-filled and empty BIC sandwich specimens.

The experimental results are summarized in the following tables. P_i, P_{mean} and P_{max} refer initial peak force, average force and maximum peak force, respectively. Absorbed energy was obtained by taking the integral of the force values with respect to the displacement values in each curve. In the tables, absorbed energies by sandwich specimens are given at the compression level of 20 mm where the densification starts. Then, specific absorbed energy (SAE) values were calculated dividing absorbed energy

by the total mass of the core materials. Face sheets were not taken into consideration. Finally, crushing force efficiency (CFE) which is the ratio of P_{mean} to P_{max} was provided for each type of specimens. The closer value of CFE to "1" is aimed to have a better crashworthiness performance as previously mentioned in the literature review part.

Table 5.1. Crashworthiness parameters of IC, OS and BIC sandwich specimens under quasi-static loading

Sandwich Specimen	**P_i (kN)**	**P_{mean} (kN)**	**P_{max} (kN)**	**Absorbed Energy @20 mm (J)**	**SAE @20 mm (kJ/kg)**	**CFE**
IC	8.3	36.8	57.2	740.0	29.9	0.64
OS	36.5	43.8	70.0	860.0	31.2	0.62
BIC	38.5	89.0	123.2	1807.4	34.8	0.72

Table 5.2. Crashworthiness parameters of IC, OS and BIC sandwich specimens under dynamic loading

Sandwich Specimen	**P_i (kN)**	**P_{mean} (kN)**	**P_{max} (kN)**	**Absorbed Energy (J)**	**Def. (mm)**	**SAE (kJ/kg)**	**CFE**	**Test Conditions**
IC	15.8	31.8	58.6	611.5	19.1	22.5	0.54	15.63kg 10 m/s
OS	32.0	43.6	77.3	675.8	15.4	24.8	0.56	18.63kg 10 m/s
BIC	94.1	67.9	117.2	586.0	8.6	11.3	0.58	18.63kg 10 m/s

In the quasi-static compression tests, all types of sandwich specimens were deformed up to the same amount of deformation level. Thus, it is easy to evaluate the crashworthiness parameters. BIC sandwich specimen absorbs the highest amount of energy while IC sandwich specimen exhibits the lowest energy absorbing capacity. The same ranking is also valid for the specific absorbed energies in the quasi-static tests.

In the drop-weight tests, the sandwich specimens could not be crushed to their densification levels due to too high force responses. Instead, to examine the parameters, the maximum compression level of BIC sandwich specimen was focused on. Absorbed energy values at the compression level of 8.6 mm are provided in another table.

Table 5.3. Comparison of the energy absorption amounts of the sandwich specimens under different loading conditions.

Test Type	Sandwich Specimen	Absorbed Energy @8.6 mm (J)	SAE @8.6 mm (kJ/kg)
Quasi-static	IC	232.8	9.4
	OS	273.7	10.1
	BIC	529.1	10.2
Drop-weight	IC	248.3	10.0
	OS	295.6	10.9
	BIC	586.0	11.3

At the same compression level, the energy absorption capacities of each sandwich specimen increase as the loading rate increases. This can be explained by the effects of the inertia and rate sensitivity.

In order to gain a complete insight into the interaction of inertial and rate sensitivity properties of the proposed sandwich type, several numerical studies were conducted. Rate sensitive and rate insensitive numerical codes were prepared and they were run with different constant crushing velocities, which are 50 m/s, 100 m/s and 150 m/s.

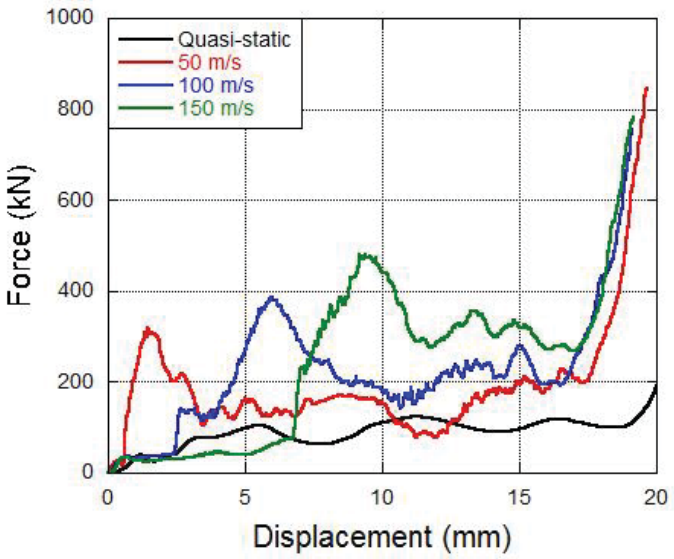

Figure 5.25. The force-displacement curves of the rate sensitive numerical models with constant upper plate velocities.

Enhancement in the load-carrying capacity of the proposed geometry was revealed as the loading rate increases in the previous tables which present the comparison of the quasi-static and drop-weight tests. However, it becomes more apparent when the crushing velocity is increased in the higher degree as seen in Figure 5.26. Absorbed energies in each simulation were also graphed against the crushing displacements.

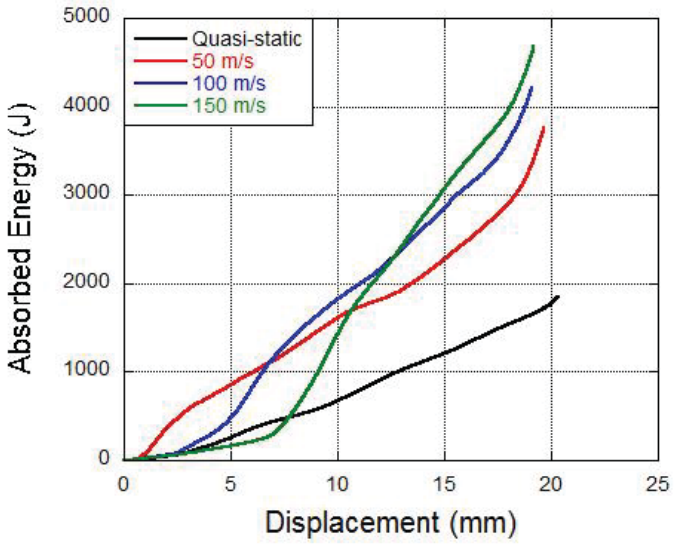

Figure 5.26. The absorbed energy-displacement curves of the rate sensitive numerical models with constant upper plate velocities.

The final views of the numerically deformed BIC sandwich specimens under the constant crushing velocities of 50 m/s, 100 m/s and 150 m/s are given in Figure 5.27 . Even all they are deformed in diamond mode, the erosion level increases prominently at the higher velocities.

(a)

(b)

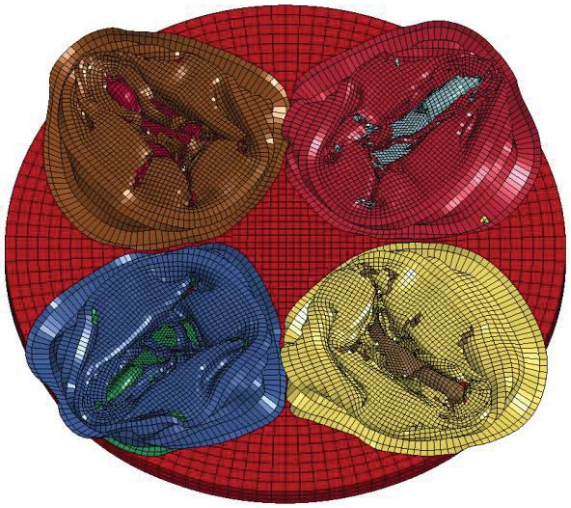

(c)

Figure 5.27. Numerically deformed BIC sandwich specimen under the velocities of a) 50 m/s, b) 100 m/s, c) 150 m/s

In addition, rate sensitive and rate insensitive numerical models with the constant upper plate velocity of 50 m/s were prepared to see the effect of rate sensitivity and inertia separately. In the Johnson-Cook material model, "C" parameter was taken as zero to neglect the strain rate effects. The force-displacement curves of rate sensitive and rate insensitive model are sketched together with that of quasi-static model.

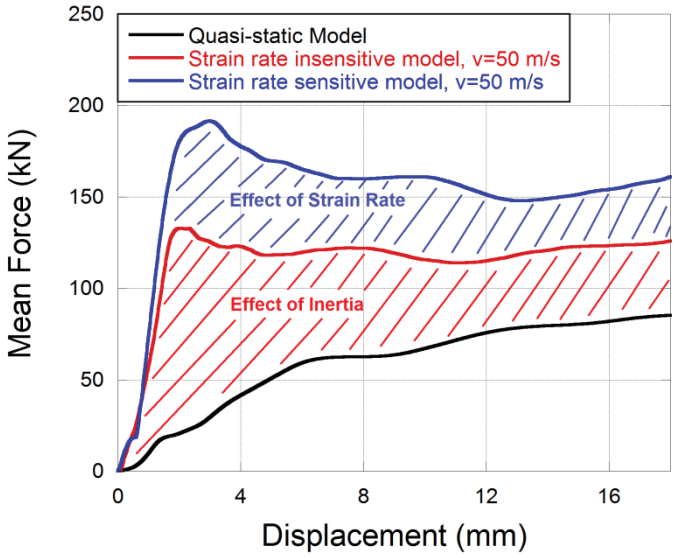

Figure 5.28. The force-displacement curves of rate-sensitive and rate insensitive models.

In Figure 5.28, the rise in the force values of the rate insensitive model in comparison with the quasi-static model is sourced by only the inertial effects while the rate sensitivity and inertial effects play role together in the rising force response of the strain rate sensitive model.

Finally, the results of the gas gun tests are presented. The first group of tests was carried out with the impact velocities of 120 m/s, 125 m/s, 150 m/s, 180 m/s using spherical penetrator. In the second group, cube edge penetrator was used and the impact velocity of 235 m/s was tried in addition to the same velocities in the first group. The high speed camera views which belong the tests with the highest impact velocities in each group are provided in the following figures.

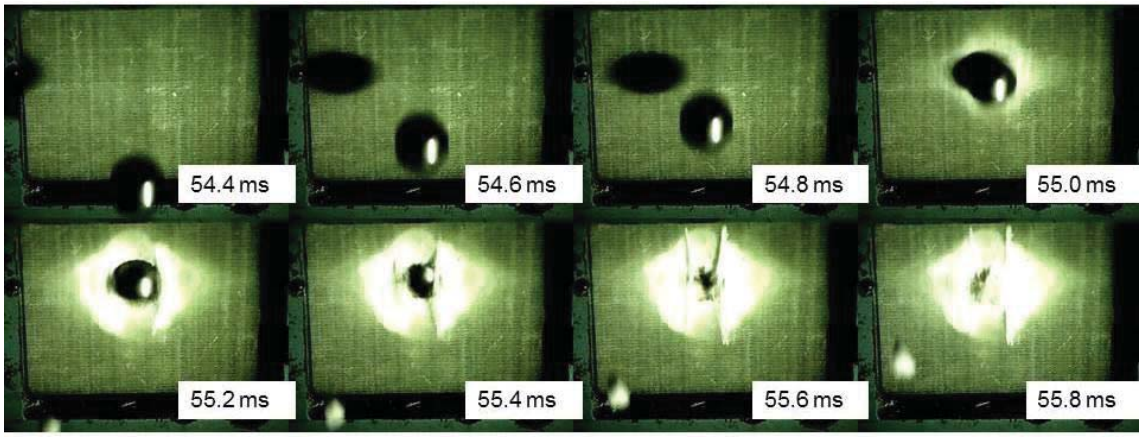

Figure 5.29. High speed camera views in the gas gun test (Spherical penetrator, 180 m/s).

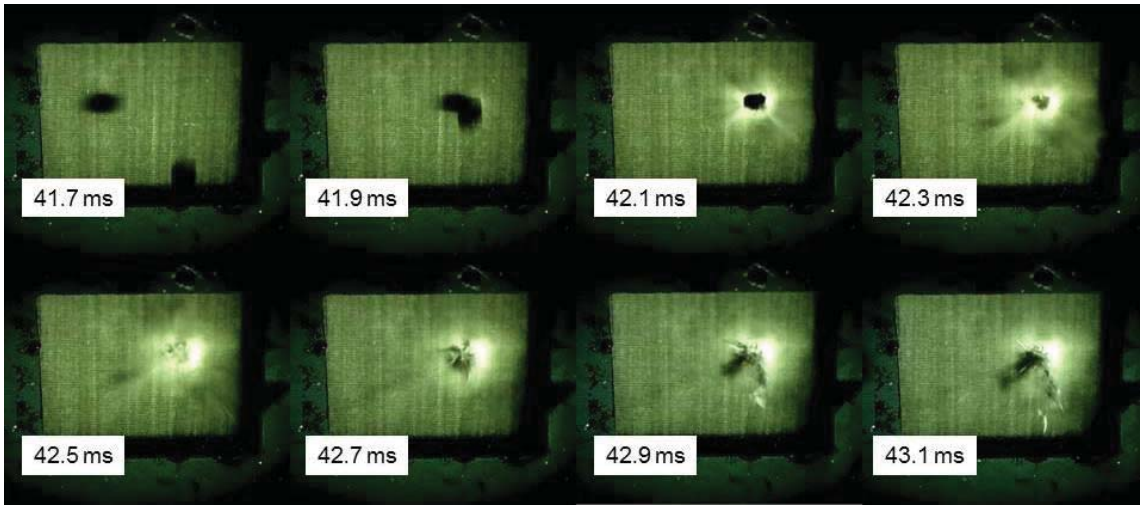

Figure 5.30. High speed camera views in the gas gun test (Cubical penetrator, 235 m/s).

Only penetration was observed in the tests which were carried out using cubical penetrator due to its relatively smaller mass. However, in the test which was performed with the spherical penetrator and the impact velocity of 180 m/s, perforation was seen. The terminal velocity of the penetrator was measured as 68 m/s. The damages on the front composite facing and the bio-inspired cores of several tests are given between Figure 5.31 and Figure 5.37.

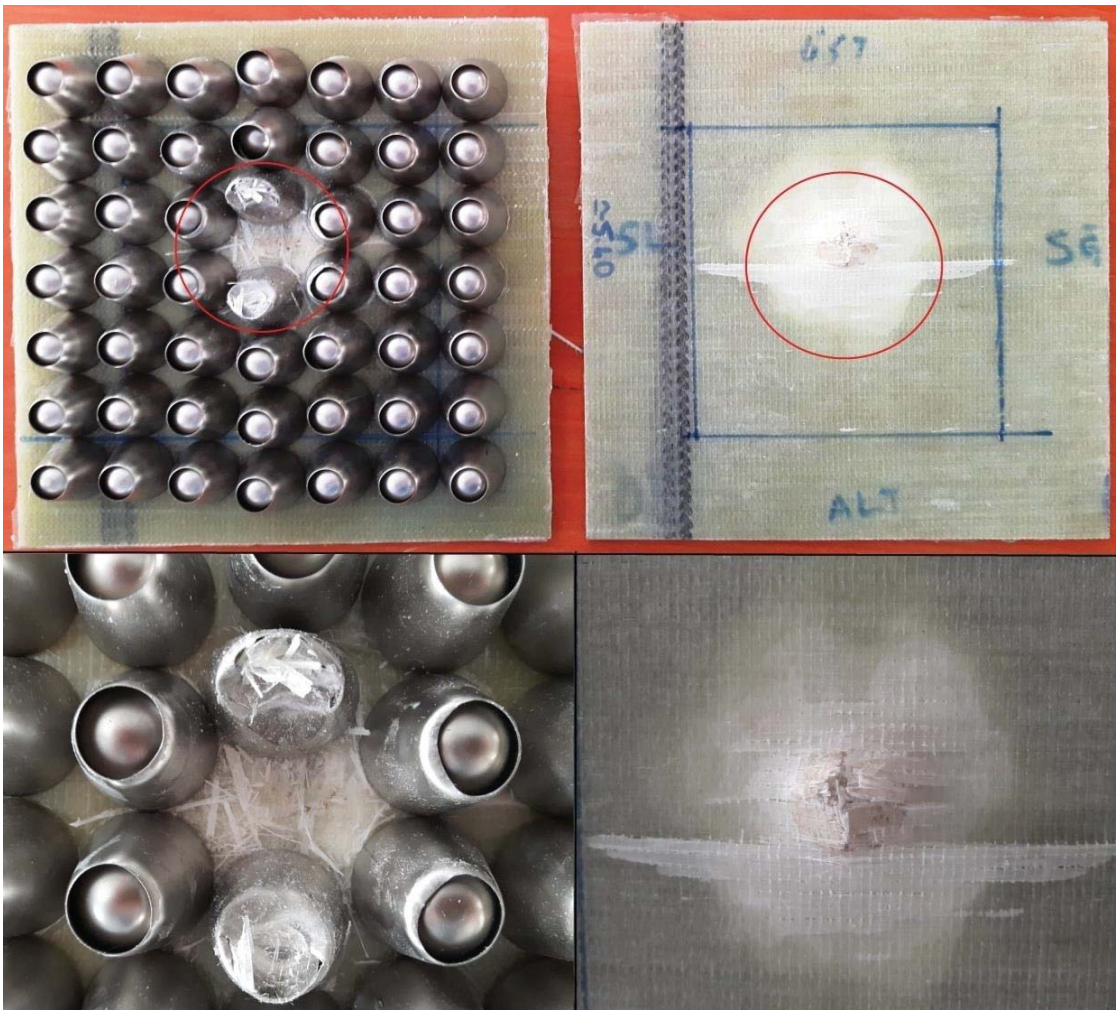

Figure 5.31. Gas gun test with spherical penetrator and the impact velocity of 150 m/s

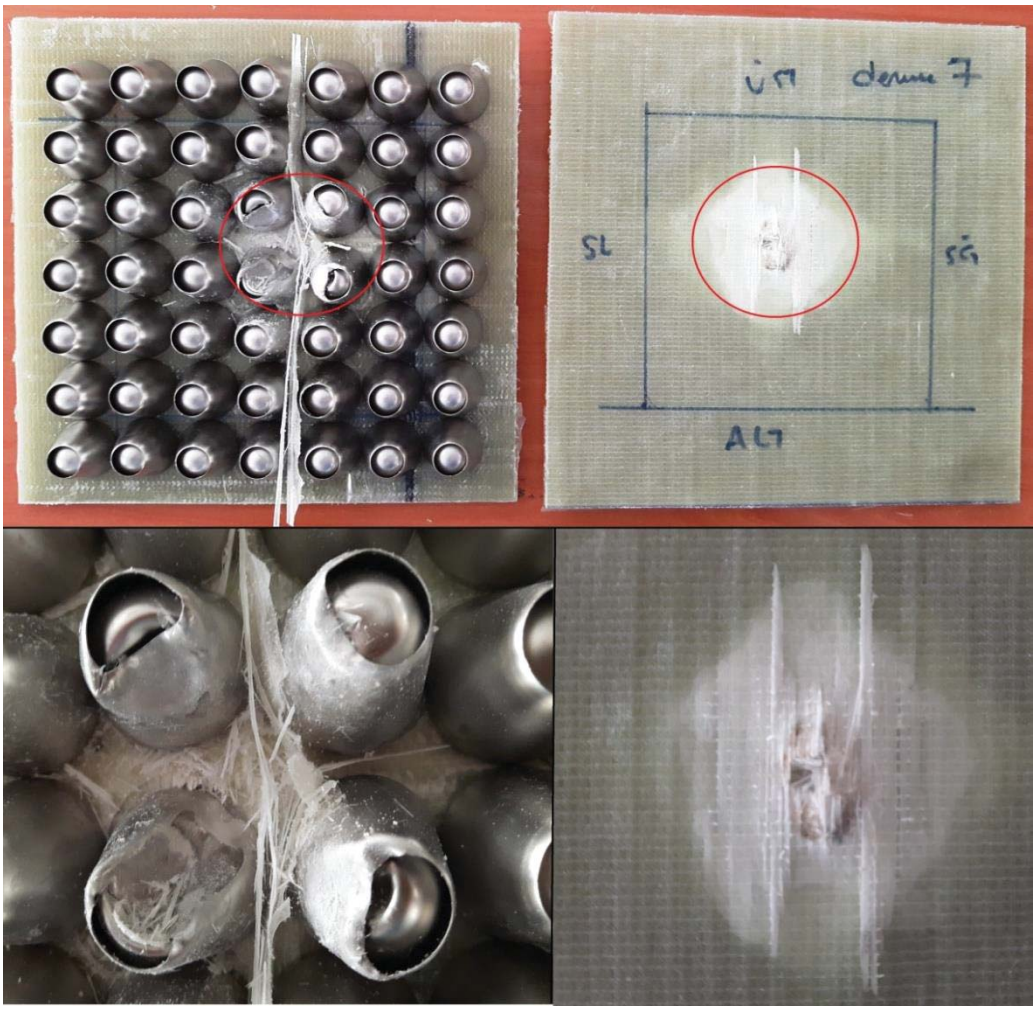

Figure 5.32. Gas gun test with spherical penetrator and the impact velocity of 180 m/s

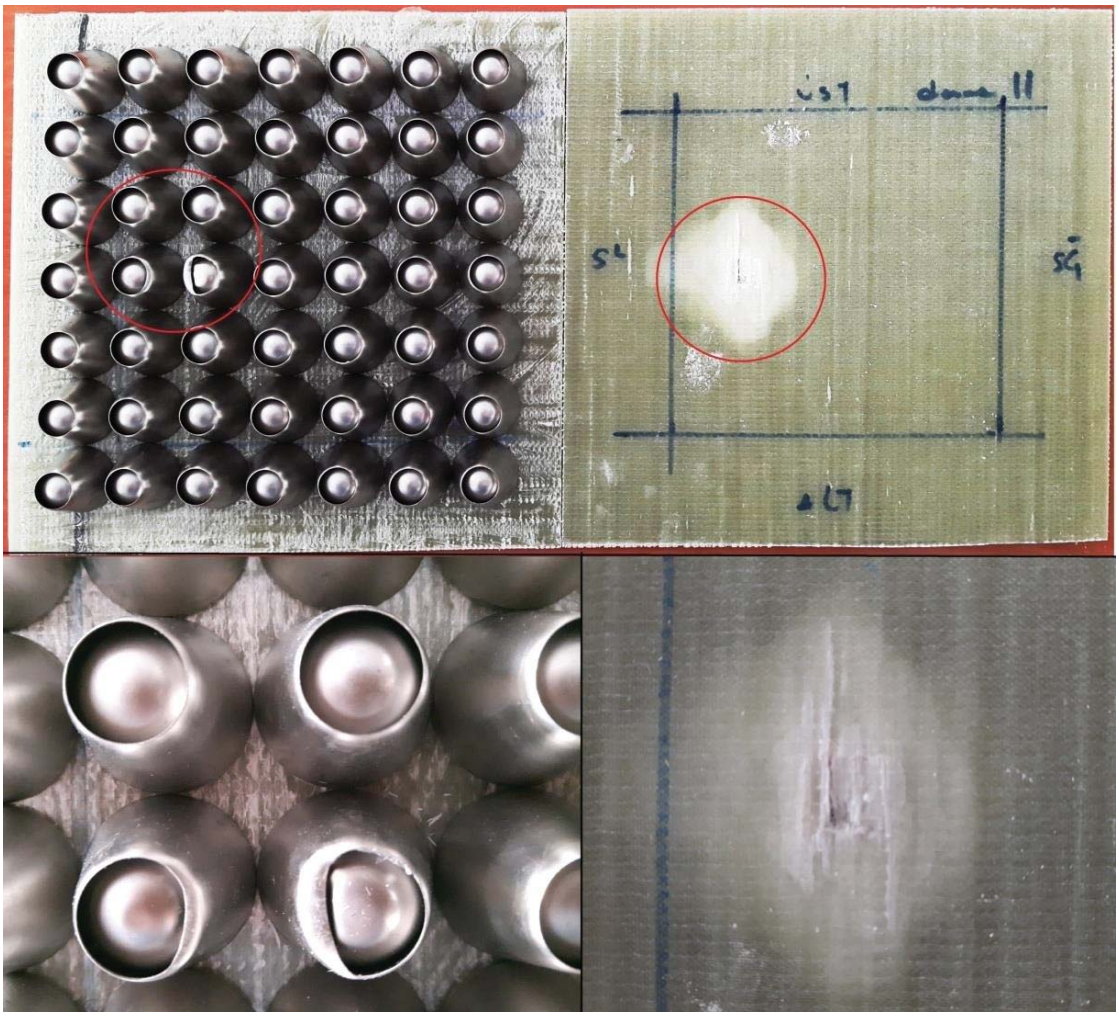

Figure 5.33. Gas gun test with cubical penetrator and the impact velocity of 120 m/s

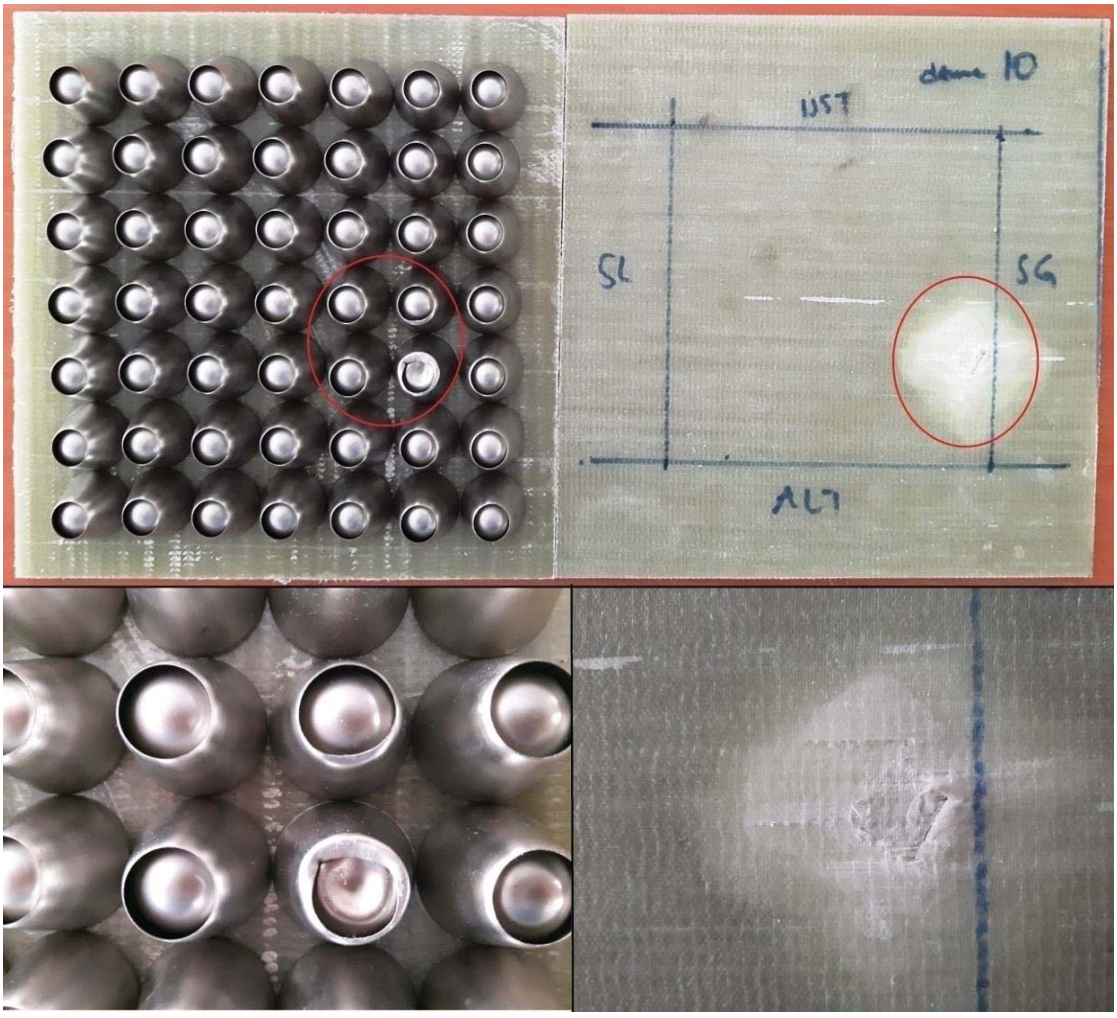

Figure 5.34. Gas gun test with cubical penetrator and the impact velocity of 125 m/s

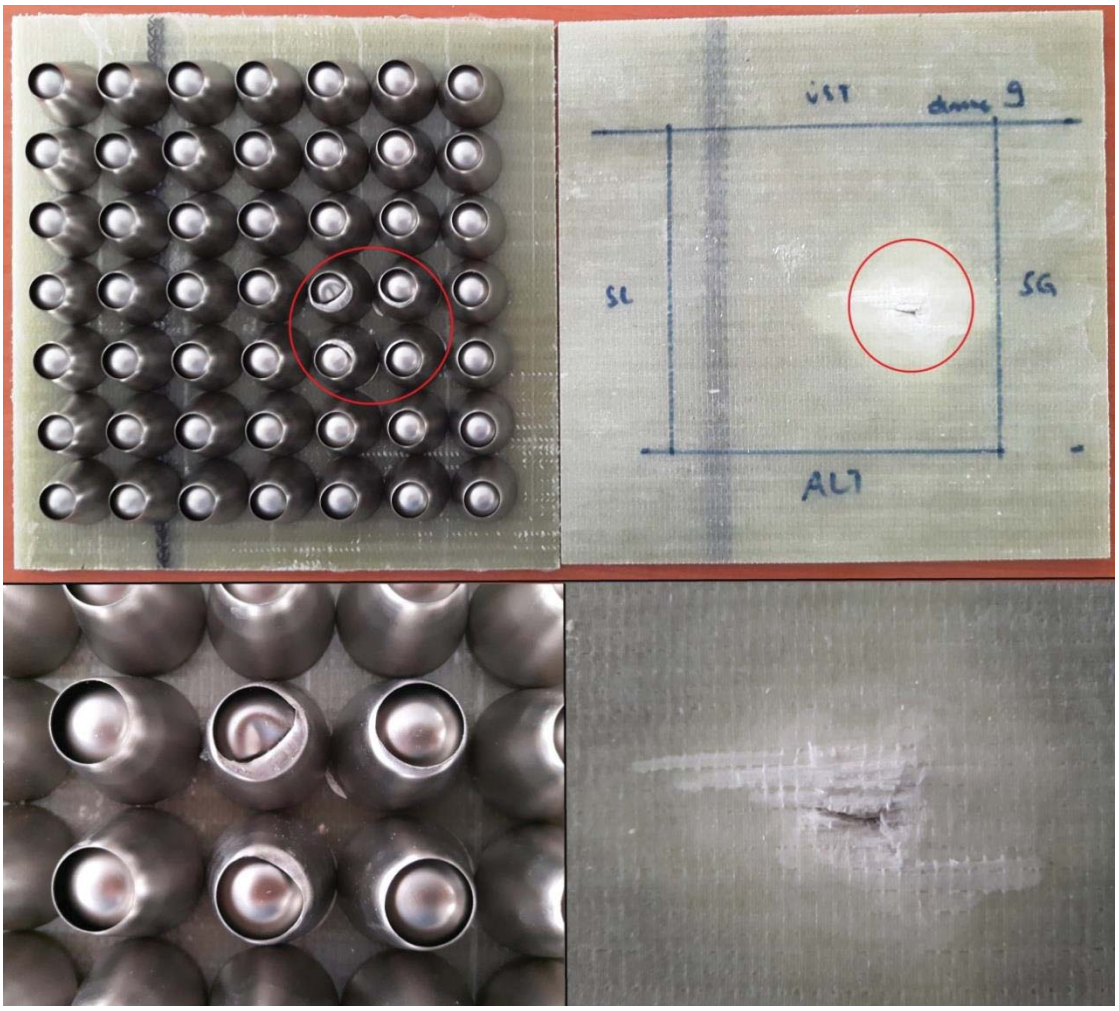

Figure 5.35. Gas gun test with cubical penetrator and the impact velocity of 150 m/s

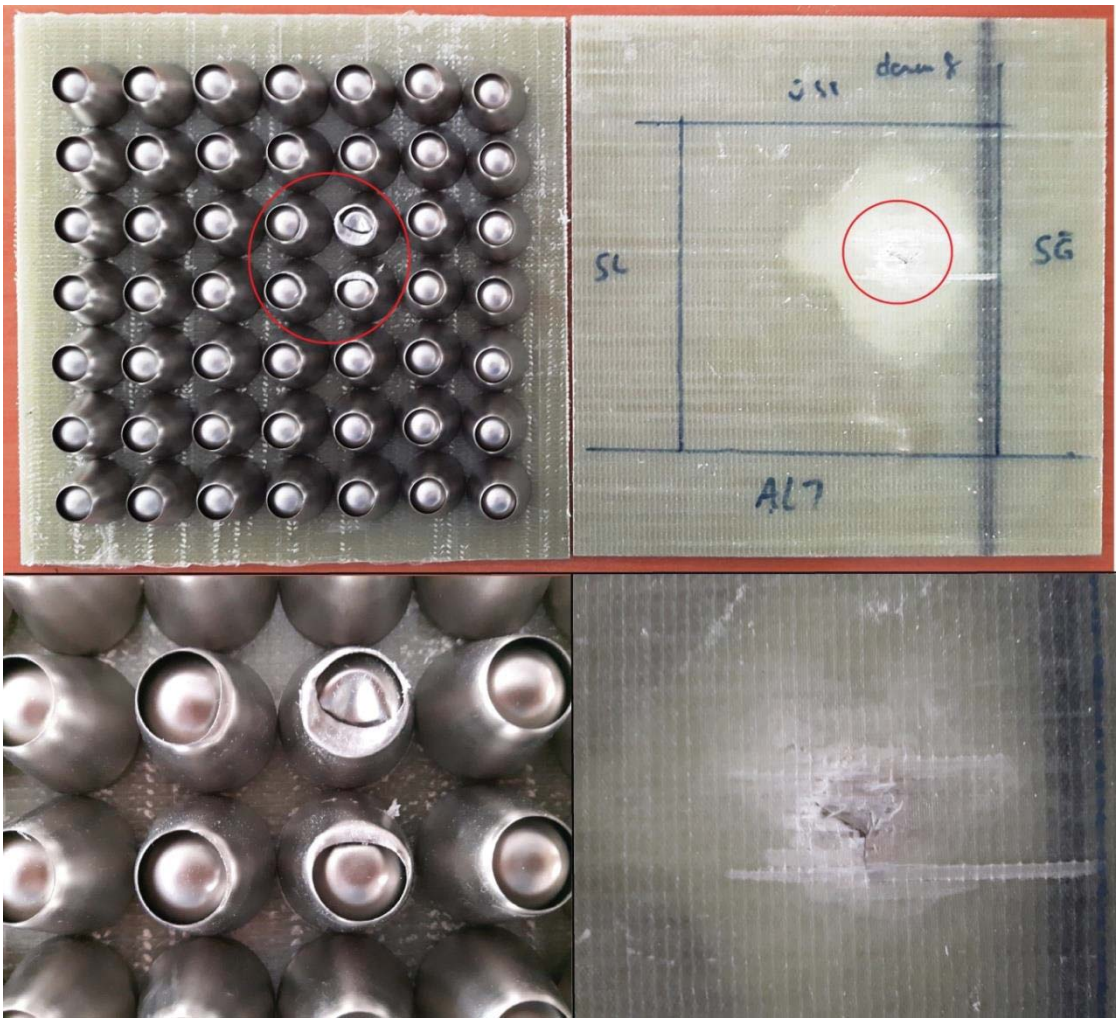

Figure 5.36. Gas gun test with cubical penetrator and the impact velocity of 180 m/s

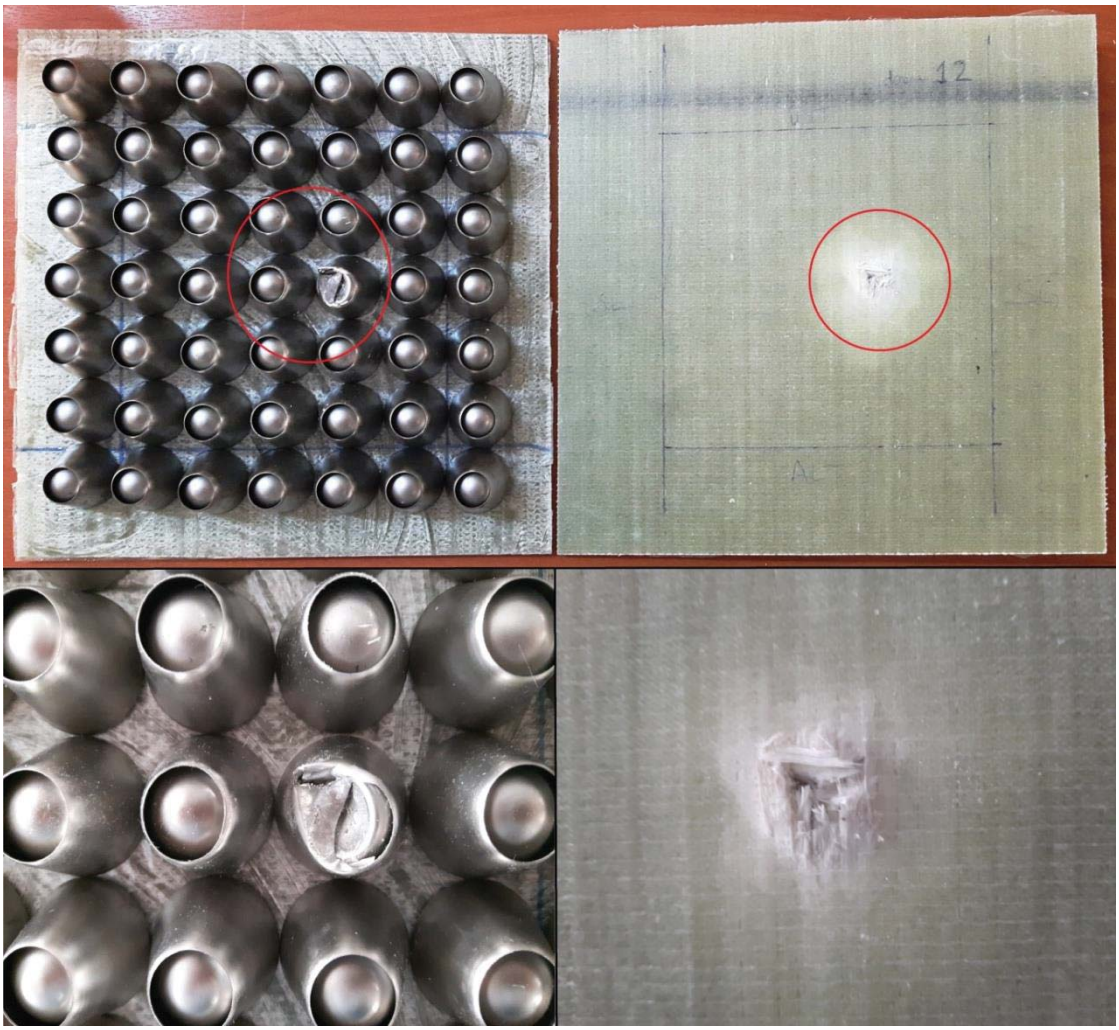

Figure 5.37. Gas gun test with cubical penetrator and the impact velocity of 235 m/s

The amount of permanent deformation of the front composite facing (delamination, fiber and matrix damages) and the amount of plastic deformation in the core structures increase directly proportional with the increase in impact velocity as can be seen in figures given above. In case of using spherical penetrator, usually 4-6 pieces of bio-inspired cores participate in the resistance against penetration. The relatively small geometric dimensions of the cubical penetrator cause a deformation in a smaller area involving maximum 4 pieces of bio-inspired cores. Due to the sharp edges of the cubical penetrator, tearing was also observed in several tests.

One of the penetration tests (spherical penetrator, 180 m/s) was modeled in LS-DYNA to better understand the crushing behavior of the proposed structure and to

demonstrate the success of the composite material model. In Figure 5.38, numerically deformed cores and the delamination on the front composite facing are given. A quite similarity was noted between the deformation modes of experimentally and numerically crushed sandwich structures.

(a)

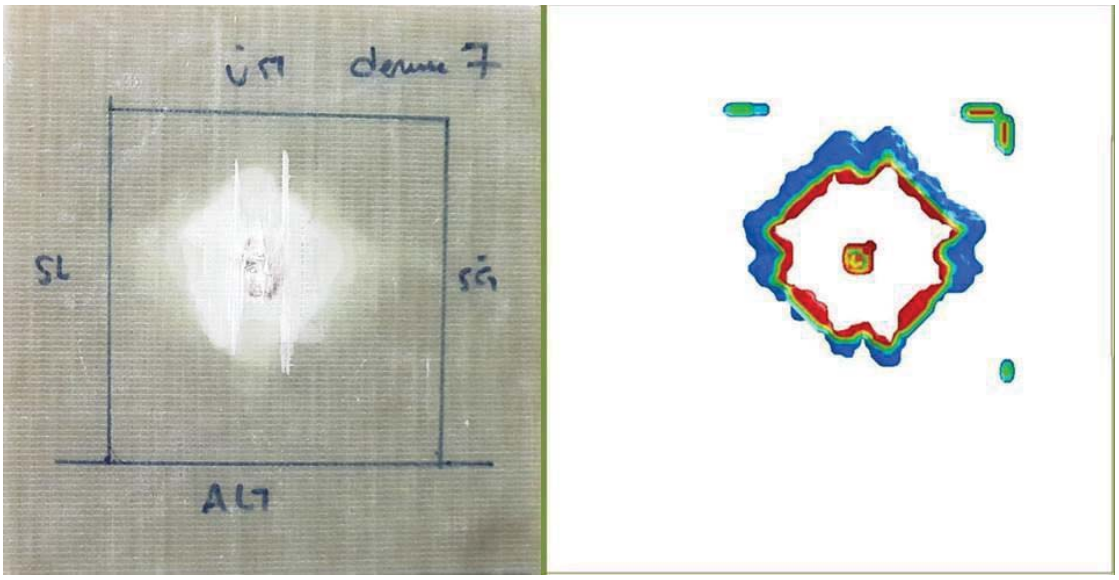

(b) (c)

Figure 5.38. (a) The deformed bio-inspired cores and the damage on composite facing in (b) experiment and (c) numerical model.

In the test which perforation was observed, the impact energy was equal to 1782 J. 76% of the impact energy was spent to puncture the front face, the core layer and the back face, respectively and the residual energy was calculated as 254 J. The energy

absorption percentage is highly satisfying in comparison with the results in the related papers, especially the ones which are studied on the sandwich structures that have close core layer thickness to that of the current bio-inspired sandwich structure. In the study that is carried out by C. Liu *et al*, sandwich panels with metal fibre laminate skins and aluminum core were investigated. A spherical projectile with the impact velocity of 200 m/s and the mass of only 7.05 g was fired to inspect the high velocity impact responses of the structure. 71% of the impact energy was absorbed while the residual velocity was measured as 107.8 m/s. (C. Liu, Zhang, & Ye, 2017). In another study, sandwich structures with honeycomb core were examined numerically. Much lighter spherical projectile (1.7 g) was used in gas gun models. Only 47% energy absorption was observed while the velocity of the projectile decreases to 210 m/s from 287 m/s. (Buitrago, Santiuste, Sánchez-Sáez, Barbero, & Navarro, 2010)

CHAPTER 6

CONCLUSION

In the current study, a sandwich structure with a novel core geometry was designed and manufactured. AISI 304L stainless steel was chosen as the core material. Then, the sandwich structures with different face sheets (AISI 304L stainless steel and E-glass/polyester) were crushed under quasi-static and dynamic loading rates. Also, the penetration and perforation characteristics of the proposed sandwich structure were examined. Aforementioned studies were carried out both experimentally and numerically. Experimental and numerical results have shown a quite well agreement. Validation of the numerical models is a significant gain for the future works. In the literature review part, mainly thin-walled structures were inspected and related investigation methods were pointed out. Within this framework; the effect of foam filling, deformation rate and inertial effects were mainly concentrated on.

The following conclusions can be reached based upon the results of experimental and numerical studies:

- The inspired living creature has been adapted into the core material geometry in the most appropriate way which provides easy, rapid and cost-effective manufacturing process. In the light of these requirements, the method of deep drawing was preferred. Its contribution to the crashworthiness performance of the sandwich structure was revealed. Also, the significance of taking the modeling of manufacturing process into consideration was demonstrated. A good agreement was noted in the thickness variations of experimentally and numerically prepared thin-walled geometries.
- The importance of using a pattern in the assembly process of the sandwich structures was indicated in terms of obtaining consistent results.
- Since the proposed geometry consists of two concentric conical-like geometries, each geometry (inner core & outer shell) was investigated individually at first. Then, in order to show the interaction affect between inner core and outer shell, arithmetic addition of the individual load-

carrying performances with respect to the crushing displacements was given in the same graph with that of bio-inspired core (combination of inner core and outer shell). Approximately 15% increase in absorbed energy was noted in the crushing of bio-inspired cores compared to the arithmetic addition of inner cores and outer shells.

- A comparison was made between the energy absorbing capabilities of the sandwich structure with four bio-inspired cores and the single bio-inspired core multiplied by the scale factor of four. A slight enhancement was observed in the performance of the sandwich, in particular, at the compression level where densification is about to start.
- It has been demonstrated that the type of face sheet material has insignificant effect on the energy absorbing capacity and the deformation modes of core geometries. In both cases, core materials were collapsed in diamond mode.
- The effects of using polyurethane foam as the filler material were shown. An increase of 10% in the amount of absorbed energy was noticed in case of using foam-filled bio-inspired cores instead of empty ones. However, at lower strain rate levels, it can be said that foam filling shows ineffectiveness when the SAE values are considered. On the other hand, in the drop-weight tests, using polyurethane foam filler is impressively beneficial in the reduction of deformation amount to absorb the same amount of kinetic energy with the empty equivalent absorbs.
- Confinement effect on the load-carrying capacity of the each sandwich specimen was exhibited. While the confinement effect makes itself evident after the compression level of ~15 mm particularly in the crushing of OS and BIC sandwich specimens, IC sandwich specimens is not affected on a big scale due to having comparatively smaller bottom diameter.
- The validation of crushing models performed in LS-DYNA was presented. Not only the force-displacement curves but also the deformation modes of the core materials in experimental and numerical studies perfectly match up with each other. It enables to investigate the proposed geometry extensively and provides an ease for the future

works. It has been detected that the formation of foldings in the collapse of bio-inspired cores results in the generation of local maximum and local minimum points in the force-displacement curves.

- At both quasi-static and dynamic deformation rates, while BIC sandwich specimen exhibits the most excellent performance IC sandwich specimen has the lowest performance. Moreover, at the deformation level of 8.6 mm (the maximum deformation level of BIC sandwich specimen), energy absorption capacities and specific absorbed energies of each type of sandwich specimen were tabulated. It has been revealed that the identical sandwich specimens show better energy absorption characteristics at higher deformation rates.
- Relying on the consistency of the numerical models which can be verified by the experimental results, the specimen was exposed to the higher crushing velocities: 50 m/s, 100 m/s, 150 m/s. Thus, the increase in the energy absorption capability with increasing deformation rate was demonstrated more clearly.
- Further, the effect of inertia and deformation rate on the load-carrying capacity was clarified in details by running rate sensitive and rate insensitive numerical models. When only the inertial effects play a role on load-carrying capacity, the mean force shows an increase of 46% under the constant crushing velocity of 50 m/s compared to that value of quasi-statically deformed specimen. In case of including the effects of rate sensitivity, the mean force rises 85%. It has been concluded that inertial effects are more effective than strain rate in the improvement of crashworthiness performance.
- In the gas gun tests, perforation was observed only in case of using 110 g spherical projectile with 180 m/s impact velocity. Sharp edged cubical projectile only penetrated into the sandwich specimen despite the higher impact velocity due to having lower mass. The test which perforation was observed in was modeled in LS-DYNA and quite well agreement observed in the deformation modes of both the bio-inspired cores and the front face sheet.

Eventually, following suggestions can be made for the future works based on the current study:

- An initial blank material with different thickness can be chosen in the first step of manufacturing process to see the effects of the wall thickness on the dynamic crushing behavior of the proposed geometry.
- The distance between adjacent bio-inspired cores can be varied to see how the energy absorption capability is affected by the change of interaction level.
- The effect of material type might be investigated. Different materials can be employed instead of AISI 304L stainless steel.
- It might be beneficial to investigate the crushing behavior of the proposed core geometry under oblique loading.

REFERENCES

Ahmad, Z., & Thambiratnam, D. P. (2009). Dynamic computer simulation and energy absorption of foam-filled conical tubes under axial impact loading. *Computers and Structures*, *87*(3–4), 186–197. http://doi.org/10.1016/j.compstruc.2008.10.003

Akbulut, F. (2017). *The investigation of the static and dynamic crrushing behavior of an energy absoring biomimetic armor* (Master's thesis, İzmir Institute of Technology, İzmir, Turkey).

Alavi Nia, A., & Khodabakhsh, H. (2015). The effect of radial distance of concentric thin-walled tubes on their energy absorption capability under axial dynamic and quasi-static loading. *Thin-Walled Structures*, *93*, 188–197. http://doi.org/10.1016/j.tws.2015.03.023

Alkateb, M., & Mahdi, E. (2004). On the energy absorption capability of axially crushed composite elliptical cones. *Composite Structures*, *66*, 495–501. http://doi.org/10.1016/j.compstruct.2004.04.078

Azarakhsh, S., & Ghamarian, A. (2017). subjected to axial and oblique loads, *112*(November 2016), 1–11.

Bitzer, T. (1997). *Honeycomb Technology: Materials, Design, Manufacturing, Applications And Testing*. *Chapman & Hall, London*. http://doi.org/10.1007/978-94-011-5856-5

Buitrago, B. L., Santiuste, C., Sánchez-Sáez, S., Barbero, E., & Navarro, C. (2010). Modelling of composite sandwich structures with honeycomb core subjected to high-velocity impact. *Composite Structures*, *92*(9), 2090–2096. http://doi.org/10.1016/j.compstruct.2009.10.013

Calladine, C. R., & English, R. W. (1984). Strain-rate and inertia effects in the collapse of two types of energy-absorbing structure. *International Journal of Mechanical Sciences*, *26*(11–12), 689–701. http://doi.org/10.1016/0020-7403(84)90021-3

Compston, P. (2006). Low Energy Impact Damage Modes in Aluminum Foam and Polymer Foam Sandwich Structures. *Journal of Sandwich Structures and Materials*, *8*(5), 365–379. http://doi.org/10.1177/1099636206064824

Deshpande, V. S., & Fleck, N. A. (2001). Collapse of truss core sandwich beams in 3-point bending. *International Journal of Solids and Structures*, *38*(36–37), 6275–6305. http://doi.org/10.1016/S0020-7683(01)00103-2

Fan, H. L., Meng, F. H., & Yang, W. (2007). Sandwich panels with Kagome lattice cores reinforced by carbon fibers. *Composite Structures*, *81*(4), 533–539. http://doi.org/10.1016/j.compstruct.2006.09.011

Ghamarian, A., Zarei, H. R., & Abadi, M. T. (2011). Experimental and numerical crashworthiness investigation of empty and foam-filled end-capped conical tubes. *Thin-Walled Structures*, *49*(10), 1312–1319. http://doi.org/10.1016/j.tws.2011.03.005

Guden, M., Yüksel, S., Taşdemirci, A., & Tanoğlu, M. (2007). Effect of aluminum closed-cell foam filling on the quasi-static axial crush performance of glass fiber reinforced polyester composite and aluminum/composite hybrid tubes. *Composite Structures*, *81*(4), 480–490. http://doi.org/10.1016/j.compstruct.2006.09.005

Gupta, N. K. (1998). Some aspects of axial collapse of cylindrical thin-walled tubes. *Thin-Walled Structures*, *32*(1–3), 111–126. http://doi.org/10.1016/S0263-8231(98)00029-9

Gupta, N. K., Mohamed Sheriff, N., & Velmurugan, R. (2008). Analysis of collapse behaviour of combined geometry metallic shells under axial impact. *International Journal of Impact Engineering*, *35*(8), 731–741. http://doi.org/10.1016/j.ijimpeng.2008.01.005

Gupta, N. K., & Venkatesh. (2004). Experimental and numerical studies of dynamic axial compression of thin walled spherical shells. *International Journal of Impact Engineering*, *30*(8–9), 1225–1240. http://doi.org/10.1016/j.ijimpeng.2004.03.009

Gupta, P. K., & Gupta, N. K. (2013). A study on axial compression of tubular metallic shells having combined tube-cone geometry. *Thin-Walled Structures*, *62*, 85–95. http://doi.org/10.1016/j.tws.2012.07.018

Haldar, S., & Bruck, H. A. (2014). Mechanics of composite sandwich structures with bioinspired core, *95*, 67–74. http://doi.org/10.1016/j.compscitech.2014.02.011

Hazizan, A., & Cantwell, W. J. (2002). the Low Velocity Impact Response of Sandwich Structures, *33*.

Hazizan, A., & Cantwell, W. J. (2003). The low velocity impact response of an aluminium honeycomb sandwich structure, *34*, 679–687. http://doi.org/10.1016/S1359-8368(03)00089-1

Hong, S. T., Pan, J., Tyan, T., & Prasad, P. (2008). Dynamic crush behaviors of aluminum honeycomb specimens under compression dominant inclined loads. *International Journal of Plasticity*, *24*(1), 89–117.

http://doi.org/10.1016/j.ijplas.2007.02.003

Kavi, H., Toksoy, A. K., & Guden, M. (2006). Predicting energy absorption in a foam-filled thin-walled aluminum tube based on experimentally determined strengthening coefficient. *Materials and Design*, *27*(4), 263–269. http://doi.org/10.1016/j.matdes.2004.10.024

Lee, S. M., & Tsotsis, T. K. (2000). Indentation failure behavior of honeycomb sandwich panels. *Composites Science and Technology*, *60*(8), 1147–1159. http://doi.org/10.1016/S0266-3538(00)00023-3

Liu, C., Zhang, Y. X., & Ye, L. (2017). High velocity impact responses of sandwich panels with metal fibre laminate skins and aluminium foam core. *International Journal of Impact Engineering*, *100*, 139–153. http://doi.org/10.1016/j.ijimpeng.2016.09.004

Liu, W., Lin, Z., Wang, N., & Deng, X. (2016). Dynamic performances of thin-walled tubes with star-shaped cross section under axial impact. *Thin-Walled Structures*, *100*, 25–37. http://doi.org/10.1016/j.tws.2015.11.016

McCormack, T. M., Miller, R., Kesler, O., & Gibson, L. J. (2001). Failure of sandwich beams with metallic foam cores. *International Journal of Solids and Structures*, *38*(28–29), 4901–4920. http://doi.org/10.1016/S0020-7683(00)00327-9

Meo, M., Vignjevic, R., & Marengo, G. (2005). The response of honeycomb sandwich panels under low-velocity impact loading. *International Journal of Mechanical Sciences*, *47*(9), 1301–1325. http://doi.org/10.1016/j.ijmecsci.2005.05.006

Najafi, A., & Rais-Rohani, M. (2011). Mechanics of axial plastic collapse in multi-cell, multi-corner crush tubes. *Thin-Walled Structures*, *49*(1), 1–12. http://doi.org/10.1016/j.tws.2010.07.002

Paik, J. K., Thayamballi, A. K., & Kim, G. S. (1999). The strength characteristics of aluminum honeycomb sandwich panels. *Thin-Walled Structures*, *35*, 205–231.

Pérez-Losada, M., Høeg, J., & Crandall, K. (2004). Unraveling the Evolutionary Radiation of the Thoracican Barnacles Using Molecular and Morphological Evidence: A Comparison of Several Divergence Time Estimation Approaches. *Systematic Biology*, *53*(2), 244–264. http://doi.org/10.1080/10635150490423458

Rubino, V., Deshpande, V. S., & Fleck, N. A. (2008). The dynamic response of end-clamped sandwich beams with a Y-frame or corrugated core. *International Journal of Impact Engineering*, *35*(8), 829–844. http://doi.org/10.1016/j.ijimpeng.2007.10.006

Tang, Z., Liu, S., & Zhang, Z. (1998). Thin-walled structures. *Thin-Walled Structures*, *7*, 841. http://doi.org/10.1016/0263-8231(89)90022-0

Tasdemirci, A., Kara, A., Turan, K., & Sahin, S. (2015). Dynamic crushing and energy absorption of sandwich structures with combined geometry shell cores. *Thin-Walled Structures*, *91*, 116–128. http://doi.org/10.1016/j.tws.2015.02.015

Tunusoglu, G. (2011). The effects of light-weight interface material on the stress wave propagation in the multilayered composite armored system. (Master's thesis, İzmir Institute of Technology , İzmir, Turkey).

Ullah, I., Elambasseril, J., Brandt, M., & Feih, S. (2014). Performance of bio-inspired Kagome truss core structures under compression and shear loading. *Composite Structures*, *118*(1), 294–302. http://doi.org/10.1016/j.compstruct.2014.07.036

Vinayagar, K., & Kumar, A. S. (2017). Thin Walled Structures, *112*(December 2016), 184–193. Retrieved from papers2://publication/uuid/A9DA5EB4-25B8-4436-9288-5B84DDC9A53D

Vincent, J. F. V, Bogatyreva, O. A., Bogatyrev, N. R., Bowyer, A., & Pahl, A.-K. (2006). Biomimetics: its practice and theory. *Journal of the Royal Society*, *3*(April), 471–482. http://doi.org/10.1098/rsif.2006.0127

Wang, B., & Lu, G. (2002). Mushrooming of circular tubes under dynamic axial loading. *Thin-Walled Structures*, *40*(2), 167–182. http://doi.org/10.1016/S0263-8231(01)00057-X

Yamashita, M., Gotoh, M., & Sawairi, Y. (2003). Axial crush of hollow cylindrical structures with various polygonal cross-sections: Numerical simulation and experiment. *Journal of Materials Processing Technology*, *140*(1–3 SPEC.), 59–64. http://doi.org/10.1016/S0924-0136(03)00821-5

Zarei, H. R., & Kröger, M. (2008). Optimization of the foam-filled aluminum tubes for crush box application. *Thin-Walled Structures*, *46*(2), 214–221. http://doi.org/10.1016/j.tws.2007.07.016

Zhang, X., & Huh, H. (2009). Energy absorption of longitudinally grooved square tubes under axial compression. *Thin-Walled Structures*, *47*(12), 1469–1477. http://doi.org/10.1016/j.tws.2009.07.003

Zheng, G., Wu, S., Sun, G., Li, G., & Li, Q. (2014). Crushing analysis of foam-filled single and bitubal polygonal thin-walled tubes. *International Journal of Mechanical Sciences*, *87*, 226–240. http://doi.org/10.1016/j.ijmecsci.2014.06.002